

INFORMATION TO USERS

This manuscript has been reproduced from the microfilm master. UMI films the text directly from the original or copy submitted. Thus, some thesis and dissertation copies are in typewriter face, while others may be from any type of computer printer.

The quality of this reproduction is dependent upon the quality of the copy submitted. Broken or indistinct print, colored or poor quality illustrations and photographs, print bleedthrough, substandard margins, and improper alignment can adversely affect reproduction.

In the unlikely event that the author did not send UMI a complete manuscript and there are missing pages, these will be noted. Also, if unauthorized copyright material had to be removed, a note will indicate the deletion.

Oversize materials (e.g., maps, drawings, charts) are reproduced by sectioning the original, beginning at the upper left-hand corner and continuing from left to right in equal sections with small overlaps. Each original is also photographed in one exposure and is included in reduced form at the back of the book.

Photographs included in the original manuscript have been reproduced xerographically in this copy. Higher quality 6" x 9" black and white photographic prints are available for any photographs or illustrations appearing in this copy for an additional charge. Contact UMI directly to order.

UMI

A Bell & Howell Information Company
300 North Zeeb Road, Ann Arbor MI 48106-1346 USA
313/761-4700 800/521-0600

AIRCRAFT SURVEILLANCE AND COLLISION AVOIDANCE USING GPS

A DISSERTATION

SUBMITTED TO THE DEPARTMENT OF AERONAUTICS AND ASTRONAUTICS

AND THE COMMITTEE ON GRADUATE STUDIES

OF STANFORD UNIVERSITY

IN PARTIAL FULFILLMENT OF THE REQUIREMENTS

FOR THE DEGREE OF

DOCTOR OF PHILOSOPHY

By

Ran Y. Gazit

August 1996

UMI Number: 9702894

UMI Microform 9702894
Copyright 1996, by UMI Company. All rights reserved.

**This microform edition is protected against unauthorized
copying under Title 17, United States Code.**

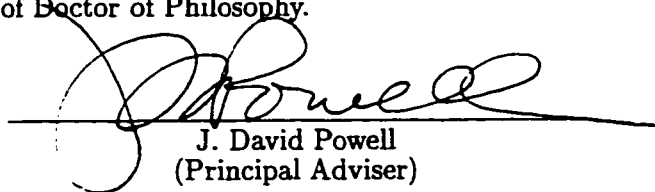
UMI
300 North Zeeb Road
Ann Arbor, MI 48103

© Copyright 1996

by

Ran Y. Gazit

I certify that I have read this thesis and that in my opinion
it is fully adequate, in scope and in quality, as a dissertation
for the degree of Doctor of Philosophy.



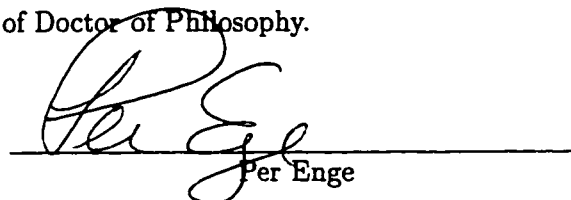
J. David Powell
(Principal Adviser)

I certify that I have read this thesis and that in my opinion
it is fully adequate, in scope and in quality, as a dissertation
for the degree of Doctor of Philosophy.



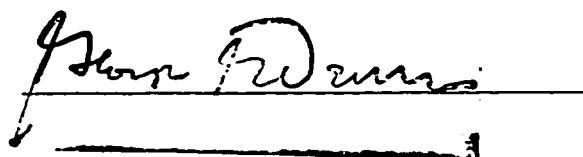
Bradford W. Parkinson

I certify that I have read this thesis and that in my opinion
it is fully adequate, in scope and in quality, as a dissertation
for the degree of Doctor of Philosophy.



Per Enge

Approved for the University Committee on Graduate Studies:



John F. Williams

Abstract

Avoidance of in-flight collisions requires accurate and timely information on aircraft position and velocity. This information is obtained today by a ground-based surveillance system that is limited in accuracy, coverage and automation. A new concept for integrated navigation and surveillance suggests that every aircraft will periodically broadcast its position as determined by an on-board GPS receiver. The position reports will be received by Air Traffic Control ground facilities and will be used for aircraft tracking and conflict resolution.

The key to the successful application of this concept is a reliable data link architecture that will allow all aircraft within a specified detection range to exchange information at a required rate. In this research, the basic parameters and relationships that govern the data link channel capacity are identified, and bounds on the performance of several random-access and self-organized communication protocols are set.

Unique adaptive algorithms for aircraft tracking are designed and tested. The resulting tracking accuracy is shown to be superior to the performance of modern, multiple-model radar trackers. The improvement in tracking accuracy provides the means to reduce aircraft separation standards and to decrease the runway spacing required for independent parallel approaches, all without affecting the safety level.

Moreover, since each aircraft can receive the position reports of its neighbors, a highly accurate airborne collision avoidance system can be designed. The three-dimensional positioning information provided by GPS, coupled with new collision detection and avoidance algorithms can provide timely alarms with a low false alarm rate. This significantly improves the performance of the current airborne collision avoidance system.

Acknowledgments

I would like to thank my advisor, Professor J. David Powell, for introducing me to GPS and to Air Traffic Control, and for giving me the opportunity to pursue this research. His comprehensive knowledge and clear guidance are greatly appreciated. I wish also to thank my defense and reading committee, including Professors Bradford W. Parkinson and Per Enge for their constructive evaluation and criticism of this manuscript.

I would like to thank all of the GPS graduate students for their assistance throughout my research. I would especially like to express my thanks to Y.C. Chao for reviewing my early papers and for his invaluable help and expertise in GPS data collection. In addition, I gratefully acknowledge the Federal Aviation Administration (FAA) Satellite Program Office for sponsoring this research.

I would like to thank my parents, Rachel and Jacob Gazit, for their love and support and for the motivation they have given me during my academic studies. Finally and most importantly, I express special thanks to my wife Yifat for her help, advice and encouragement which made this work possible. Although much smaller in scale to what she has given to me, this work is dedicated to her.

Contents

Abstract	iv
Acknowledgments	v
Nomenclature	xiv
1 Introduction	1
1.1 Associated Work	3
1.2 Contributions	5
2 Aircraft Surveillance	7
2.1 ATC Surveillance Systems	7
2.1.1 Pilot Position Reports	8
2.1.2 Primary Surveillance Radar	8
2.1.3 Secondary Surveillance Radar	9
2.2 Automatic Dependent Surveillance	10
2.2.1 System Concept	10
2.2.2 GPS Role	11
2.2.3 Anticipated Benefits	12
2.2.4 Current Status	14
3 Communication Protocols	16
3.1 Introduction	16

3.2	Probability of Clear Reception	17
3.2.1	Exact Expression	18
3.2.2	Exponential Approximation	20
3.3	Channel Capacity	22
3.3.1	Capacity as the Maximal Throughput	22
3.3.2	Organized Channel	24
3.3.3	Capacity for a Given Reliability Level	26
3.4	Capture Effects	28
3.5	Conflict Resolution and Self Organization	30
3.5.1	Basic Requirements	31
3.5.2	Perfect Self-Organization	33
3.5.3	Negative Acknowledgments	34
3.5.4	Self Adapting TDMA	36
3.5.5	Random Switching	36
3.6	Design Alternatives	38
3.7	Conclusion	40
4	Aircraft Tracking	42
4.1	Introduction	42
4.2	Error Model Identification	43
4.2.1	Data Analysis	44
4.2.2	Simple Gauss-Markov Processes	45
4.2.3	A General 3rd Order Gauss-Markov Process	47
4.3	Dynamic Aircraft Models	47
4.4	Tracking Filter Design	48
4.4.1	Correlated Measurement Noise	49
4.4.2	Filter Initialization	51
4.4.3	Error Model Selection	53
4.4.4	Aircraft Model Selection	54

4.4.5	Data Link Effect	56
4.4.6	Multiple-Model Estimation	58
4.4.7	Velocity Reports	61
4.4.8	Update Rate	62
4.5	Performance Study	63
4.6	Conclusion	65
5	Separation Standards	67
5.1	Introduction	67
5.2	Radar Separation Minima	69
5.2.1	Probability of Close Approach	69
5.2.2	Distribution of Surveillance Errors	70
5.2.3	Analysis	71
5.3	Parallel Runway Separation	73
5.4	Blunder Prediction	76
5.4.1	Probability of Late Alarm	77
5.4.2	Probability of False Alarm	78
5.4.3	Effect on Runway Spacing	79
5.5	Conclusion	82
6	Airborne Collision Avoidance	83
6.1	Introduction	83
6.2	TCAS Overview	84
6.2.1	Operation	84
6.2.2	Status	85
6.3	Traffic Display	86
6.3.1	TCAS II Display	87
6.3.2	GPS-based Traffic Display	88
6.4	Collision Detection	89
6.4.1	Basic Algorithms	89

6.4.2	Analysis	96
6.5	Collision Avoidance	103
6.6	Conclusion	108
7	Conclusion	109
A	ADS Message Format and Reporting Rate	113
A.1	ADS	113
A.2	GNSS Transponder	115
A.3	ADS Mode-S (GPS Squitter)	115
A.4	ADS-B Extended Squitter	117
B	Probability of Clear Reception	119
B.1	Random Channel	119
B.2	Random Slot Selection	120
B.3	Capture Effects	124
C	Aircraft Traffic Density	128
D	Correlation Functions	131
D.1	Theory	131
D.2	Examples	132
E	Correlated Measurement Noise	134
E.1	Reduced Order Model	134
E.2	Filter Design	138
E.3	Filter Initialization	140
E.4	Examples	142
F	Runway Spacing Components	146

G Monte Carlo Simulations	150
G.1 Random Air Traffic Communication Network	150
G.2 Random Approach Simulation	152
G.3 Random Encounters in “Free Flight”	153
Bibliography	165

List of Tables

4.1	Statistical Properties of the Data Base	44
4.2	Representative Trajectories	63
4.3	Average Tracking Errors with GPS (SA on)	64
4.4	Average Tracking Errors with ATC Radars	64
A.1	ADS message formats	114
A.2	GNSS transponder message format	115
A.3	ADS Mode-S message format	116
A.4	ADS-B message format (RTCA SC-186)	117
A.5	ADS-B message format (RTCA SC-186) - cont.	118
F.1	Model Parameters for Parallel Runway Separation	148
G.1	“Free Flight” Simulation Parameters	155

List of Figures

3.1	Probability of Clear Reception vs. Range	20
3.2	Probability of Clear Reception vs. Aircraft Number	23
3.3	Channel Throughput	23
3.4	Channel Capacity - 100 Kbps	25
3.5	Channel Capacity - 1 Mbps	25
3.6	Capacity for Multiple Transmission Attempts	27
3.7	Effective Update Rate	28
3.8	Capacity Gain due to Capture	30
3.9	Minimum Bit Rate for an Organized Channel	32
3.10	Negative Acknowledgments	35
3.11	Self Adapting TDMA and Random Switching	37
3.12	Capacity of Design Alternatives	40
4.1	Autocorrelation Functions	46
4.2	Error Model Selection	54
4.3	Average Tracking Errors – Uniform Motion	55
4.4	Average Tracking Errors – Coordinated Turn	55
4.5	Data Link Effects	57
4.6	Tracking Filters Comparison	60
4.7	Constellation Change Effect	61
5.1	PDF of GPS Position Errors	70
5.2	Probability of Unobserved Close Approach	72

5.3	GPS Equipage Effect	73
5.4	Runway Separation vs. Surveillance Accuracy	75
5.5	Prediction Effect on Late Alarms	78
5.6	Prediction Effect on False Alarms	79
5.7	Prediction Effect on NOZ and DZ	80
5.8	Prediction Effect on Runway Separation	81
6.1	TCAS II Traffic Display	87
6.2	GPS-based Traffic Display	87
6.3	Collision Plane	91
6.4	Protection Volumes	92
6.5	Reachability Regions	95
6.6	Probability of False Alarm in Constant Velocity, Planar Encounters	98
6.7	Probability of Late Alarm in Constant Velocity, Planar Encounters	98
6.8	Probability of False Alarm in Planar Encounters	99
6.9	Probability of Late Alarm in Planar Encounters	99
6.10	Probability of False Alarm, 3-D Encounters	102
6.11	Probability of Late Alarm, 3-D Encounters	102
6.12	CDF of Miss Distance	106
6.13	Distribution of the Closest Point of Approach (CPA) Distance	107
B.1	Interference Region in a Slotted Channel	121
B.2	Interference Region with Capture	125
C.1	Traffic Count	130
C.2	Average Traffic Density	130
G.1	Distribution of Aircraft Turn Rate	154

Nomenclature

Roman Symbols

A	area of interest for probability calculation
a_r	relative acceleration
B	bit rate
C	channel capacity
c	speed of light
d	minimum safety distance
D_m	range threshold
K_{CR}	capacity gain due to capture
K_n	capacity gain due to multiple transmission attempts
M	total number of aircraft
m	miss distance
N	average number of aircraft in range
N_2	average number of aircraft in a $2R$ circle
N_r	channel throughput
n	number of transmission attempts
n_m	number of bits in a message
p	probability that an aircraft is in range
P_{ca}	probability of unobserved close approach
P_{fa}	probability of false alarm

P_d	probability of transmitter–receiver interference
P_{la}	probability of late alarm
P_n	probability of clear reception with n attempts
P_o	probability of message overlap inside a slot
P_r	probability of clear reception
Q	spectral density
q	probability of changing time slot selection
R	detection range
r	transmitter–receiver range
s	number of time slots in a frame
T	sampling interval
t_d	propagation delay guard band
t_f	frame length (update interval)
t_{go}	time to the point of closest approach
t_m	message length
t_p	prediction time
t_r	required frame length
t_s	time slot length
t_w	warning time
V	aircraft speed
V_R	relative velocity
w	white noise
v	white measurement noise
v_{\perp}	cross track velocity
y_{\perp}	cross track position
z	measurement vector
z_{\perp}	predicted cross track position

Greek Symbols

α	linear capture ratio
β	distance measure of the capture ratio
γ	aircraft heading
ϵ	Gaussian mixture coefficient
λ	average number of received messages per second
σ	average number of aircraft per unit area
Φ	aircraft model dynamics matrix
ϕ	autocorrelation
Ψ	error model dynamics matrix
ω	aircraft turn rate

Acronyms

ADS	automatic dependent surveillance
APAS	automatic position advisory system
ARSR	air route surveillance radar
ARTS	automated radar terminal system
ASR	airport surveillance radar
ATC	air traffic control
ATCRBS	air traffic control radar beacon system
CPA	closest point of approach
CR	capture ratio
CZ	correction zone
DGPS	differential GPS
DZ	detection zone
FAA	federal aviation administration

FANS	future air navigation system
FMA	final monitor aid
GNSS	global navigation satellite system
GPS	global positioning system
IAS	indicated air speed
ICAO	international civil aviation organization
IFR	instrument flight rules
ILS	instrument landing system
IMC	instrument meteorological conditions
IMM	interacting multiple model
INMARSAT	international maritime satellite
NOZ	normal operating zone
PDOP	position dilution of precision
RTCA	radio technical commission for aviation
SA	selective availability
SSR	secondary surveillance radar
TCAS	traffic alert and collision avoidance system
TDMA	time division multiple access
VFR	visual flight rules
VHF	very high frequency
VMC	visual meteorological conditions
WAAS	wide area augmentation system

Chapter 1

Introduction

Avoidance of in-flight collisions requires accurate and timely information on aircraft position and velocity. This information is obtained by the Air Traffic Control (ATC) surveillance system, which is almost totally dependent today on voice communication and ground-based radar systems. The current surveillance system is limited in accuracy, coverage and automation, and is very expensive to maintain and operate.

However, the proliferation of Global Navigation Satellite Systems such as the GPS (Global Positioning System) makes it now possible for each aircraft to determine its own position much more accurately than obtainable with the present surveillance systems. With the addition of an appropriate communication link, each aircraft could broadcast its position as derived by an onboard GPS receiver. The position reports will be received by ATC ground facilities and will be used for aircraft tracking and conflict resolution, in a similar fashion to the way radar measurements are used today.

This concept is referred to as Automatic Dependent Surveillance (ADS). It can provide the ATC system with highly accurate surveillance information, even in areas which are not covered today by radar. ADS is expected to decrease aircraft separation requirements and to allow a more effective control of aircraft movements. Eventually, it should provide the freedom to select random routing and optimum altitudes for time and fuel savings.

ADS has also the potential to replace the large and expensive rotating radar beacons by

simple, fixed omni directional antennas for receiving the position reports. This can reduce substantially the cost of the overall surveillance system. Moreover, since each aircraft can also receive the position reports of other nearby aircraft, it is actually provided with a highly accurate collision avoidance system, at a price which is affordable to all aviation.

Although this concept is being evaluated now in trials all around the world, there are many questions which are still open. We can classify these questions into the following areas:

- **Communication:** The communication architecture should enable all aircraft to share a common channel and exchange information at a required rate. What is the communication architecture that will handle the largest number of aircraft? What are the parameters that govern this result? What is the probability of clear reception under various architectures?
- **Tracking:** The ground-based control center is required to track the position reports of each aircraft and estimate its velocity vector. What is the appropriate tracking algorithm? How is it different (in structure and performance) from the tracking filters which are currently used with radar measurements?
- **Separation standards:** The tracking filter is expected to provide highly accurate estimates of the aircraft position and velocity. What is the effect of the improved tracking accuracy on aircraft separation standards? Is it possible to reduce the current separation standards without affecting the safety level?
- **Airborne collision avoidance:** Under ADS, every aircraft could be provided with the position of all nearby aircraft. How can this information be used to detect and avoid possible midair collisions? How will the performance of this new system be different from the performance of the current airborne collision avoidance system, which uses only range measurements?

These are some of the questions to be answered in this work.

1.1 Associated Work

Most of the published work on ADS concentrates on the communication aspect of this system. The other areas defined above are studied here in detail for the first time.

Communication

ADS position reports can be relayed to ATC on ground via communication satellites or through a terrestrial data link. The satellite data link, intended for use in the oceanic airspace, was thoroughly studied before [1-4] and will not be considered in this work.

Different communication architectures for a terrestrial ADS data link were proposed during 1992-1994 by Nilsson [5-8] from the Swedish civil aviation administration, Orlando et. al. [9-13] from MIT's Lincoln Laboratory and others (Beining [14], Moody and Peed [15, 16], Spellman [17] and Villani [18]). These architectures use different frequencies, bandwidth, update rate and communication protocols, and it is required to evaluate their performance on a common basis in order to determine their relative capacities.

An attempt to perform a more general analysis of the data link was done in 1993 by Jones [19]. This work does not show the basic relationship between the channel capacity and the detection range. Moreover, it does not present a solid conclusion regarding the relative capacities of the suggested communication architectures.

Tracking

Lefas et. al. [20-25] studied during 1982-1994 the possibility of downlinking aircraft derived data (such as air speed, magnetic heading or roll angle) in order to *assist* radar tracking systems. The basic position measurement in this case was still being made by radar.

Palsson [26] implemented in 1992 a simple ADS tracking filter, using an identical approach to that used for coasting radar tracks. The tracking filter design in this case did not consider the unique characteristics of GPS measurement errors.

Separation Standards

The effect of GPS on oceanic separation standards was analyzed in 1990 by Rome [27] and in 1993 by Coote et. al. [28]. The considerations for the domestic airspace are very different from the oceanic airspace, and so are the considerations leading to the required separation between parallel runways. The effect of GPS-based surveillance in these areas was not analyzed yet.

Airborne Collision Avoidance

Most of the work on collision detection and avoidance assumes that the airborne equipment can measure only range to other aircraft. Morrel [29] in 1958, Holt [30] in 1970, and Ford [31-33] during 1986-1990 are just a few examples.

More recent work on GPS-based collision avoidance proposed different collision detection algorithms: Deckert [34] suggested in 1992 to use similar algorithms to those used by the current airborne collision avoidance system; Pilley [35] suggested comparing a simple linear projection of aircraft position to a circular protection zone defined around each aircraft; and Winer [36] described in 1995 a GPS-based collision detection algorithm which looks for the intersection of the aircraft's reachability regions. In all cases the algorithms were evaluated in a very restricted environment, and without considering the associated probabilities of false and late alarm.

1.2 Contributions

The objective of this work is twofold: to analyze the basic relationships and requirements for the operation of a GPS-based surveillance system, and to evaluate the potential benefits of this system in certain aircraft operations. The contributions presented in this dissertation are as follows:

Communication [Chap. 3]

- *Analysis framework*: derivation of a basic framework for analysis of spatial Time Division Multiple Access (TDMA) protocols, where users are distributed on a plane, and each one has a finite detection range. The main result of this analysis is the relationship between the detection range and the channel capacity.
- *Capture*: analysis of the effect of co-channel interference, or “capture”, on the capacity of random access protocols.
- *Self Organized protocols*: examination of several self-organized communication protocols, using a detailed simulation of random air traffic.
- *Relative capacity of suggested architectures*: comparison of the suggested communication architectures, with a specific conclusion regarding their relative benefits.

Tracking [Chap. 4]

- *GPS-based tracking filter*: derivation and analysis of an adaptive filter specifically matched to track GPS position reports received through an imperfect radio data link.
- *High order correlated measurement noise*: providing a general solution for optimal tracking filter design in systems with high order correlated measurement noise, including a consistent initialization procedure.

Separation Standards [Chap. 5]

- *Radar separation standards:* evaluation of the possible effect of GPS-based surveillance on aircraft separation standards in the domestic airspace.
- *Parallel runway separation:* evaluation of the effect of GPS-based surveillance on the required spacing between parallel runways which allows independent approaches under instrument meteorological conditions.
- *Alert algorithm:* study the effect of blunder prediction on parallel runway spacing.

Airborne Collision Avoidance [Chap. 6]

- *GPS-based collision detection and avoidance:* derivation and analysis of a collision detection and avoidance algorithm which fully utilizes the three dimensional positioning information provided by GPS.
- *Free-flight simulation:* evaluation of the new algorithm effectiveness through an extensive simulation of a free-flight environment.

The dissertation opens with chapter 2, which provides a brief overview of the current Air Traffic Control surveillance system and describes the Automatic Dependent Surveillance concept. Chapters 3,4,5 and 6 are devoted to an in-depth study of the different research areas defined above. Chapter 7 concludes the dissertation with a summary and some recommendations for future research. Several appendices provide detailed derivations that were omitted from the body of this work in order to improve its clarity.

Chapter 2

Aircraft Surveillance

Safe and efficient operation of the Air Traffic Control (ATC) system requires accurate and timely indication of an aircraft's identity and position in space. The air traffic controller uses this information to monitor an aircraft's flight progress, ensure safe separation of aircraft, and provide air traffic management functions such as traffic advisories, unsafe conditions alerts, vectoring and navigational assistance [4].

The information about the current location of aircraft is obtained by the surveillance function of the ATC system. The surveillance systems used today are briefly described in the first section of this chapter. The second section describes a concept for surveillance in the next century, known as Automatic Dependent Surveillance. The objective of the chapter is to provide a broader perspective and a more detailed background for the research described in this dissertation.

2.1 ATC Surveillance Systems

The current surveillance system consists of pilot-provided position reports, primary surveillance radar and secondary surveillance radar. ATC uses the data collected by these systems to track all aircraft flying under Instrument Flight Rules (IFR), where all aircraft flying through clouds or above 18,000 ft are required to be IFR. ATC also tracks most Visual Flight Rules (VFR) flights so they can warn IFR pilots of their existence and, workload

permitting, provide traffic advisories to VFR flights.

2.1.1 Pilot Position Reports

While flying an IFR flight plan that is not being tracked by radar, pilots are required to verbally report their position at designated points along the route of flight, roughly 160 km apart while over land and 10° longitude apart while over the ocean [37].

In the oceanic airspace, pilot-filed progress reports provide the only surveillance data currently available, since radar coverage is limited to a range of 200 miles. The quality of these reports may be impaired by a number of factors [38], such as erroneous position and/or time information, communication difficulties and crew preoccupation with other matters.

Note also that the VHF radio used for voice communication in the domestic airspace is a line-of-sight system, limited by the Earth's curvature: the maximum range for VHF communication at an altitude of 39,000 ft is 240 nmi [39]. Aircraft surveillance over the ocean is therefore based on hourly position reports, verbally by the pilot, using HF radio which is severely affected by ionospheric propagation conditions and electrical storms [1].

2.1.2 Primary Surveillance Radar

Primary Surveillance Radar or Air Route Surveillance Radar (ARSR) transmits a pulse of radio frequency energy from a rotating antenna. The pulse strikes an aircraft and a portion of that energy is reflected back toward the emitting antenna. Aircraft range is determined from the elapsed time between transmission and reception of the reflected pulse. Aircraft bearing is determined from the direction the antenna was pointing when the reflected pulse was received. Primary radar is also known as *independent surveillance* or *noncooperative surveillance* because the radar does not rely on aircraft equipage in order to perform its function [4].

Primary radar efficiency and operation depends on a number of variables, including transmitter power, aircraft size and distance from the radar antenna, atmospheric conditions, and obstructions that may interfere with the transmitted radar signal. When using

primary radar the controller can not determine the aircraft's altitude and must depend on accurate altitude verbal reports from the pilot. In addition, the controller must initially identify each aircraft and maintain this identification while the aircraft is under his control. The Secondary Surveillance Radar can be used to alleviate these deficiencies.

2.1.3 Secondary Surveillance Radar

Secondary Surveillance Radar (SSR) or Air Traffic Control Radar Beacon System (ATCRBS) works only with transponder-carrying aircraft, and is therefore known as *cooperative surveillance*. The SSR rotating antenna transmits interrogation signals at 1030 MHz. The interrogation signal triggers the aircraft transponder into emitting a reply at 1090 MHz. Aircraft range is determined from the time elapsed between the interrogation and the reply. Aircraft bearing is determined from the antenna direction at time of reception.

Two types of interrogations are used: Mode A, which elicits a reply that contains one of 4,096 codes assigned by a controller to the pilot of each aircraft; and Mode C, which elicits a similar 12-bit reply that contains the aircraft's barometric altitude. Altitude-encoded transponders are required within 30 miles of congested terminal areas or above 10,000 ft.

ATCRBS has several limitations that are incompatible with increased airspace congestion [40, 41]: limited surveillance of closely spaced aircraft (synchronous garbling); signal interference (fruit reply) and false targets generation; over interrogation in regions with high sensor density; limited number of identification codes; and poor azimuth accuracy. These limitations are alleviated in the Mode-S secondary radar.

A Mode-S (for Select) SSR employs a monopulse beacon which offers better azimuth determination accuracy and avoids multiple interrogations. The Mode-S transponder replies with the aircraft's altitude and a 24-bit identification code, which is permanently assigned by the International Civil Aviation Organization (ICAO) to an airframe and is unique to each aircraft throughout the world. This makes possible selective interrogation of individual aircraft, and eliminates the synchronous garbling experienced by SSR Mode A/C.

In addition, all Mode-S transponders broadcast a short message with their identification

code about once per second, even without radar interrogation. This spontaneous transmission is referred to as a “squitter”. The requirement to transmit squitters was adopted as a Mode-S standard mainly because of its usefulness in air-to-air surveillance [42, 43]. The squitter is an integral part of one of the major candidate designs for the future surveillance system, described in the next section.

Mode-S radar is being gradually introduced to replace existing ATCRBS all over the world. Its greater precision and reliability, coupled with cost considerations are causing some administrations to abandon the use of primary surveillance radar and rely exclusively on Mode-S, particularly for en-route surveillance [38]. Recently, the FAA announced its plan to eliminate most long range, enroute primary radar sites in the U.S. by the end of the century, mainly due to the high costs of maintenance and dwindling availability of parts [44]. To help compensate for the loss of primary radars, the FAA would rely on improved secondary radars and Automatic Dependent Surveillance procedures.

2.2 Automatic Dependent Surveillance

2.2.1 System Concept

The International Civil Aviation Organization (ICAO) has defined a concept for an integrated Communications, Navigation and Surveillance system for the next century known as the Future Air Navigation System (FANS) [45]. A corner stone of FANS is Automatic Dependent Surveillance (ADS), defined as:

“A surveillance technique in which aircraft automatically provide, via a data link, data derived from on-board navigation and position-fixing systems, including aircraft identification, four-dimensional position, and additional data as appropriate [46].”

In contrast to radar based surveillance, ADS *depends* on the navigation equipment on-board the aircraft, and it is not an independent position measurement.

ADS takes two forms, termed ADS and ADS-B (for Broadcast). In the first, aircraft position reports are relayed to ATC ground facilities via communication satellites, such as those operated by the International Maritime Satellite (INMARSAT) organization. This approach is primarily intended for use in the oceanic airspace or over sparsely-populated land regions where there are no ATC facilities within line of sight.

In ADS-B the aircraft broadcasts its position omni-directionally for all listeners within range to receive: ATC ground facilities as well as nearby aircraft. ADS-B is implemented through a terrestrial (line-of-sight) data link, such as the Mode-S squitter or a VHF channel. In ADS-B each aircraft can receive the position reports of other nearby aircraft, thus providing the pilot of the receiving aircraft with situational awareness of nearby traffic. Global traffic information, traditionally available to ATC only, can thus be distributed to all aircraft without an additional uplink channel.

2.2.2 GPS Role

The ICAO definition of ADS as given above clearly allows ADS to be operated with any navigation system. However, the success of ADS as a replacement or substitute for traditional surveillance methods depends primarily on the navigation system which provides the data for the ADS report. GPS has a number of strengths that are relevant to ADS [47]:

- GPS is available world-wide with uniform accuracy, controlled by the GPS ground segment. The accuracy of inertial systems is controlled by crew initialization and inertial sensor drift rates and therefore changes in time and varies from aircraft to aircraft.
- The 2-D surveillance information provided by GPS is with respect to a common grid reference, WGS-84.
- GPS provides time to a precision better than a micro second. The automatic provision of time in GPS (which does not rely on the crew setting a clock, as does the current systems), and the common reference it provides for time can serve as a basis for optimization of the ADS communication channel.

- The typical redundancy of GPS coverage allows the user to directly and automatically check the integrity of the position solution.
- A GPS receiver is considerably cheaper than an inertial platform. A basic GPS receiver fully approved to the relevant Technical Standards Order costs around \$3,000 whereas a Ring Laser Gyro inertial system is around \$100,000. This allows all aircraft to derive the benefit of ADS, including smaller general aviation aircraft.

2.2.3 Anticipated Benefits

ADS has the potential to offer increased safety and capacity, and to allow more efficient operation of aircraft at a reduced cost. Some of the anticipated benefits to ADS users are:

- *Accuracy:*

ADS, properly integrated with GPS will provide aircraft position measurements with an accuracy which in most instances far exceeds that available from ATC radars. GPS can also provide very accurate measurements of ground speed and heading, which in the case of radar must be computed by the ground-based systems.

This will permit highly accurate conflict prediction by both ground-based ATC computers and airborne collision avoidance systems. The direct result of the improved accuracy will be increased safety margins.

- *Safety:*

ADS will permit air traffic controllers to track aircraft in regions with incomplete or no radar coverage. This will enable potential conflicts to be managed and reduce the probability of gross navigational errors going unnoticed. ADS-B can also provide pilots with an increased situational awareness with respect to other aircraft, thus distributing the responsibility for aircraft separation among the aircraft themselves.

In addition, the automatic data link provided by ADS will help to reduce the workload of both air crew and ATC ground controllers. This will tend to further increase levels of safety [48].

- *Availability and capacity:*

The application of ADS to oceanic separation, where no radar surveillance data is available, provides significant potential for improvement in oceanic traffic management. A direct result of the improved visibility to controllers should lead to reduced aircraft separation, thereby offering the possibility of increased capacity.

Extension of the ADS concept to the domestic airspace will provide the key element to the implementation of a “free flight” air traffic control environment. Most of the US airspace is under positive control, where controllers closely monitor and direct aircraft operating under instrument flight rules through a restricted airway system. Free flight would require IFR pilots to assume more responsibility for safe aircraft separation, but would free them to fly unrestricted, efficient, direct routes to their destinations. This will permit a significant increase in airspace capacity, as well as substantial savings for all.

- *Savings:*

ADS has already demonstrated a significant cost benefit for operations in the Pacific region [48]. Fuel savings have been realized through flexible routings which reduce flight times. Reduced fuel loads also allow carriers to increase the commercial payload, and reduced flight time provides benefits for the passenger as well as allowing more flexibility in scheduling aircraft and aircrew.

In the domestic airspace, the number of radar sites needed to provide surveillance coverage can be minimized by overlaying gaps in coverage by a supplementary ADS capability. ADS has thus the potential to reduce the need for radar, which will reduce the cost of the total surveillance system.

2.2.4 Current Status

- *ADS:*

The preliminary requirements for satellite based ADS and its effect on oceanic ATC were thoroughly studied and are very well understood. See for example the requirements for oceanic ATC in [4, 2], the capacity for aeronautical mobile satellite ATC services in [3], and the effect of ADS on oceanic separation standards in [27, 28]. The message format for ADS as defined by the ICAO FANS committee is described in Appendix A.

Experimental trials and international ATC development programs incorporating ADS for oceanic flight control were set up in Iceland [26], Canada, Spain and Portugal [1]. The European community set up a project called “ADS Europe” which involves organizations from the UK, France and the Netherlands as well as four commercial airlines: Air France, British Airways, KLM and Lufthansa [48]. ADS engineering trials were also conducted over the pacific ocean region, involving the FAA, Japan and Australia [39].

In 1995 ADS entered into operational service in the South Pacific region. The driving force behind this implementation was the user requirement to shorten the flight time between the United States to Australia and New Zealand using flexible routing [48]. Starting in 1998 over the Atlantic, aircraft position reports derived from GPS navigation data will begin to be sent automatically to the appropriate Oceanic ATC facility via a communication satellite [49].

- *ADS-B:*

Various implementations of ADS-B have been proposed and tested. The two options under most intense investigation are ADS Mode-S [9-13], being actively tested in the United States by MIT’s Lincoln Laboratory, and the GNSS Transponder [5-8] being tested in Sweden. The message format and reporting rate of these two options are described in Appendix A. This appendix also provides the latest message format

definition as suggested by the Radio Technical Commission for Aviation (RTCA) Special Committee 186.

The research on ADS-B and the associated terrestrial data link is not so developed as the research on the satellite-based ADS concept. This dissertation is devoted therefore to a study of the ADS-B concept and its possible effect on air traffic control.

Chapter 3

Communication Protocols

3.1 Introduction

The key issue in the design of ADS-B is a communication architecture that will allow up to several hundred aircraft within reception range to broadcast their position at a required rate, with an acceptable level of mutual interference, so that an airborne receiver or a ground-based controller would be able to receive these position reports with adequate reliability [50].

The communication architectures considered in this work are based on sharing a single frequency channel among all aircraft, using Time Division Multiple Access (TDMA) protocols. Other multiple access forms, such as Frequency Division Multiple Access (FDMA) or Code Division Multiple Access (CDMA) can achieve similar or somewhat better performance over pure TDMA, at the cost of increased transceiver complexity and/or increased spectrum use. For example, FDMA requires simultaneous processing of each subchannel in addition to transmission frequency agility [19]. The narrower bandwidth allocations associated with FDMA would also require significantly more stable reference frequency oscillators and enhanced selectivity in order to offer equivalent performance gain [51].

In addition, using a TDMA-based architecture would maximize the utilization of the existing communication infrastructure, since both the ground and airborne operational environments are currently more suited to support a TDMA approach over other multiple

access forms [51]. It seems therefore that the selection of a TDMA-based architecture would minimize the incremental cost of an ADS-B unit relative to the purchase of a GPS receiver alone. This will make ADS-B affordable also to the general aviation community. Hence, this chapter is devoted to an analysis of TDMA protocols for ADS-B.

The communication schemes suggested so far can be divided into three groups, according to the level of required synchronization between the aircraft. At the lowest level, no synchronization is required, and aircraft are allowed to transmit whenever they wish. The next level of synchronization is achieved by dividing the time axis into slots, and allowing each aircraft to transmit at slot beginning only, where transmission slots are selected at random.

In section 2 of this chapter we derive analytical expressions for the probability of clear reception under these two protocols. The expressions are validated by using a Monte Carlo simulation of random air traffic, and are used in section 3 to obtain the average throughput and capacity of the channel.

The highest level of synchronization between the aircraft can be achieved by assigning specific time slots to specific aircraft such that no transmission conflicts occur. Several methods for autonomous (self-organized) time slot selection are examined in section 4, using the Monte Carlo simulation described in Appendix G. The general analysis detailed in sections 2–4 is finally applied in section 5 to a comparison of several specific communication alternatives.

3.2 Probability of Clear Reception

Consider M aircraft, uniformly distributed over large area A . All aircraft generate short messages periodically, once every t_f seconds. Each message is t_m seconds long. An aircraft can receive messages sent by other aircraft, only if they are within its detection range R . The detection range is identical for all aircraft.

We assume that whenever two or more messages overlap at some receiver, all are lost and can not be received correctly by this receiver. We further assume that the channel is

noiseless, such that errors caused by random noise are neglected in comparison with errors caused by messages overlap. The only activity in the channel is due to the periodical reports generated by the aircraft. We consider two random access protocols:

- **Random reporting**, where aircraft select a random transmission time between 0 and t_f .
- **Random slot selection**, where the time axis is divided into slots, which are organized into frames t_f seconds long. Aircraft select at random one transmission slot each frame, and send their message at slot beginning. It is assumed that a global, accurate time base is available to all aircraft. When using GPS, this is an integral part of the navigation solution.

In order to get the channel capacity, we are interested in the average probability of clear reception, which is the probability of receiving a message correctly from any aircraft within range.

3.2.1 Exact Expression

In Appendix B we derive an exact expression for the average probability of clear reception under both of these random access protocols. It is given by:

$$P_r = (1 - \frac{P_d}{s})(1 - \frac{\pi R^2 P_o}{A s})^{M-2} \quad (3.1)$$

where P_d is the probability of direct transmitter-receiver interference, and P_o is the probability of message overlap inside a time slot. Both P_d and P_o are equal to 1 in a random channel, and depend on the ratio t_m/t_d in a slotted channel:

$$P_d = \begin{cases} 1 & t_m \geq t_d \\ (t_m/t_d)^2 & t_m < t_d \end{cases} \quad (3.2)$$

$$P_o = \begin{cases} 1 & t_m \geq t_d \\ \frac{1}{3}(t_m/t_d)^4 - 2(t_m/t_d)^2 + \frac{8}{3}(t_m/t_d) & t_m < t_d \end{cases} \quad (3.3)$$

where t_m is the message length, and t_d is the propagation delay guard band. The guard band is sized according to the maximum expected propagation delay, determined by the detection range R :

$$t_d = R/c \quad (3.4)$$

where c is the speed of light. The slot size is therefore $t_s = t_m + t_d$ and the number of slots in a frame is:

$$s = \begin{cases} t_f/2t_m & \text{Random channel} \\ t_f/(t_m + t_d) & \text{Slotted channel} \end{cases} \quad (3.5)$$

The slots in a random channel are introduced here for notation purposes only.

The first term in equation 3.1 is the probability that the receiver itself is not transmitting when a message arrives. The second term is the probability that all aircraft beside the receiver and the transmitter are either out of range, or that their messages do not overlap with the message sent by the transmitter. Note that this expression for the probability of clear reception differs from the common exponential expression used in previous works on ADS data link [11, 19, 10]. The exponential expression assumes an infinite aircraft population, and is further discussed below.

In the following example (and throughout this chapter) we assume a 250-bit message. For comparison, the current format suggested for ADS-B is based on two 112-bit reports, and the system suggested by the Swedish Civil Aviation Administration uses a 256-bit message (see Appendix A for more details.)

Figure 3.1 depicts the average probability of clear reception in a random channel and a slotted channel as a function of the detection range, based on the exact expression described above. The points marked along the curves were obtained by using a Monte Carlo simulation of random air traffic. We obtained excellent agreement between the analytical expressions and the simulation results, for many different combinations of the channel parameters. The dotted lines in this figure represent the exponential approximation of the average probability, to be derived next.

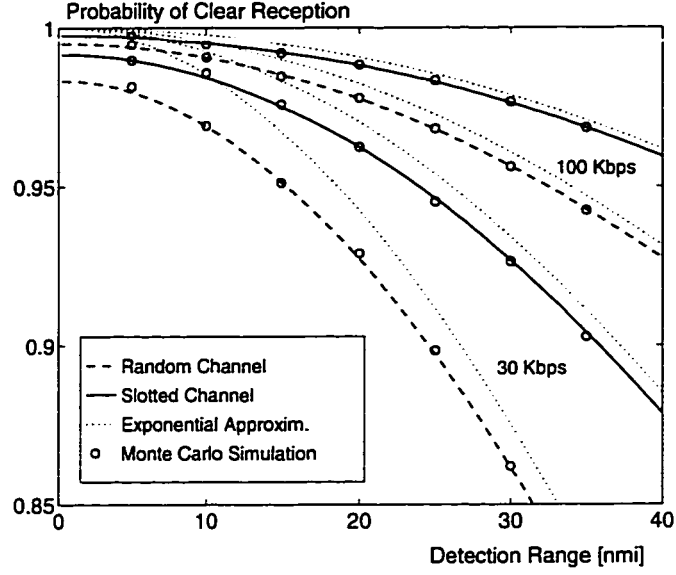


Figure 3.1: **Probability of Clear Reception vs. Range**

Shown for bit rates of 30 & 100 Kbps. We assume 200 aircraft inside a 150-nmi radius circle. Each aircraft transmits a 250-bit message, once per second. For this set of parameters, the probability of clear reception in a slotted channel is always higher than the probability in a random channel.

3.2.2 Exponential Approximation

When the message length is very small compared to the frame length ($t_m \ll t_f$), we can neglect the probability of direct transmitter-receiver interference. If we further assume an infinite large population of aircraft, we can approximate the average probability of clear reception in both random and slotted channels, as

$$P_r = \exp\left(-N \frac{P_o}{s}\right) \quad (3.6)$$

where N is the average number of aircraft in the detection range, P_o is the probability of message overlap inside a time slot given by equation 3.3, and s is the number of slots in a frame, given by equation 3.5.

This expression for P_r can also be derived by describing the messages arrival time as a Poisson process. In that case the probability of receiving n messages during a time

period t is:

$$P[n] = \frac{(\lambda t)^n}{n!} \exp(-\lambda t)$$

where $\lambda = N/t_f$ is the average number of received messages per second. In a random channel, the length of the vulnerable period is $2t_m$ (see Appendix B), and the probability that no messages arrive during this period is

$$P[n = 0] = \exp\left(-\frac{N}{t_f} 2t_m\right) = \exp\left(-\frac{N}{s}\right)$$

where the frame length t_f was divided into s virtual slots, each with duration equal to twice the message duration.

In a slotted channel, when $t_m \geq t_d$, the vulnerable period for each message is equal to the slot length, and the probability that no messages arrive during this period is

$$\exp[-\lambda(t_m + t_d)] = \exp\left(-\frac{N}{s}\right)$$

When $t_m < t_d$, the average vulnerable period is smaller than the slot length. The reduction factor is P_o , and the probability of no conflict during this time is

$$\exp[-\lambda(t_m + t_d)P_o] = \exp\left(-N \frac{P_o}{s}\right)$$

Figure 3.1 shows the exponential approximation for the average probability of clear reception, together with the exact values. As the bit rate becomes higher, the message length becomes shorter relatively to the fixed frame length, and the exponential approximation is better. The approximation is also better when the detection range is larger and the average number of aircraft in range is higher. In that case the description of the received messages as a Poisson process is more accurate.

The exponential expression is commonly used in the analysis of communication systems [52, 53] due to its analytical simplicity. In the next section we use it to derive the capacity of the communication channel.

3.3 Channel Capacity

3.3.1 Capacity as the Maximal Throughput

The channel throughput is the average number of messages received correctly by any aircraft during one frame:

$$N_r = NP_r \approx N \exp\left(-N \frac{P_o}{s}\right) \quad (3.7)$$

The channel capacity is usually defined as the maximum value of the throughput [53]. It is obtained for $N = s/P_o$, and is equal to:

$$C = \max(N_r) = \frac{s}{eP_o} \quad (3.8)$$

In a random channel, $s = t_f/2t_m$ and $P_o = 1$. The capacity is:

$$C_{\text{random}} = \frac{t_f}{2t_me}$$

In a slotted channel, the number of slots is $s = t_f/(t_m + t_d)$. If $t_m \geq t_d$, $P_o = 1$, and:

$$C_{\text{slotted}} = \frac{t_f}{(t_m + t_d)e}$$

It is clear that $C_{\text{slotted}} > C_{\text{random}}$ in this case. When $t_m \gg t_d$, we get the well known result that the capacity of a slotted channel is twice as large as the capacity of a random channel [52, 53]. This is the case in most computer networks, where the propagation delay is very small compared to the packet transmission time.

When $t_m = t_d$ the capacity of both channels is equal. When $t_m < t_d$, C_{slotted} is always smaller than C_{random} . In terms of range, the capacity of a slotted channel is smaller than that of a random channel, for any detection range R which is greater than ct_m .

Figure 3.2 depicts the average probability of clear reception as a function of N , the average number of aircraft in range, for various values of the propagation delay t_d . In this case the message is 250 bits long, and the bit rate is 100 Kbps. The message length is $t_m = 2.5$ msec. As expected, the clear reception probability in a slotted channel is higher than that of a random channel only when $t_m > t_d$.

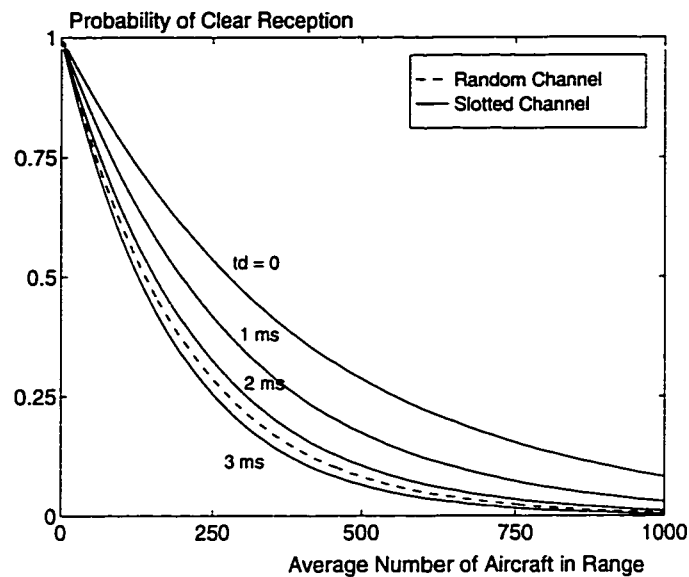


Figure 3.2: Probability of Clear Reception vs. Aircraft Number

Using a 250 bit message at 100 Kbps bit rate and 1 second update interval. t_d is the propagation delay guard band.

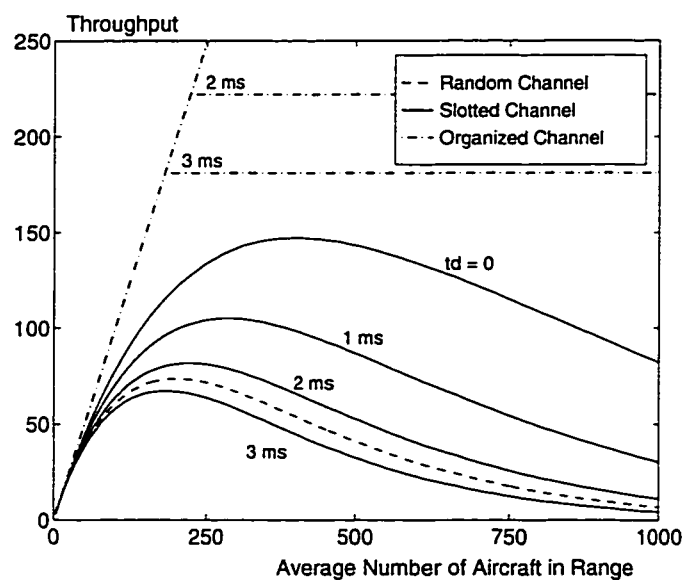


Figure 3.3: Channel Throughput

Using a 250 bit message at 100 Kbps bit rate and 1 second update interval. t_d is the propagation delay guard band. The throughput in the organized channel is equal to the number of aircraft, bounded by the number of slots in a frame.

The channel throughput, which is the average number of messages received correctly during one frame is depicted in figure 3.3 as a function of N . The channel capacity, which is the maximum value of the throughput, is depicted in figure 3.4 as a function of both the propagation delay t_d and the detection range $R = ct_d$.

The capacity of a slotted channel starts at a value which is twice as large as the capacity of a random channel. As the propagation delay gets higher, the slot size increases and the number of available time slots in a fixed size frame gets smaller. This reduces the capacity of a slotted channel, but does not affect the random channel.

When the propagation delay is equal to the message length, the capacity of both channels is equal. This occurs when $R = ct_m$, in this case 405 nmi. At any range greater than 405 nmi, the capacity of a random channel is higher than the slotted channel.

A higher bit rate of 1Mbps decreases the message length to 0.25 msec. In this case, shown in figure 3.5, a slotted channel has higher capacity only up to a range of 40.5 nmi. Note however the capacity scale change between figures 3.4 and 3.5.

3.3.2 Organized Channel

The capacity of a slotted channel can be increased by using a protocol which assigns specific time slots to specific aircraft, such that no transmission conflicts occur. In case of perfect assignment, the average number of messages received correctly during a frame should be equal to the average number of aircraft in range, bounded by the number of time slots in a frame. This is demonstrated in figure 3.3.

The upper bound for the capacity of a slotted channel is equal therefore to the number of time slots in a frame. Figures 3.4 and 3.5 show the capacity of a perfectly organized channel as a function of the propagation delay. The large capacity improvement that can be achieved in short range by using an organized protocol is evident from these figures. Note however, that in the case of a self-organized protocol, the message length should be increased in order to include the information required for the channel organization. This will decrease the number of available time slots, and the actual capacity would be lower than the upper bound shown in figures 3.4 and 3.5. This is further studied in section 3.5.

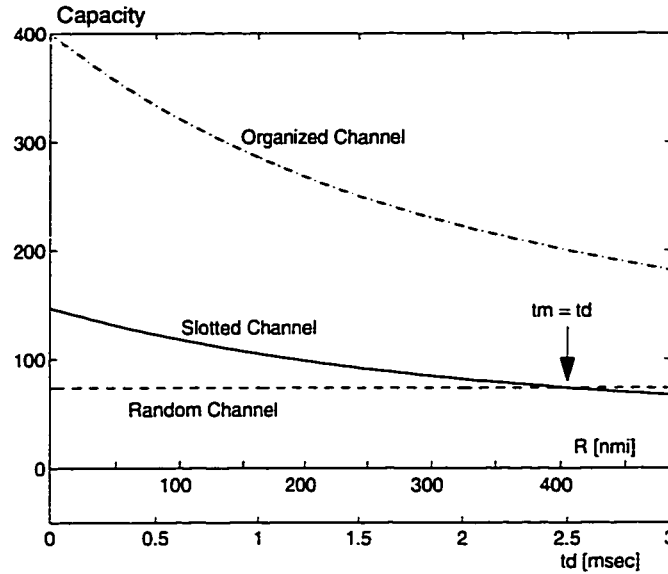


Figure 3.4: Channel Capacity - 100 Kbps

Using a 250 bit message and 1 second update interval. t_m is the message length, t_d is the propagation delay guard band and R is the detection range. Organized channel capacity is equal to the number of slots in a frame.

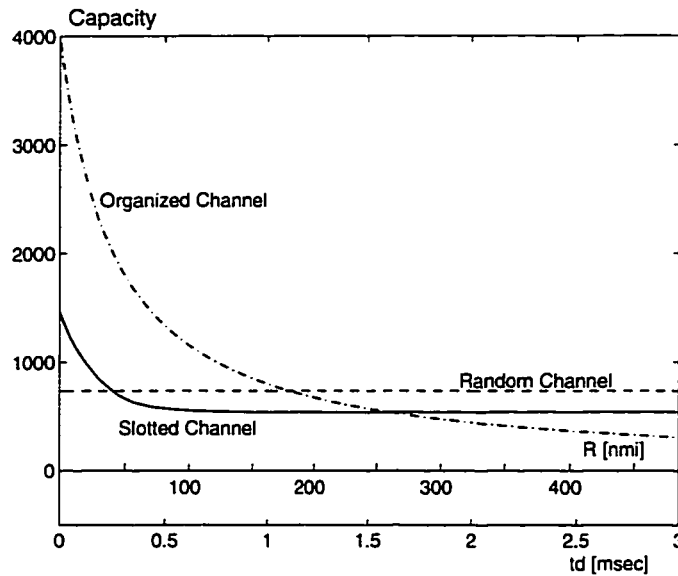


Figure 3.5: Channel Capacity - 1 Mbps

Using a 250 bit message and 1 second update interval. t_d is the propagation delay guard band and R is the detection range. Organized channel capacity is equal to the number of slots in a frame.

3.3.3 Capacity for a Given Reliability Level

The channel capacity during a required frame length can be increased by dividing the frame into several sub frames, and repeating the message each sub frame. This increases the probability that at least one message will be received during the required frame length. The probability that at least one out of n transmissions is received correctly, is:

$$P_n = 1 - (1 - P_r)^n \quad (3.9)$$

where P_r is the average probability of clear reception in a random or slotted channel. We can define another measure of the channel capacity, as the maximum number of aircraft in range that the protocol can handle, such that P_n is greater than or equal to a given reliability level [10]. Taking P_r from equation 3.6 and solving (3.9) for N , we get:

$$N = -\frac{s}{P_o} \ln[1 - (1 - P_n)^{1/n}] \quad (3.10)$$

First, we note that N can be expressed as $N = K_n C$, where $C = s/eP_o$ is the channel capacity obtained previously and K_n is a constant factor. Since K_n depends only on the given reliability level P_n and the number of transmission attempts, the relations between C_{slotted} and C_{random} previously described hold also for this measure of capacity.

Next, we consider a required frame length t_r , divided into n sub frames. The sub frame length is $t_f = t_r/n$, and the number of slots in a sub frame is $s = t_f/t_s$. The channel capacity is:

$$N = -\frac{t_r}{P_o t_s} \left\{ \frac{1}{n} \ln[1 - (1 - P_n)^{1/n}] \right\} \quad (3.11)$$

The number of sub frames n that maximizes this expression is clearly a function of P_n only. For example, when $P_n = 0.995$, we get $n = 8$. Figure 3.6 shows the number of aircraft in range such that the probability of clear reception is greater than or equal to 99.5%. The required frame length is 5 seconds, and the message is repeated 1,2,4 and 8 times in the 5 seconds period. Note that the point where the capacity of a slotted channel is equal to the capacity of a random channel is the same for all n , and would be the same for any reliability level P_n . The uppermost line in this figure represents an organized channel. The capacity

in this case is given by the number of slots in a 5 second period and it represents the upper bound for the performance of a slotted protocol.

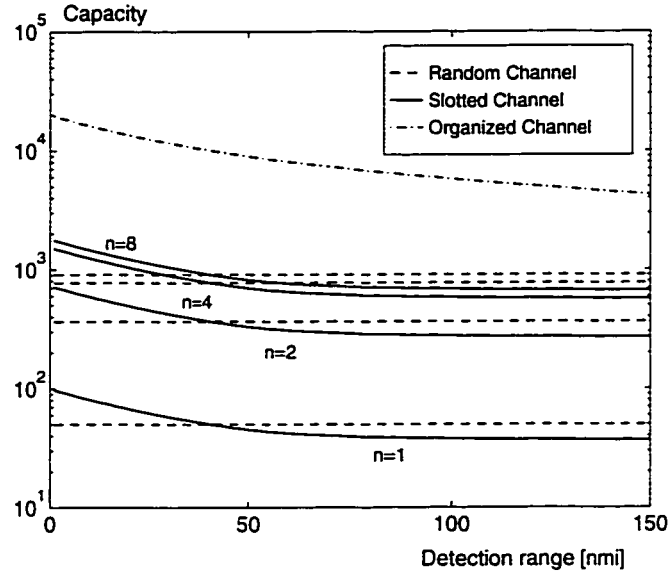


Figure 3.6: Capacity for Multiple Transmission Attempts

This figure shows the channel capacity for n transmission attempts in a 5 seconds frame. The capacity here is the maximum number of aircraft in range such that the probability of receiving at least one of the n messages is greater than 99.5% (using 250 bit message, 1 Mbps bit rate.)

Finally, equation (3.9) can also be solved for n , yielding

$$n = \log(1 - P_n) / \log(1 - P_r) \quad (3.12)$$

By fixing the number of aircraft per unit area, we can get the effective update rate as a function of the detection range. The effective update rate, shown in figure 3.7, indicates how often an aircraft can receive a message, with a probability that is higher than the given reliability level. Thus for example, consider the case where a 250-bit message is sent at random once every 0.5 seconds, and the traffic density is 0.1 aircraft per square nmi. If the detection range is less than 20 nmi, the message can be received every second with probability higher than 99.5%. However, if the detection range is 50 nmi, the effective update rate is smaller, and the message can be received only every 5 seconds with the

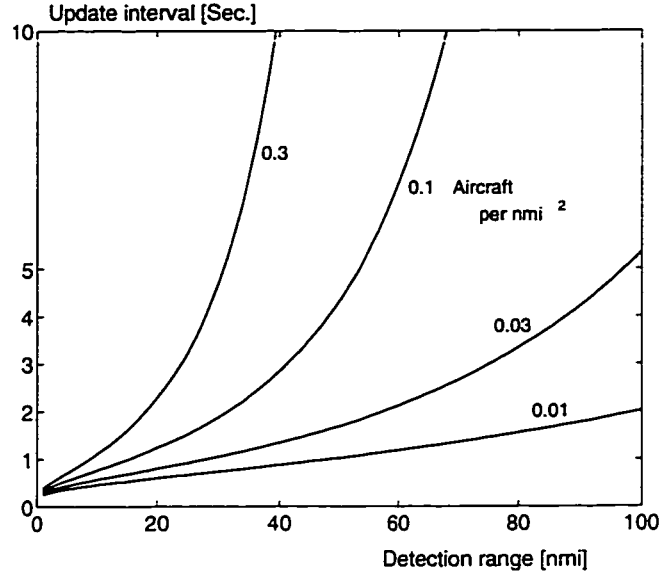


Figure 3.7: **Effective Update Rate**

This figure indicates how often an aircraft can receive a message with probability higher than 99.5%, given a random protocol with 0.5 second update interval (using 250 bit message, 1 Mbps bit rate.) See Appendix C for information on the interpretation of aircraft traffic density figures.

same reliability level. Additional information on the correct interpretation of aircraft traffic density figures is given in Appendix C.

3.4 Capture Effects

The previous analysis was based on the pessimistic assumption that whenever several messages overlap at the receiver, all are lost. This assumption provides a lower bound to the performance of real broadcast channels, since many receivers can correctly receive the strongest of several interfering signals, if the received power of the next to strongest is down by several dB. This phenomenon is referred to as capture [54, 53]. In mobile radio systems it is referred to as the co-channel interference characteristic [15]. Generally, it is a function of the modulation and coding technique used for transmission. However, in this work we look only at the channel capacity which is not affected significantly by the use of coding or the change of packet lengths [55].

In Appendix B we derive the average probability of clear reception under capture conditions, by assuming that an aircraft will correctly receive a message from another aircraft at distance r , if it does not overlap with any of the messages sent by aircraft within distance αr , where α is related to the capture ratio:

$$CR = 20 \log \alpha \quad \alpha \geq 1 \quad (3.13)$$

The probability of clear reception in that case is:

$$P_r = \frac{\beta}{N/s} + (1 - \beta - \frac{\beta}{N/s}) \exp(-\frac{N}{s}) \quad (3.14)$$

where $\beta \triangleq 1/\alpha^2$, N is the average number of aircraft within range, and s is the number of time slots in a frame (Eq. 3.5). The channel throughput NP_r is the average number of messages received correctly during a frame. The channel capacity, defined as the maximum value of the throughput, is obtained for

$$\frac{N}{s} = \frac{1}{1 - \beta}$$

and can be expressed as $C_{CR} = K_{CR}C$, where C is the capacity calculated previously for “no capture”, and K_{CR} is a constant factor which depends only on the capture ratio:

$$K_{CR} = e[\beta + (1 - \beta) \exp(\frac{1}{\beta - 1})]$$

K_{CR} is depicted in figure 3.8 as function of the capture ratio. It is equal to one for “no capture” ($\beta = 0$), and is greater than one for any other value of the capture ratio. For example, a capture ratio of 6dB will increase the capacity of both a random and a slotted channel by $K_{CR} = 1.218$. The ratio between the capacity of the two channels is not changed, since both values are multiplied by the same factor. Note however, that the maximum capacity obtained by using an organized channel is not affected by the capture ratio, and remains an upper bound on the performance of a slotted protocol.

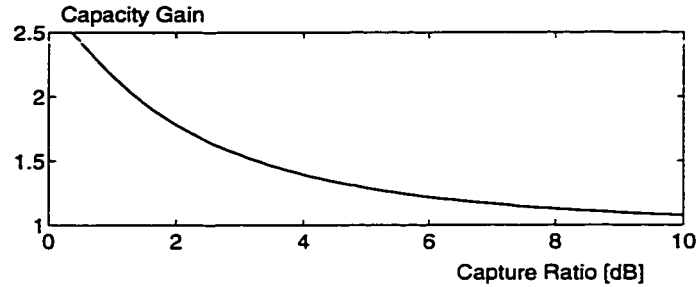


Figure 3.8: Capacity Gain due to Capture

3.5 Conflict Resolution and Self Organization

In the previous sections we looked at the probability of transmission conflicts and their effect on the channel capacity. In this section we analyze several methods for resolving or preventing these conflicts. It is clear that solving at least part of the conflicts can yield a higher channel capacity, and we might get closer to the upper boundary on the capacity of a slotted channel.

If all aircraft in some region are in direct contact with a central controller, conflict resolution can be achieved by polling or by any other multiple access protocol that uses global knowledge. However, for ADS-B to be available in remote areas (beyond line-of-sight of any ATC control facility), and to retain easy access to the airspace for General Aviation pilots, the candidate network designs should not depend upon central control or management. We wish therefore to examine communication protocols that would enable all aircraft to operate autonomously, and to resolve conflicts without relying on a ground facility for coordination.

We will start with the basic requirements for a conflict-free channel, and then analyze several self-organized communication protocols, using a Monte Carlo simulation of random air traffic.

3.5.1 Basic Requirements

We wish to construct a protocol for conflict-free access to the communication channel, based on time slot assignment. The slot assignment should be executed in a completely distributed manner, i.e., no central information or centralized control is assumed. This can be accomplished by exchanging connectivity information between neighboring aircraft. The term *neighbor* is defined as follows:

1. P is a *neighbor* of Q if P is within the detection range of Q .
2. P is a *2-neighbor* (read: second neighbor) of Q , if P is a neighbor of some neighbor of Q .

To eliminate transmission conflicts, the following two conditions [56, 57] must hold for every aircraft P :

1. All neighbors of P do not transmit at the same slot as P . (An aircraft can not send and receive simultaneously.)
2. Every two neighbors of P transmit at a different slot. (An aircraft can not receive simultaneously two transmissions.)

These two conditions provide “conflict free” communication. Violation of condition 1 causes a direct conflict, where two neighbors interfere with each other. Violation of condition 2 might cause an indirect conflict, where messages of two non-neighboring aircraft interfere at a third aircraft, which is a common neighbor to both of them.

These conditions imply that every aircraft needs a time slot that is different from any of its neighbors and 2-neighbors. When aircraft are uniformly distributed on a plane, the average number of neighbors and 2-neighbors is bounded by the average number of aircraft inside a $2R$ radius circle

$$N_2 = 4\pi R^2 \sigma \quad (3.15)$$

where R is the detection range and σ is the average number of aircraft per unit area. The number of available time slots should therefore be equal at least to N_2 , in order to allow

for self organization of the aircraft into a conflict-free channel. By using the definitions of a slotted channel parameters we can solve for the minimum bit rate requirement:

$$B = \frac{n_m}{t_f/N_2 - R/c} \quad (3.16)$$

where n_m is the number of bits in a message, and t_f is the frame length.

Figure 3.9 describes the required bit rate as a function of the detection range, for several values of aircraft traffic density. If the detection range is 10 nmi, and the bit rate in the channel is 10 Kbps, an organized protocol could work up to a traffic density of 0.03 aircraft per squared nmi. If the traffic density is higher, we need to increase the bit rate or the frame length, in order to create more time slots.

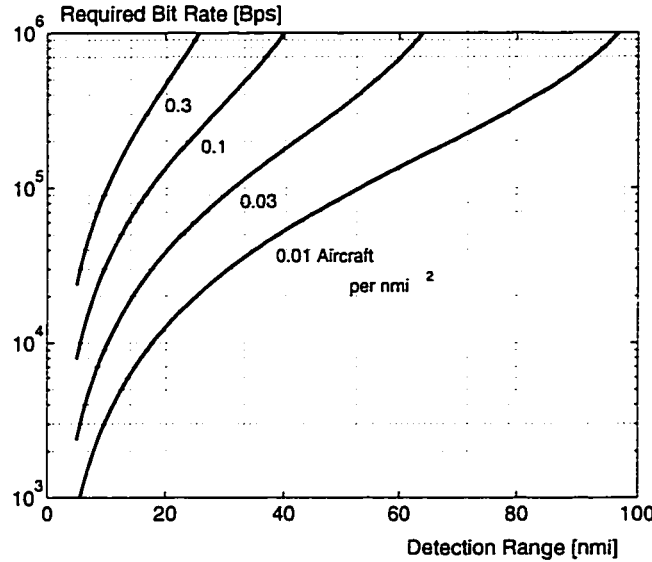


Figure 3.9: Minimum Bit Rate for an Organized Channel

Requirement for a self organized channel, in Bits per second (assuming 250 bit message, 1 second update interval.)

In the following subsections we examine several communication protocols that attempt to resolve at least part of the transmission conflicts in the channel. Since mathematical analysis of these protocols in arbitrary topologies is not feasible [57], we conduct our investigation by using a detailed simulation of random air traffic.

3.5.2 Perfect Self-Organization

We saw that each aircraft needs a time slot that is different from any of its neighbors and 2-neighbors. This can be accomplished in a distributed manner if each aircraft will include in its message the slots assignments of all neighbors, in addition to its own slot assignment and position report [58, 59]. Another possibility is to transmit the identities of all neighbors [60], in addition to own identity and position report. In this way each aircraft becomes aware of the slot assignments or identities of all its neighbors and their neighbors. If all aircraft use the same algorithm for selecting a time slot based on this information, a conflict free access to the channel can be guaranteed. The outline of an algorithm which uses the aircraft identities can be given as follows [56]:

Use the current time slot if your identity number is highest among all neighbors and 2-neighbors who did not transmit yet in the current frame.

This communication protocol provides each aircraft with a time slot in each frame, in which it is guaranteed that its message will be correctly received by all its neighbors.

The cost of this conflict free communication is the large amount of information that should be transmitted by each aircraft. If an aircraft identity is 24-bit long, then 10 neighbors would almost double the 250-bit position report. This problem can be solved by transmitting the connectivity information at a much lower update rate than the position reports, or by using a different control or coordination channel for the transmission of this information. Note that the coordination channel is subject to the same difficulties in scheduling the transmissions [61].

This protocol is expected to perform perfectly up to the point where the average number of neighbors and 2-neighbors is larger than the number of time slots. As stated earlier, this is a basic limitation of any self organized protocol. When this happens, a modification of the algorithm can extend the frame length as required, and generate local update rates to accommodate any traffic density [62].

3.5.3 Negative Acknowledgments

Assume that aircraft can distinguish between a garbled (multiple usage) time slot and the background noise in the channel. In that case, we can construct a communication protocol where each aircraft is required to transmit a list of time slots that were detected as garbled in the previous frame. An aircraft that finds its own time slot in one of the lists transmitted by its neighbors, will then change its time slot selection to another unoccupied slot. This is a form of “negative acknowledgment” [63] for a broadcast channel, proposed by Jones [19] for the ADS-B data link.

Under certain conditions, the list of garbled time slots is the minimum amount of information that can be exchanged between the aircraft. However, it does not contain all the information required for conflict-free communication. We can identify two mechanisms that will create transmission conflicts in this protocol :

1. Two neighboring aircraft share the same time slot, and have no common neighbor to identify the conflict.
2. An aircraft selects a new time slot which is occupied by a 2-neighbor.

The first type of conflict will occur at low traffic density areas, and when the detection range is small. A possible solution is that aircraft in low density areas would switch time slots in a random fashion, or listen periodically at their own time slot. These options are further studied below.

The second type of conflict should be resolved within one frame. However, when the number of available time slots is close to the average number of neighbors and 2-neighbors, any new selection is likely to be occupied by some 2-neighbor, and the conflict can not be resolved.

Figure 3.10 shows the probability of clear reception as obtained by a Monte Carlo simulation, using the communication protocol described above. The labels attached to the curves denote the number of aircraft inside a circular area with 150-nmi radius. As the number of aircraft gets lower, the probability of clear reception for short detection range

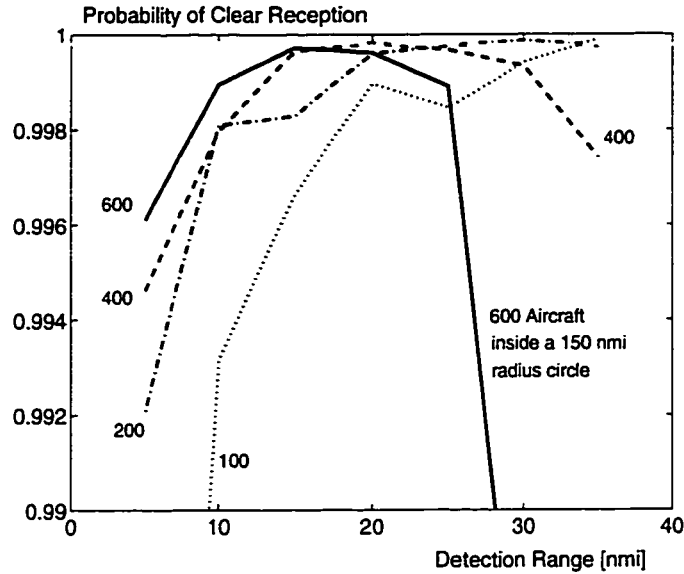


Figure 3.10: **Negative Acknowledgments**

Probability of clear reception for 30 Kbps bit rate, 250 bit message, 1 second update interval. The highest number of aircraft (600) represents a traffic density of about 0.01 aircraft per square nmi.

gets smaller, due to the first type of conflict described above. On the other hand, when the detection range is large, the probability of clear reception drops down as the number of aircraft grows. This is due to the second type of conflict.

When the number of aircraft in the playing area is 600, the probability of clear reception drops below 0.99 at a detection range of 30 nmi. Referring back to the required bit rate analysis (figure 3.9), we can see that this was expected at these values (30 Kbps, $\sigma = 0.01$ aircraft per square nmi).

The basic assumption that an aircraft can distinguish between a garbled slot and a free one is problematic [64]. Usually, message interference is hard to distinguish from the noise that is always present in the channel, and a communication protocol which does not rely on the ability to detect multiple-usage slots is likely to be more reliable [61].

3.5.4 Self Adapting TDMA

Self adapting TDMA is a communication scheme suggested by A. Beining [14], as part of a general concept called Automatic Position Advisory System (APAS). In this scheme, no additional information beside the position reports is exchanged between the aircraft. Instead, each aircraft monitors its currently selected time slot by periodically, at random intervals, listening only instead of transmitting. If another message is received in the currently selected time slot, the aircraft selects another unoccupied time slot. In addition, each aircraft is required to transmit its message in any time slot that was detected as garbled in the previous frame.

The first part of this protocol can solve direct conflicts, where two neighboring aircraft use the same time slot. It can not, however, solve indirect conflicts. These should be handled by the second part of the protocol.

We have checked the effect of the first part in a simulation of random air traffic. The upper curve in figure 3.11 shows the probability of clear reception in a slotted channel where time slots are changed according to the algorithm described above. Each aircraft in the simulation selects a random number of transmission frames that should pass before a silent frame. This number is uniformly distributed between 5 and 10, and is reselected after the silent frame.

The increase in the probability of clear reception over a slotted channel is evident, but it is still much lower than the probability that could be obtained by exchanging information between the aircraft. Note that part of the increase in the probability is due to the fact that at any given frame, a large fraction of the aircraft population is not transmitting. This reduces the number of transmission conflicts, but also reduces the effective update rate.

3.5.5 Random Switching

Another way to resolve part of the transmission conflicts without adding information to the transmitted message, is to continuously change the time slot being used, and select another unoccupied slot. This technique is used in Sweden's GNSS Transponder system [5], when

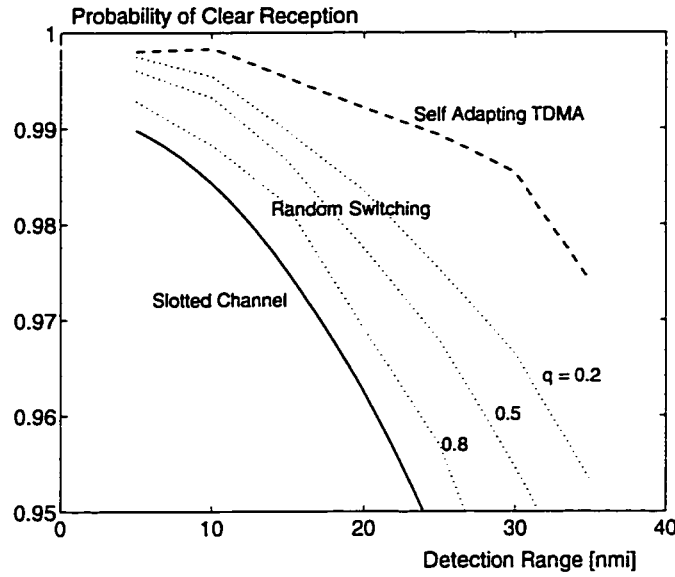


Figure 3.11: Self Adapting TDMA and Random Switching

Probability of clear reception for 200 aircraft in a 150 nmi radius circle (traffic density is about 0.003 aircraft per square nmi), assuming 250 bit message at 30 Kbps bit rate, and 1 second update interval. The probability in a slotted channel is based on equation 3.1.

aircraft are out of range of ground stations.

In our simulation check, aircraft decide before each frame whether to change their selected time slot with probability q . Figure 3.11 shows the probability of clear reception as a function of the detection range, for several values of q . It seems that careful selection of this parameter can improve the channel capacity. However, the probability of clear reception is still lower than the probability achieved by using the protocols described previously.

3.6 Design Alternatives

This section provides a brief description of the major design candidates for the ADS-B data link, and compares their maximum capacities. The various alternatives are:

- **ADS Mode-S (GPS Squitter)**

Proposed by MIT's Lincoln Laboratory [9-13], this approach is based on using a modified Mode-S transponder to broadcast aircraft identity and position at the existing SSR downlink frequency (1090 MHz). Since this channel is already used for the SSR replies, it is impossible to coordinate the aircraft position reports and a random reporting protocol must be used. The main advantage of this approach is the high bandwidth (1 Mbps) associated with the Mode-S downlink frequency.

- **GNSS transponder**

A system designed and tested by the Swedish Civil Aviation Administration [5-8] uses a dedicated 25 KHz bandwidth VHF channel, with only 9600 bps. Time slots for transmission are assigned by the ATC ground system, or selected autonomously when aircraft are out of range of ground stations. In this case the communication protocol is a Self organized TDMA, based on randomly changing the time slot selection to an unoccupied time slot. This future time slot is reserved by adding its address to the aircraft position report.

- **Automatic Position Advisory System**

A technique proposed by A. Beining [14] and studied at Hughes Aircraft is based on using modified Mode-S transponders in a similar way to ADS Mode-S. However, the protocol used is a self-adapting TDMA protocol, as described in section 3.5.4. This approach is based on the assumption that the current communication traffic in the Mode-S frequency will be eliminated upon the introduction of ADS-B.

- **GNSS Augmentation Data Link**

Moody and Peed [15, 16] propose to use an unassigned Tactical Air Navigation / Distance Measuring Equipment (TACAN/DME) half channel (967 MHz), with a signal structure derived from a European digital mobile telephone system known as Global System Mobile (GSM). The raw channel bit rate in this case is 270 Kbps, but selecting another signal structure could more fully utilize the 1 MHz bandwidth. This unused channel allows a slotted protocol, and it is proposed that users will select time slots on a random basis.

We now wish to compare the maximum capacity of these architectures on a common basis. We assume a 250 bit message and a required update interval of 5 seconds. In the VHF frequencies, the highest available bit rate is 30 Kbps. Selection of an unused channel allows the use of a self-organized protocol, optimized for maximum capacity. We assume that the organized protocol is perfect, such that no transmission conflicts occur.

The capacity of the organized channel is represented by the number of available time slots during the 5 second period. Note that this is an upper bound on the possible performance of the VHF channel, and the actual capacity of any self organized protocol would be lower than this value, as demonstrated in the previous section.

The Mode-S frequency option provides a high bit rate of 1 Mbps. However, the requirement for coexistence of the ADS reports with the random traffic currently in this channel, dictates the use of a random reporting protocol. We assume that the message is repeated 8 times in the 5 seconds frame. The channel capacity in this case is the maximum number of aircraft in range such that the probability of receiving correctly at least one of these 8 reports in a frame is greater than or equal to a reliability level of 99.5%.

As can be seen in figure 3.12, the capacity of a random channel at 1 Mbps is higher than the capacity of fully organized channel at 30 Kbps, for any realizable detection range. Also shown is the capacity of an organized channel at 1 Mbps. This represents the maximum possible performance of the TACAN/DME channel, or the Mode-S frequency when all the current traffic in this channel is phased out.

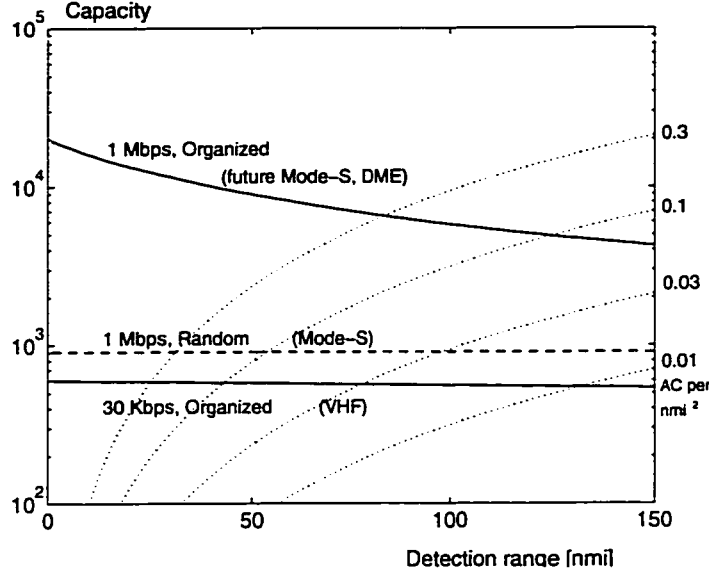


Figure 3.12: **Capacity of Design Alternatives**

Assuming 250 bit message and 5 seconds required update interval. The capacity in the organized protocol is equal to the number of slots in the 5 seconds frame. The capacity in the random protocol is based on 8 transmission attempts in the 5 second frame, and a reliability level of 99.5%. The dotted lines represent constant traffic density over a circle with a radius of the detection range. The density values are denoted on the right.

3.7 Conclusion

Using the channel capacity as a measure of performance, we have compared three groups of communication protocols for GPS-based air traffic control: a random scheme, where aircraft transmit whenever they wish; a slotted channel, where transmission is restricted to time slots selected randomly by the aircraft, and an organized protocol, where time slot selection is made such as to eliminate transmission conflicts.

It was shown that the capacity of a slotted channel is higher than the capacity of a random channel only for short detection range, where the message length is longer than the propagation delay guard band. The capacity can be increased by using self-organized protocols for conflict resolution. In this case the capacity is limited by the average number of neighbors. The selection of a specific self organized protocol involves a compromise between high capacity with large amounts of information exchanged between the aircraft, and lower

capacity without information exchange.

By evaluating the maximum possible capacity of specific design alternatives, we can conclude that a random protocol at the Mode-S frequency is a superior design to an organized protocol at the VHF frequency, due to the higher capacity at the higher frequency and the reduced complexity of the random protocol.

Chapter 4

Aircraft Tracking

4.1 Introduction

The tracking filter is a major element in any ATC surveillance system. Based on noisy position measurements, it provides smooth estimates of the aircraft position, velocity and heading. Most of the existing research on aircraft tracking and tracking filter design assume that the aircraft position is measured by radar [65-68]. Using an airborne GPS receiver as the position sensor requires a new design of the tracking filter, since the nature of the measurement errors in this case is very different from the nature of the current radar measurement errors.

In addition to the geometric difference between the two systems - radar accuracy depends on the distance from the radar, whereas GPS accuracy is uniform worldwide - we observe a much larger time constant in GPS position errors than the almost white radar measurement errors. An appropriate measurement error model should be identified and incorporated in the new tracking filter design. Other possible error sources should be identified and treated appropriately.

The objective of this chapter is therefore to design an aircraft tracking filter, which uses measurements provided by airborne GPS receivers. Through the tracking filter design process, we wish to identify and solve the major problems that might occur in GPS-based

aircraft tracking. We will then study the performance of the new tracking filter and compare its tracking accuracy with the performance of current ATC radar trackers.

We treat the GPS receiver as a standalone sensor, unaided by data from other sources or differential corrections. In that case the position measurement errors are governed by Selective Availability (SA). Note that these errors are different from pure ranging errors, and the work done on SA model identification [69] is not directly applicable in this case. An appropriate measurement error model is identified in section 2 of this chapter, by analyzing actual GPS data. The data is analyzed with special emphasis on the relationship between the position and velocity errors, since we would like to determine the possible benefits of including velocity information in the message transmitted by each aircraft.

The tracking filter should combine the measurement error model with a dynamic model for the aircraft motion. Section 3 provides a brief description of various aircraft models, and the tracking filter design is described in section 4. Section 5 compares the GPS tracking accuracy with the accuracy of ATC radar trackers, and section 6 concludes the chapter.

4.2 Error Model Identification

The first step in tracking filter design is identification of the error model. This was done by analyzing a data base composed of several five-hour-long recordings of GPS position and velocity errors. The recordings were made at a basic sampling rate of 1Hz, on different days, at different times of the day¹, using a static Trimble 4000-SSE receiver located at Stanford University. The receiver output is given as latitude, longitude, altitude and their rates of change. These values were transformed to position and velocity errors in a Local Level Local North (LLLN) coordinate system, using classical transformations [70] and the surveyed location of the antenna site.

¹The dates and start times of the four recordings described in table 4.1 are: 12-7-94 10:49 AM, 12-13-94 16:35 PM, 12-14-94 22:30 PM, 12-15-94 09:28 AM.

4.2.1 Data Analysis

Table 4.1 summarizes some of the statistical properties of four different recordings. The time constants shown in the table were estimated at the point where the autocorrelation function of the measurement error reaches $1/e$ of its value at zero lag.

		1	2	3	4
Avg. PDOP		2.38	2.34	2.23	2.64
Avg. No. Sat.		6.67	6.37	7.31	6.25
1 σ East position	[m]	19.55	16.32	17.55	15.75
1 σ North position	[m]	20.82	23.9	19.69	20.68
1 σ Up position	[m]	45.01	44.59	39.67	48.24
1 σ East velocity	[m/s]	0.19	0.16	0.17	0.17
1 σ North velocity	[m/s]	0.21	0.22	0.22	0.23
1 σ Up velocity	[m/s]	0.45	0.4	0.41	0.55
τ East position	[s]	147	139	137	119
τ North position	[s]	135	166	131	130
τ Up position	[s]	122	141	139	123
τ East velocity	[s]	80	76	77	80
τ North velocity	[s]	76	77	100	79
τ Up velocity	[s]	78	75	82	90

Table 4.1: Statistical Properties of the Data Base

Note that the standard deviation of the position error in the north-south coordinate is larger than the standard deviation of the position error in the east-west coordinate. As the latitude increases, this ratio can go up to a 22% larger RMS error in the north-south coordinate [71]. The same behavior was observed for the velocity errors.

The average time constant of the position error in the north-south direction is 139.7 seconds. This is smaller than the value usually associated with SA, which is 190 seconds [69, 72]. This indicates that SA models are not directly suitable to model the position errors. The average time constant of the velocity error is significantly large (83.1 sec). The velocity error is therefore not white as sometimes assumed [73], but rather correlated.

In order to identify the possible benefits of additional velocity reports, we are interested in a dynamic model that matches the autocorrelation of both position and velocity errors. This requires some analysis of the relationship between the two error components.

We compared between the velocity solution of the receiver and the velocity estimated by first difference of the position solution. The difference between the two values was smaller than 0.05 m/s for about 80% of the time. This is one of the indications that the velocity error can usually be treated as a derivative of the position error.

We have observed sharp transitions between periods of agreement and non-agreement of the two velocity values. The transitions were always associated with a satellite constellation change. Sudden steps in GPS error due to satellite set transitions can be a major error source in aircraft tracking [74], and we must pay special attention to these transitions when designing the tracking filter.

The transfer function between the position and velocity errors was estimated by computing the ratio between their power spectral densities. The results showed that we can consider the velocity error as a derivative of the position error and use one dynamic model for both errors.

The identification of the dynamic error model is based on estimating the sample autocorrelation function of the data in each coordinate, using [75]:

$$\phi_{xx}(kT) = \frac{1}{N-k-1} \sum_{i=1}^{N-k} (x_k - m)(x_{i+k} - m)^T$$

where m is the mean of the data

$$m = \frac{1}{N} \sum_{i=1}^N x_i$$

We then fit the estimated autocorrelation function with autocorrelation functions of known models.

4.2.2 Simple Gauss-Markov Processes

Simple Gauss-Markov processes can be described by the following transfer function:

$$x(s) = \frac{\beta^n}{(s + \beta)^n} w(s) \quad (4.1)$$

where $w(s)$ describes a zero mean white noise input $w(t)$, with spectral density Q , and n is the process order. For $n = 1$, $x(t)$ is an exponentially correlated signal. The rate of change of an exponentially correlated signal is white, whereas the experimental data clearly shows that the velocity error is correlated. This leads us to higher order models.

We derived the correlation functions of high order ($n = 2, 3, 4$) simple Gauss Markov processes (see Appendix D) and selected the time constant and the spectral density of the driving white noise to match the value of the experimental position autocorrelation at zero lag and at the $1/e$ point. This however does not guarantee that the *velocity* autocorrelation will match the experimental data, as shown in figure 4.1 for $n=2$ (the behavior of higher order simple processes is similar.) Matching both position and velocity autocorrelations, at both zero lag and $1/e$ points requires four free parameters, where simple Gauss Markov processes have only two (Q and β .) This leads to a general 3rd order process.

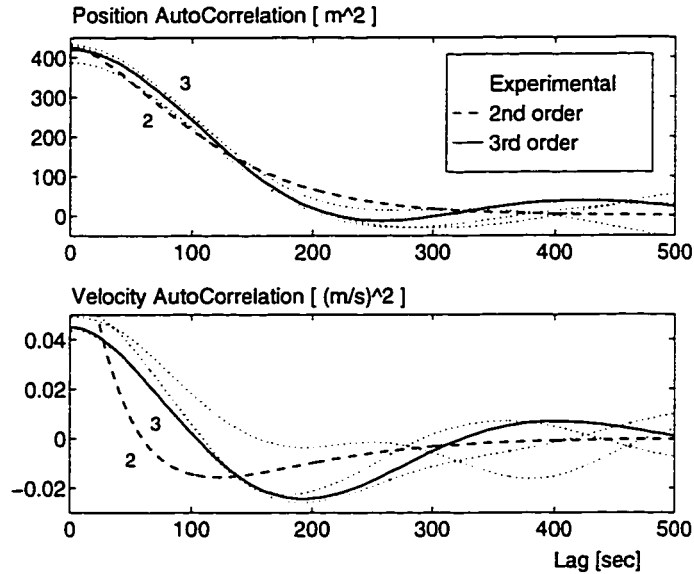


Figure 4.1: Autocorrelation Functions

The dotted lines are autocorrelations of three different five-hour-long recordings of GPS position and velocity errors. The dashed line shows the autocorrelations of a simple 2nd order GM process with $\beta=0.0165\text{sec}^{-1}$. The solid line describes a general 3rd order GM process with $a=0.0067\text{sec}^{-1}$, $\omega=0.01634\text{sec}^{-1}$ and $\zeta=0.3057$. In both cases Q is set such that $\sigma_x=20.6$ meters.

4.2.3 A General 3rd Order Gauss-Markov Process

A general 3rd order Gauss-Markov process can be described by the following transfer function:

$$x(s) = \frac{a\omega^2}{(s+a)(s^2 + 2\zeta\omega s + \omega^2)}w(s) \quad (4.2)$$

The correlation functions of this model are given in Appendix D. In this case we have four free parameters (a, ω, ζ and Q), and we can use them to match the experimental correlation functions of both position and velocity errors at the required time points. The results depicted in figure 4.1 show good agreement up to 300 seconds lag.

The measurement error model should be combined with a dynamic model for the aircraft motion. The next section proposes several such models.

4.3 Dynamic Aircraft Models

Civil aircraft have two basic modes of flight: uniform motion and maneuvering. The uniform motion mode can be described by a 2nd order kinematic (constant velocity) model:

$$\dot{x}(t) = v_x(t) \quad (4.3)$$

$$\dot{v}_x(t) = w_v(t) \quad (4.4)$$

where $w_v(t)$ is zero mean white noise with appropriate spectral density, which accounts for the small acceleration disturbances in this stage of flight. The same equations apply in the y direction. This model is the basis for the simple tracking filter that was used in ADS trials to track aircraft position reports [26]. Without a measurement error model, this filter simply interpolates the position between measurements, assuming constant velocity.

In order to account for the aircraft accelerations during maneuvers, the model order can be increased:

$$\dot{x}(t) = v_x(t) \quad (4.5)$$

$$\dot{v}_x(t) = a_x(t) \quad (4.6)$$

$$\dot{a}_x(t) = w_a(t) \quad (4.7)$$

where $w_a(t)$ is zero mean white noise, which accounts for acceleration increments ('jerks') during aircraft maneuvers. The aircraft acceleration is assumed to be nearly constant in this model.

A more accurate description of the kinematic behavior during a turn is given by the coordinated turn model, which assumes a constant turn rate at a constant speed:

$$\dot{x}(t) = V \cos \gamma(t) + w_x(t) \quad (4.8)$$

$$\dot{y}(t) = V \sin \gamma(t) + w_y(t) \quad (4.9)$$

$$\dot{\gamma}(t) = \omega + w_\gamma(t) \quad (4.10)$$

where γ is the aircraft heading, and ω is the turn rate. The various disturbances and modeling errors are accounted for by adding the appropriate noise terms [67]. The turn rate ω in this model can be set to a fixed, preselected value, or extracted from the estimated state vector. In that case the discrete time model is nonlinear in ω , and requires an Extended Kalman Filter.

More elaborate models may include the thrust and control surface settings of the aircraft in addition to its position and orientation [76]. These models usually involve Euler angle measurements [22, 23, 25, 77], and do not seem to be directly applicable in our case.

4.4 Tracking Filter Design

The tracking filter should combine a measurement error model with an aircraft model. The general problem of tracking filter design with correlated measurement noise is discussed first. We then select a simple aircraft model, combine it with several error models and compare the performance of the resulting tracking filters by using a Monte Carlo simulation. Based on this study we decide on a specific error model to be used in the tracking filter, and check its performance with several aircraft models.

4.4.1 Correlated Measurement Noise

The aircraft model and the measurement error model can be described by the following linear systems:

$$x(k+1) = \Phi x(k) + w(k), \quad w \sim N(0, W) \quad (4.11)$$

$$e(k+1) = \Psi e(k) + v(k), \quad v \sim N(0, V) \quad (4.12)$$

where x is the aircraft state vector, e is the state vector of the measurement error model, and w and v are independent, zero mean white noise vectors. The measurement vector z is a linear combination of x and e :

$$z(k) = Cx(k) + De(k) \quad (4.13)$$

The tracking filter should provide an optimal estimate of the aircraft state vector x . In order to use the Kalman Filter formulation, the dynamic model (Eqs. 4.11-4.13) should be expressed as a linear system with white process and measurement noise. This is usually achieved by augmenting the aircraft state vector with the error model state vector:

$$x_a = \begin{bmatrix} x \\ e \end{bmatrix}$$

The augmented state space system is:

$$\begin{bmatrix} x(k+1) \\ e(k+1) \end{bmatrix} = \begin{bmatrix} \Phi & 0 \\ 0 & \Psi \end{bmatrix} \begin{bmatrix} x(k) \\ e(k) \end{bmatrix} + \begin{bmatrix} w(k) \\ v(k) \end{bmatrix} \quad (4.14)$$

and the measurement equation is:

$$z_k = \begin{bmatrix} C & D \end{bmatrix} \begin{bmatrix} x(k) \\ e(k) \end{bmatrix} \quad (4.15)$$

The augmented system has white plant noise as required, but has no measurement error, since the white noise driving the error model is now part of the augmented process noise. This may cause the covariance matrix of the state estimate to become singular, since linear combinations of the augmented state elements are known perfectly [78, 79]. Moreover, the

information form of the Kalman filter can not be used, since the inverse of the measurement noise covariance matrix is an explicit part of this form of the filter.

A possible solution to this problem is to assign some small artificial value to the measurement noise covariance matrix. This value accounts for unmodeled measurement errors, and serves as a design parameter, chosen to match some specific performance requirements. Note that some white noise does exist in the measurement error, mainly due to receiver noise. However, in our case SA dominates the measurement error and the white noise does not show up in the measurement error model.

A more rigorous solution to this problem was described first by Bryson and Henrikson [79]. It is based on generating a pseudo-measurement, which is a linear combination of two consecutive measurements. This pseudo-measurement is corrupted by white noise, and the Kalman filter equations can now be applied without state augmentation. A similar approach was described also by Chui and Chen [80].

These solutions have a definite restriction [78, 81]: the dimension of the error model must be equal to the dimension of the measurement vector. Due to this restriction, the application of the pseudo-measurement approach to tracking filters was limited to the case where only position is measured, and the position error is exponentially correlated [82-85]. The cases where both position and velocity are measured, or where the error model is of higher order could not be solved with this approach.

We have extended the procedure suggested by Henrikson [86], and formulated an optimal tracking filter, without any restrictions on the order of the error model. The dimension of the tracking filter is reduced, and it is smaller than the dimension of the filter obtained by state augmentation. The derivation of this reduced order tracking filter and its associated initialization procedure are detailed in Appendix E. Simulation studies we made showed that the performance of the reduced order filter is similar to the performance of the full order augmented state filter with the addition of small artificial measurement noise.

4.4.2 Filter Initialization

Appendix E derives an initialization procedure for the reduced order filter, using the first available measurements and the correlation matrix of the error model. Following this derivation, the initial estimate of the augmented state vector $\hat{x}_a(0)$ is obtained after the first two position measurements:

$$\hat{x}(0) = \begin{bmatrix} z(0) \\ [z(0) - z(-1)]/T \\ 0 \\ 0 \end{bmatrix} \quad (4.16)$$

where T is the sampling interval, and z is the position measurement. The initial covariance matrix is:

$$\hat{P}(0) = \begin{bmatrix} \phi_{xx}(0) & \Delta\phi_{xx} & -\phi_{xx}(0) & -\phi_{xv}(0) \\ \Delta\phi_{xx} & 2\Delta\phi_{xx}/T & -\Delta\phi_{xx} & -\Delta\phi_{xv} \\ -\phi_{xx}(0) & -\Delta\phi_{xx} & \phi_{xx}(0) & \phi_{xv}(0) \\ -\phi_{xv}(0) & -\Delta\phi_{xv} & \phi_{xv}(0) & \phi_{vv}(0) \end{bmatrix} \quad (4.17)$$

where

$$\Delta\phi_{xx} \triangleq [\phi_{xx}(0) - \phi_{xx}(T)]/T \quad (4.18)$$

$$\Delta\phi_{xv} \triangleq [\phi_{xv}(0) - \phi_{xv}(T)]/T \quad (4.19)$$

and $\phi_{xx}(\tau)$, $\phi_{xv}(\tau)$ and $\phi_{vv}(\tau)$ are the correlation functions of the specific error model. For example, if the error model is a simple second order Gauss Markov process, its correlation functions are (see Appendix D):

$$\phi_{xx}(\tau) = \frac{Q\beta}{4} e^{-\beta\tau} (1 + \beta\tau)$$

$$\phi_{vv}(\tau) = \frac{Q\beta^3}{4} e^{-\beta\tau} (1 - \beta\tau)$$

$$\phi_{xv}(\tau) = \frac{Q\beta^3\tau}{4} e^{-\beta\tau}$$

By substituting $\tau = 0$ and $\tau = T$, we get the initial covariance matrix for the case where only position is measured:

$$\hat{P}(0) = \sigma_x^2 \begin{bmatrix} 1 & f_x/T & -1 & 0 \\ f_x/T & 2f_x/T^2 & -f_x/T & \beta^2 T e^{-\beta T} \\ -1 & -f_x/T & 1 & 0 \\ 0 & \beta^2 T e^{-\beta T} & 0 & \beta^2 \end{bmatrix} \quad (4.20)$$

where $f_x \triangleq 1 - (1 + \beta T)e^{-\beta T}$. We have used here the identity $\sigma_x^2 = \phi_{xx}(0)$ to normalize $\hat{P}(0)$ by the variance of the position error.

When both position and velocity are measured, the initial estimate can be obtained after one measurement:

$$\hat{x}(0) = \begin{bmatrix} z_1(0) \\ z_2(0) \\ 0 \\ 0 \end{bmatrix} \quad (4.21)$$

where z_1 is the position measurement and z_2 is the velocity measurement. The initial covariance matrix is:

$$\hat{P}(0) = \begin{bmatrix} \phi_{xx}(0) & 0 & -\phi_{xx}(0) & 0 \\ 0 & \phi_{vv}(0) & 0 & -\phi_{vv}(0) \\ -\phi_{xx}(0) & 0 & \phi_{xx}(0) & 0 \\ 0 & -\phi_{vv}(0) & 0 & \phi_{vv}(0) \end{bmatrix} \quad (4.22)$$

For the simple second order error model discussed previously, the initial covariance matrix is:

$$\hat{P}(0) = \sigma_x^2 \begin{bmatrix} 1 & 0 & -1 & 0 \\ 0 & \beta^2 & 0 & -\beta^2 \\ -1 & 0 & 1 & 0 \\ 0 & -\beta^2 & 0 & \beta^2 \end{bmatrix} \quad (4.23)$$

We have assumed here one dimensional tracking, using a second order aircraft model, augmented by a second order error model. The extension to other models can be easily

done by following the derivation in Appendix E. Note that $\hat{P}(0)$ (Equation 4.20 or 4.23) is singular. This singularity can be avoided by using the reduced order approach discussed in Appendix E.

4.4.3 Error Model Selection

We now wish to examine the effect of different error models on the tracking accuracy. We form tracking filters that combine the constant velocity aircraft model with an exponential correlation error model, a simple second order error model, and the general third order error model.

The filter performance is checked in a Monte Carlo simulation in the following way: we select at random a 1000-second interval out of one of the five-hour long recordings of GPS measurements described previously. This is used as the input to the filter. The tracking errors are averaged over 1000 such intervals.

Figure 4.2 shows the average tracking errors in position and velocity, for an aircraft in uniform motion where only its position is measured. The tracking errors are compared with the average error obtained when not using a tracking filter. In this case the velocity is estimated by a first difference of the position measurement.

The tracking filters were successful in reducing the velocity error, but did not improve the position error. The difference between the various error models is small, and we can see that the time constant of the filter is quite large for any error model.

In order to check our results, we have repeated the same procedure with ‘simulated’ GPS position errors, using a 2nd order Gauss Markov process which is identical to the model used in the Kalman filter. The average tracking errors in this case were very similar to the case where actual GPS measurements were used. This indicates that the poor performance in position is not a result of bad modeling.

Another check we made is to compare the average position error of the 2nd order error model, with the square root of the appropriate diagonal element from the covariance matrix in the Kalman filter equations. The two values matched perfectly. This indicates that the filter initialization procedure is consistent, and completes the Kalman filter debugging

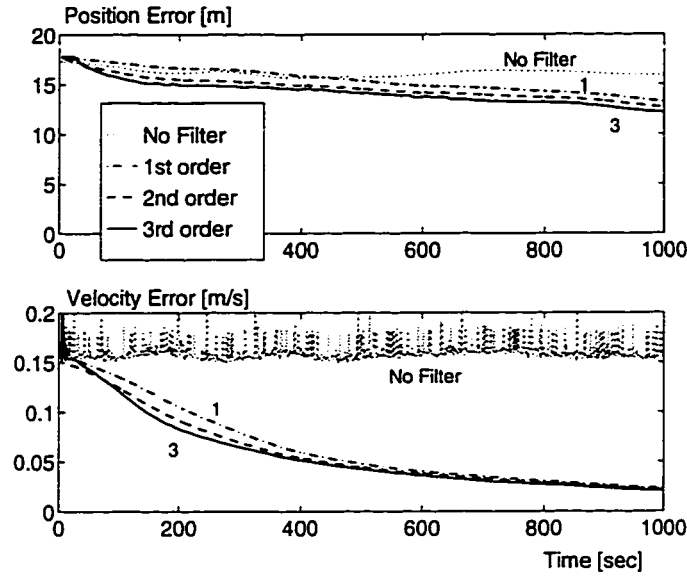


Figure 4.2: Error Model Selection

Average tracking errors during uniform motion, using different measurement error models.

process.

Due to the small differences between the error models, we have decided to use the 2nd order error model throughout the rest of this work.

4.4.4 Aircraft Model Selection

We wish now to evaluate the effect of different aircraft models on the tracking accuracy. We combine the 2nd order error model selected in the previous section, with the following aircraft models:

- CV0** Constant velocity, with zero acceleration (Eqs. 4.3–4.4, $\sigma_v=0$)
- CV1** Constant velocity, with random acceleration (Eqs. 4.3–4.4, $\sigma_v=5 \text{ m/s}^2$)
- CA** Constant acceleration, with random increments (Eqs. 4.5–4.7, $\sigma_a=1 \text{ m/s}^3$)
- CT** Constant turn rate, random disturbances (Eqs. 4.8–4.10, $\sigma_x=\sigma_y=1 \text{ m/s}^2, \sigma_\gamma=0.5^\circ/\text{s}$)

The performance of these models is compared with the case where no filter is used. This is denoted in the following discussion as **NF**.

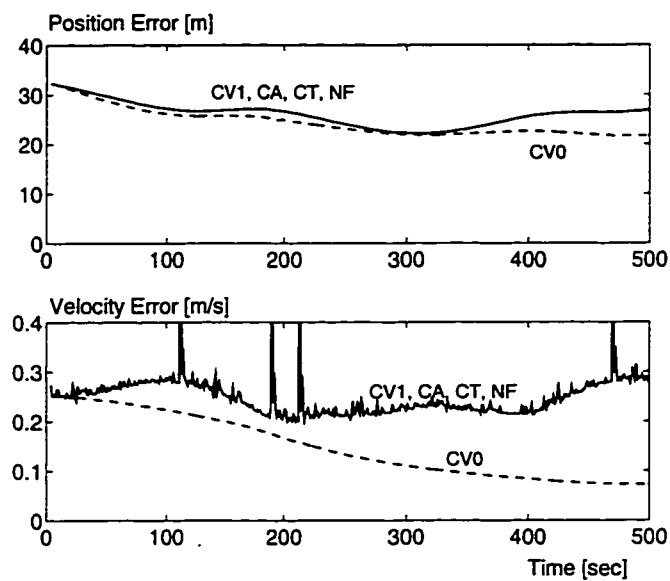


Figure 4.3: Average Tracking Errors – Uniform Motion

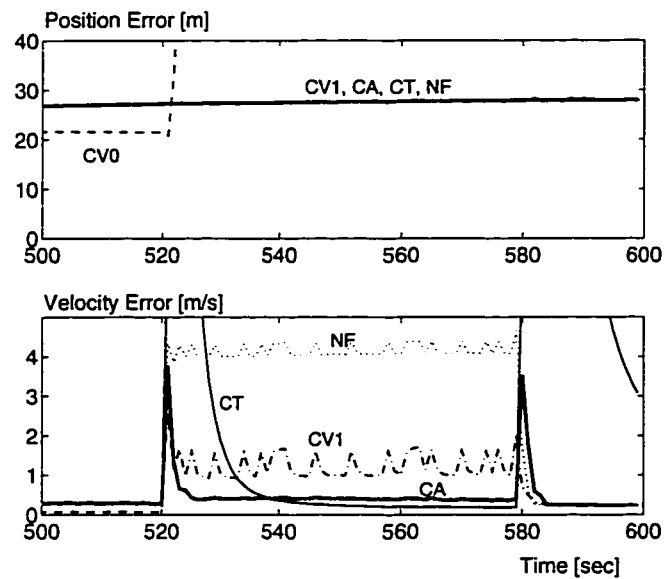


Figure 4.4: Average Tracking Errors – Coordinated Turn

Figure 4.3 shows the average tracking accuracy obtained in a 300 knot, straight line motion. All aircraft models, except **CV0** cannot do better than the raw measurement accuracy, and they provide the same tracking accuracy as **NF**. The **CV0** model cannot improve the position accuracy much, but it does improve the accuracy of the velocity estimate.

Figure 4.4 shows the average tracking errors that were observed during a $3^\circ/\text{sec}$ turn at the same speed. The turn was initiated at $t = 520$ sec and lasted for 1 minute. As expected, the **CT** model provides the best steady state accuracy during the turn. However, it has a longer transient phase than the **CA** model.

4.4.5 Data Link Effect

The input to the tracking filter is provided through a radio data link which is common to all aircraft under ADS. In the previous chapter we saw that some of the aircraft reports would be lost due to interference between messages in the radio channel. This is expected under most communication protocols. As a result of this interference, the reports arrive to the filter each update with some probability which can be estimated by (see section 3.2.2):

$$P_r = \exp\left(-N \frac{2n_m}{Bt_f}\right) \quad (4.24)$$

where N is the average number of aircraft in the detection range of the receiver, n_m is the report length in bits, B is the bit rate, and t_f is the update interval. It is assumed that aircraft send a report once every t_f seconds, and randomly change the exact transmission time. The low probability of clear reception associated with this random protocol provides us with a conservative estimate of the data link effect.

Missing data points due to interference can be handled by the tracking filter by allowing the time between measurements to vary and to be equal to the actual time between valid data measurements. This requires recomputation of the discrete time state matrices, and involves a large computational effort. A simpler approach is to set the state estimate equal to the estimate from the previous time step [87], or to set it equal to the state prediction from the time update phase of the Kalman filter in the previous step. We will use the

later approach, which is a simple and efficient way to provide a suboptimal estimate when a measurement is missing. For an analysis on the convergence of the filtering residuals in this case, see [88].

We now wish to determine the sensitivity of the various aircraft models to missing reports. The simulation study was repeated under the assumption that the position reports are received with a probability of $P_r = 0.7788$. As will be shown below, this specific value represents a future ATC environment, with 1000 aircraft within the detection range of the ATC control center.

Figure 4.5 shows the average tracking errors during the aircraft $3^\circ/\text{sec}$ turn, under the imperfect data link assumption. It seems that the CA filter is less sensitive to missing reports than the CT filter. Additional simulation studies proved the CA filter to be more robust to parameter changes, and we conclude that it is more suitable for modeling the aircraft during its maneuver phase.

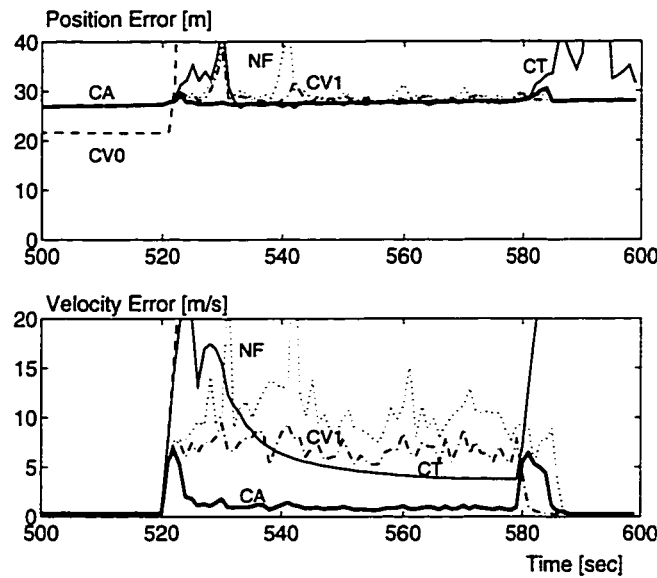


Figure 4.5: Data Link Effects

Average tracking errors during a coordinated turn, using different aircraft models, under an imperfect data link.

4.4.6 Multiple-Model Estimation

The results described above show that a tracking filter with the **CV0** model is optimal during the uniform motion phase of flight but diverges during turns. A tracking filter with the **CA** model provides good estimates during turns, however, it does not reduce the velocity error during the uniform motion phase.

In order to obtain the best estimates available during all phases of flight, we can construct the tracking filter in the following ways:

1. Use only one filter, with an aircraft model that provides acceptable behavior during all phases. In our case, this would be the **CA** model.
2. Use the constant velocity aircraft model, and adjust the process noise level to account for possible maneuvers. This scheme provides continuous transition between the **CV0** and **CV1** models [89].
3. Switch between different filters, however run only one filter at a time. The switching is done when the current filter innovations exceeds a certain threshold [90].
4. Use several aircraft models, and run in parallel a filter for each. The optimal estimate is a weighted average of the filters estimates.

Another approach to maneuvering aircraft tracking is to estimate the aircraft acceleration as an unknown input to the aircraft model [65, 91, 76, 92]. It was shown that multiple model algorithms usually perform better than input estimation schemes, and are more computationally efficient [93].

Multiple-model algorithms are composed of a parallel bank of Kalman filters, each based on a different model. The probability for each model being correct is calculated recursively, based on its likelihood function. The state estimate is a weighted average of the model-conditioned estimates, with the model probabilities as weights [65, 78].

A more elaborate scheme of multiple model estimation is the Interacting Multiple Model (IMM) filter, which assumes an underlying Markov chain that governs the probabilities of

transition between the different aircraft models. The IMM filter provided excellent position and velocity estimates during all phases of flight, in studies that used radar measurements and many different combinations of different aircraft models [66-68].

We found, however, that any multiple-model algorithm which relies on the filters innovations or likelihood functions fails when tracking GPS reports, due to satellite constellation changes. The discontinuities in position which appear whenever the GPS receiver changes the set of satellites, trigger any existing maneuver detection algorithm and cause it to switch unnecessarily from a uniform motion mode to a turn mode.

We have decided to design our tracking filter around two Kalman filters that run in parallel: one is based on the **CV0** model, and the other uses the **CA** model. The estimated state is set equal to the output of one of these filters, according to the following tests:

When the current mode of flight is uniform motion, we check the continuity of the position information. This is accomplished by computing the difference between the current position report and the previous one, and comparing it with \bar{v}_{-1} , which is the predicted velocity from the previous time step:

$$\hat{v} = \frac{z - z_{-1}}{t - t_{-1}} \quad (4.25)$$

$$\delta_v = (\hat{v} - \bar{v}_{-1})^T (\hat{v} - \bar{v}_{-1}) \quad (4.26)$$

If δ_v is greater than a specified threshold for more than one time step, we assume that a maneuver is taking place, and the flight mode is switched to the turn mode.

When the flight mode is a turn, we check the statistical significance of the estimated acceleration, in order to determine when the turn is over:

$$\delta_a = \hat{a}^T [\hat{P}_a]^{-1} \hat{a} \quad (4.27)$$

$$\rho_a = \alpha \rho_a + \delta_a \quad (4.28)$$

where \hat{a} is the estimated acceleration, and \hat{P}_a is the corresponding block from the covariance matrix of the **CA** model. ρ_a is a fading memory average of δ_a , and when it drops below a certain threshold, we assume that the turn is completed, and revert to the uniform motion mode.

The state estimate \hat{x} is set equal to the estimate of the filter that matches the current flight mode. This state estimate is used in the time update phases of both filters, so that both filters update the best estimate available.

In the following discussion we will refer to the overall filter described above as the **GPS** tracking filter. The average tracking accuracy of this filter is compared in figure 4.6 with the performance of an IMM filter and a single **CA** filter. The IMM filter we used is based on the same aircraft models as the **GPS** tracking filter (**CV0** and **CA**). We see that the **GPS** filter performs better than the other filters, during all phases of flight.

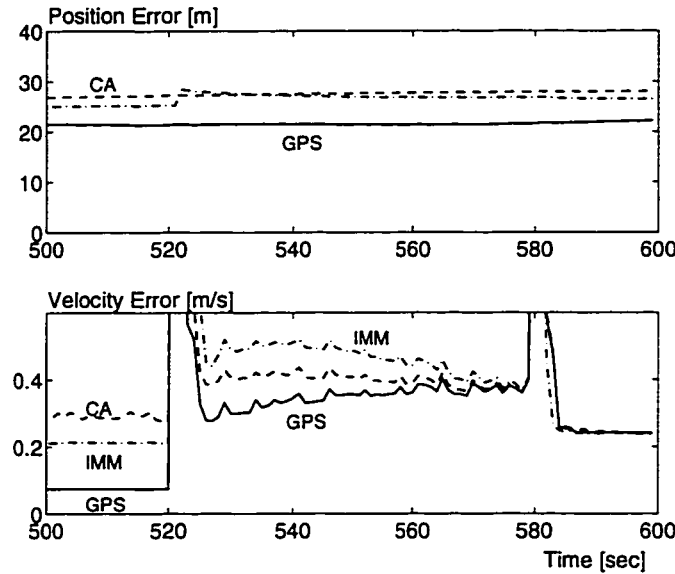


Figure 4.6: **Tracking Filters Comparison**

Average tracking errors during a coordinated turn, using different tracking filter structures.

Note that the maneuver detection scheme described above can be avoided if the aircraft will include a 'turn indicator' in its report, as suggested by MIT's Lincoln Laboratory in their ADS Mode-S concept (see Appendix A). This indicator can be used to switch between the appropriate models. However, we still have to detect satellite constellation changes and treat them appropriately.

This is done by measuring the duration of the discontinuity in the position reports. If δ_v (Eq. 4.26) is greater than the specified threshold for only one time step, we assume that a

constellation change has occurred. The state estimate for the next 5 cycles is computed by propagating the state vector through the time update phase of the current filter. The **CV0** and **CA** filters, however, continue to operate without any intervention - only the output of the overall filter is affected. After 5 cycles the transient response of the **CV0** and **CA** filters decays, and the state estimate is set equal to the output of one of them.

Figure 4.7 depicts the position measurement error during a sequence of satellite set transitions, and shows the effect of the discontinuities on the velocity tracking error of the GPS filter described above. For comparison, we show also the tracking error of a simple **CA** filter.

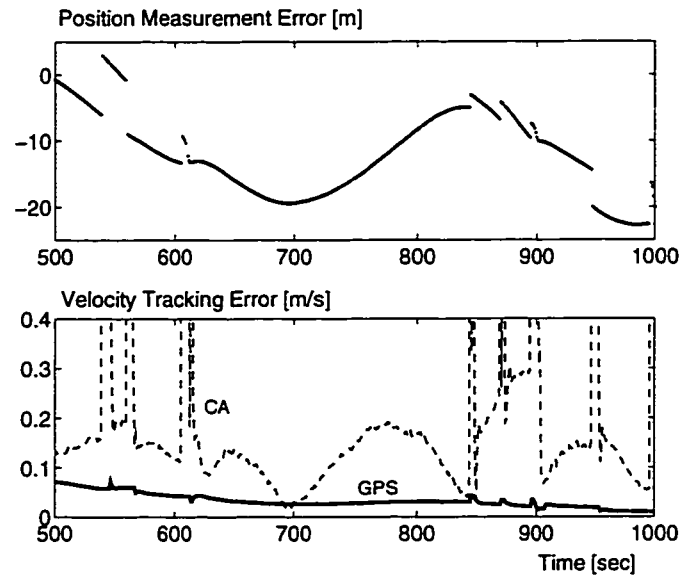


Figure 4.7: **Constellation Change Effect**

Position measurement error and velocity tracking error during a sequence of satellite set transitions.

4.4.7 Velocity Reports

The simulation studies so far assumed that only position is measured. We have repeated the same simulation trials when measuring both position and velocity and could not find any significant improvement in the tracking accuracy. Similar observations about the possible benefits of velocity information were made regarding the integration of GPS and INS [73].

As stated earlier, the velocity error is equal most of the time to the derivative of the position error. This reduces the benefits of additional velocity information, since the Kalman filter differentiates the position error anyhow, as part of its estimation process.

Moreover, adding the velocity information to the position report will increase the message length and decrease the probability of clear reception. According to the latest definition of the ADS-B message (see Appendix A), the additional velocity information will actually double the original position report length. Thus for example, if the message length increases from 125 bits to 250 bits due to the additional information, the probability of clear reception will decrease from 0.7788 to 0.6065 (based on 1Mbps bit rate, 1 second update rate and 1000 aircraft in the detection range). This caused a severe degradation in the tracking accuracy in simulation studies we made.

4.4.8 Update Rate

We have assumed up to this stage that aircraft repeat their reports once in a second. By increasing the interval between messages to 2 seconds, we can increase the probability of clear reception from 0.7788 to 0.8085 when using position measurement only (125 bit long report), or from 0.6065 to 0.7788 when using position and velocity reports (250 bit). This is supposed to increase the filter accuracy.

However, when a report is missing, the estimation error is approximately twice as large for a 2 second interval than a 1 second interval. In addition, during a coordinated turn the CA model becomes less accurate as the update interval grows. When averaging the tracking accuracy in a Monte Carlo simulation we have observed that the overall effect of decreasing the update rate is to degrade the filter performance.

The performance study in the next section assumes therefore a 1 second update rate, with position information only.

4.5 Performance Study

In order to study the performance of the proposed tracking filter, we define in table 4.2 three representative aircraft trajectories. Trajectory T1 represents typical cruise flight maneuver. T2 includes the standard $3^\circ/\text{sec}$ turn rate, and T3 represents a high speed agile target. Even though T2 is more representative of standard aircraft performance, T1 and T3 appeared in studies of ATC radar tracking, and are therefore included here for comparison.

	Speed [knot]	Turn rate [deg/sec]
T1	150	1
T2	300	3
T3	600	6

Table 4.2: **Representative Trajectories**

The average tracking accuracy is calculated over these trajectories, while using actual GPS data as described previously. The measurement errors are added to simulated aircraft motion and are sampled according to the probability of clear reception in an ATC environment.

A future ATC environment can be characterized by the following assumptions on the data link: each aircraft broadcasts a 125 bit message once a second, in a 1Mbps bit rate; there are 1000 aircraft within the detection range of the receiver. For comparison, the capacity of a Mode S sensor is 700 transponder carrying aircraft within 255 nmi [40]. The resulting probability of clear reception is $P_r=0.7788$ (Eq. 4.24). The effective update rate (which indicates how often a message from a specific aircraft is received, with a probability that is higher than a given reliability level (Eq. 3.12), is 4.58 seconds with 99.9% reliability. This is equivalent (in a probabilistic sense) to the 4 seconds rotation period of current ATC radars in the terminal areas, and considerably better than the 12 seconds rotation period of enroute radar.

Table 4.3 summarizes the average tracking errors during the uniform motion phase of flight. The table also shows the maximum tracking error immediately after a turn is

		Position [m]	Speed [m/s]	Heading [deg]
T1	uniform motion	21.5	0.07	0.04
	turn, max	21.7	1.85	1.37
	turn, after 30 sec.	22.8	0.27	0.15
T2	uniform motion	21.5	0.07	0.02
	turn, max	23.8	5.7	2.6
	turn, after 30 sec.	22.7	0.9	0.07
T3	uniform motion	21.5	0.07	0.01
	turn, max	37.1	26.7	4.9
	turn, after 30 sec.	22.5	6.5	0.24

Table 4.3: Average Tracking Errors with GPS (SA on)

		Position [m]	Speed [m/s]	Heading [deg]
T1	uniform motion	37	0.31	0.6
	turn, max	204	4.11	12
	turn, after 30 sec.	83	3.6	4
T2	uniform motion	46	0.33	0.3
	turn, max	241	6.7	20
	turn, after 30 sec.	74	3.6	5
T3	uniform motion	150	6	1.1
	turn, max	425	175	32
	turn, after 30 sec.	215	41	7.7

Table 4.4: Average Tracking Errors with ATC Radars

initiated, and the steady state tracking error during the turn. The improvement in tracking accuracy can be demonstrated by comparing these results to the tracking accuracy obtained by ATC radars, as summarized in table 4.4.

The relevant radar parameters are: on trajectories T1 and T2 the aircraft is tracked by three monopulse secondary radars, each of which has a range measurement accuracy of 110 meters and a bearing measurement accuracy of 0.07° [66]. On trajectory T3 a single radar is used, which has a bearing accuracy of 0.2° [68]. In all cases the radar rotation period is 4 seconds, and the algorithm used is the Interacting Multiple Model algorithm, which combines the constant velocity aircraft model (CV) with the constant turn rate model (CT) and its associated second order Extended Kalman Filter.

The tables clearly show the improvement in tracking accuracy which can be achieved by using GPS position reports, especially in the velocity and heading estimates. The improvement in the position estimate is especially apparent in trajectory T3, where only one radar is used to track the aircraft. Note that this improvement in tracking accuracy is achieved with SA on. When SA is eliminated or with the Wide Area Augmentation System (WAAS), tracking errors would be considerably lower yet.

4.6 Conclusion

GPS-based aircraft tracking can yield a significant improvement in the quality and extent of ATC surveillance coverage. This requires a new design of ATC tracking algorithms, since the nature of GPS measurement errors is very different from the nature of the current radar measurement errors. Constellation changes and message interference in the radio channel should be of special concern when designing the tracking filter and evaluating its performance.

The tracking filter designed here combines a 2nd order Gauss Markov process as the measurement error model, with two dynamic aircraft models, in an adaptive Kalman filter structure. Switching logic identifies aircraft maneuvers and provides smooth transition of the estimates through satellite constellation changes. The average accuracy of this filter was

estimated by using actual GPS data and simulated aircraft motion, and was compared to the performance of ATC radar trackers on several representative trajectories. The performance study showed a large improvement in tracking accuracy.

The tracking filter design and the performance study were based on data obtained by standalone GPS receivers, unassisted by differential corrections. The measurement errors were therefore dominated by SA. In case that SA is eliminated, or that the Wide Area Augmentation System (WAAS) is being used, we expect the measurement errors to be much lower, and of different dynamic characteristics. This has several consequences:

First, it can be expected that a future ATC tracking filter would have to deal with position reports from different sources, some unassisted and probably governed by SA, and some assisted by WAAS or by a local differential correction. Since the dynamic error model in this study was tailored to SA-governed errors, it would not be optimal in other cases. A Figure Of Merit (FOM) word included in the aircraft report (see Appendix A) should describe the quality of the navigation source, and thus assist the ground controller with matching optimal tracking filters to each aircraft.

Second, we can refer to the performance demonstrated here as representing a “worst case” scenario in terms of GPS measurement errors. When SA is eliminated or when WAAS is being used, the tracking errors would be considerably lower than the results shown above. However, even with SA on, the large improvement in tracking accuracy demonstrated here has the potential for reducing aircraft separation standards, as will be shown in the next chapter.

Chapter 5

Separation Standards

5.1 Introduction

Aircraft motion over most of the continental US is monitored today by surveillance radar. The radar measurements are used by air traffic controllers to alert pilots when a minimum separation standard is violated. The size of this separation standard is determined in part by the surveillance accuracy - a more accurate surveillance system will allow smaller separation between aircraft, and a subsequent increase in the airspace capacity without decreasing the safety level.

In this chapter we estimate the effect of a GPS-based surveillance system on the separation standards. We assume that every aircraft periodically broadcasts its position as derived by an onboard GPS receiver. The position reports are received by ATC ground controllers and are used for aircraft tracking and conflict resolution.

GPS-based surveillance can also be used to monitor aircraft during approach to parallel runways. Currently, independent (simultaneous) approaches to parallel runways under Instrument Meteorological Conditions (IMC) are allowed only if the runway centerlines are 4,300 ft apart or more [94]. If the parallel runways are separated by less than 4,300 ft, arriving aircraft must be dependently sequenced. This procedure poses restrictions that reduce the arrival capacity by as much as 40 percent [95].

The FAA estimated the annual airline-delay costs associated with dependent approaches relative to independent approaches, as reaching 10 M\$ by the year 2,000 in New York's JFK alone¹, and about 100 M\$ in each of the airports located at Salt Lake City, Memphis and Raleigh-Durham [97]. The runway spacing in these airports is about 3,500 ft. Reducing the required spacing for independent approaches could increase the arrival capacity, reduce airport delays, and reduce the need to build new airports or to purchase additional land to expand existing airports. We wish therefore to estimate the possible reduction in the required runway spacing due to GPS-based surveillance.

The methodology we use is similar in both cases. Given the current separation standard or runway spacing, and the performance of the current surveillance system, we find a basic risk-related parameter that should be kept when upgrading the surveillance system. Based on this parameter and on the predicted performance of a GPS-based surveillance system, we derive the new separation standard or runway spacing that will keep the current value of the selected parameter.

When dealing with radar separation standards, this parameter is the probability of unobserved close approach between aircraft, which is a measure of the collision risk, or in other terms, a measure of the system safety. In section 2 of this chapter we compute the probability of unobserved close approach as a function of the separation standard, for radar-based surveillance and GPS-based surveillance. We then derive the new separation standard that will keep the current safety level.

In section 3 we describe the procedure for conducting simultaneous parallel approaches under IMC. We analyze the various elements of the required runway spacing, and demonstrate the effect of GPS-based surveillance on this spacing. In section 4 we study the possible use of velocity estimates in predicting future conflicts, and examine the tradeoff between the probability of false alarm and the probability of late alarm as a function of the update rate and the prediction time. Section 5 concludes the chapter.

¹JFK has two sets of parallel runways, one at a separation of 3000 ft, and the other at a separation of 6600 ft [96]. This airport is therefore less affected by IMC when compared to airports with only one set of closely spaced parallel runways.

5.2 Radar Separation Minima

Safe separation between aircraft is maintained today by air traffic controllers, who monitor a minimum separation standard of 3 nmi in the terminal airspace and 5 nmi for enroute traffic. Since the surveillance information that is provided to the controllers is obtained by radar, these standards are usually referred to as *radar* separation standards and are a function of the radar accuracy.

We wish to estimate the effect of GPS-based surveillance on these standards. Since reduction of in-trail separation is limited by wake-turbulence concerns, we consider only lateral separation. Note that we do not study route spacing or track separations, which depend also on the navigation accuracy and control system delay time. These parameters will be taken into account in the next section.

5.2.1 Probability of Close Approach

The surveillance separation standard affects the collision risk, which can be measured by the probability of unobserved close approach. This is the probability that the *actual* distance between aircraft is less than the minimum safety distance, when the *measured* distance between the aircraft is equal to the minimum separation standard:

$$P_{ca} \equiv P(\Delta x_a < d \mid \Delta x_m = s) \quad (5.1)$$

where Δx_a is the actual separation between the aircraft, and Δx_m is the measured separation. s is the surveillance separation standard, and d is the minimum safety distance, represented by the horizontal size of a typical aircraft. P_{ca} can be computed by the following integral [98]:

$$P_{ca} = \int_{s-d}^{s+d} \left[\int_{-\infty}^{+\infty} f(x)f(z-x)dx \right] dz \quad (5.2)$$

where $f(x)$ is the probability distribution function of the surveillance errors.

5.2.2 Distribution of Surveillance Errors

The distribution of GPS position errors can be modeled by a mixture of two Gaussian (Normal) distributions:

$$f(x) = (1 - \epsilon)N(x|\sigma_1) + \epsilon N(x|\sigma_2), \quad 0 < \epsilon < 1 \quad (5.3)$$

where $N(x|\sigma)$ is a zero mean Gaussian density function with standard deviation σ . Mixture densities of this form are used to model heavy-tailed non-Gaussian density functions [99]. The first term models the ‘body’ of the measurement errors, and the second term models the rare large errors.

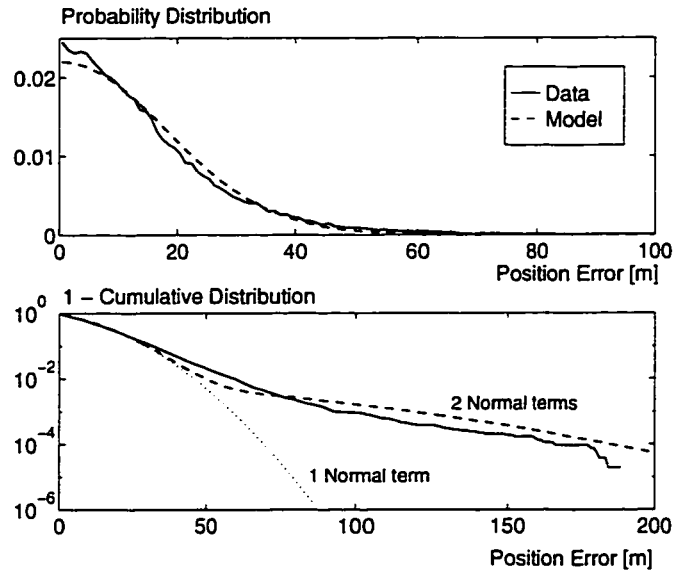


Figure 5.1: **PDF of GPS Position Errors**

Figure 5.1 shows the distribution of more than 50,000 GPS position error samples, that were collected over a period of about 6 months using four Trimble 4000-SSE receivers located at Stanford, San Diego and Arcata, California and Elko, Nevada. A Gaussian-mixture distribution (Eq. 5.3) that fits this data was obtained for $\sigma_1 = 18\text{m}$, $\sigma_2 = 72\text{m}$ and $\epsilon = 0.01$. Also shown in figure 5.1 is the effect of using only the first Gaussian term in Eq. 5.3. It is clear that the additional term is required to properly model the tail of the

experimental distribution.

This statistical model of GPS position measurement errors is different from the dynamic model presented in the previous chapter. The statistical model describes the *distribution* of the measurement errors, whereas the dynamic model describes their correlation in time. These two models were identified by using different sets of position error samples, and therefore the difference in the standard deviation of the position error between the two models.

In order to adjust the statistical model for possible SA elimination, σ_1 and σ_2 can be reduced by a factor of 5/21, which is approximately the ratio between the standard deviation of the ranging error when SA is off and when SA is on [100]. In order to model the possible effect of WAAS on the distribution of the measurement error, one should also reduce the mixture coefficient ϵ . This models the lower probability of having large measurement errors, due to the improved integrity offered by WAAS [101]. Since we do not have at the moment enough data to quantify this effect, it is left for future research.

The distribution of radar azimuth measurement errors is described by the same Gaussian-mixture distribution, with $\sigma_1=0.0987^\circ$, $\sigma_2=0.1640^\circ$ and $\epsilon=0.164$ [98]. These values are multiplied by the maximal range of the radar (200 nmi) to model en-route surveillance errors, and by 50 nmi to model terminal traffic. The radar range error is about 120 feet, and it can be neglected relatively to the azimuth errors.

5.2.3 Analysis

The probability of close approach is obtained by integration of Eq. 5.2 with the Gaussian mixture distribution from Eq. 5.3. The inner integral is evaluated analytically, being the convolution of the distribution function:

$$\begin{aligned} C(z) &= \int_{-\infty}^{+\infty} f(x)f(z-x)dx \\ &= (1-\epsilon)^2 N(z|\sqrt{2}\sigma_1) + 2\epsilon(1-\epsilon)N(z|\sqrt{\sigma_1^2+\sigma_2^2}) + \epsilon^2 N(z|\sqrt{2}\sigma_2) \end{aligned} \quad (5.4)$$

The outer integral is evaluated numerically, for several values of the separation standard and a fixed minimum safety distance, equal to $d = 200$ feet [94, 97]. The results are depicted

in figure 5.2.

We see that the enroute separation standard can be reduced to about 0.5 nmi, while keeping the same safety level that is provided today by using radar surveillance and a 5 nmi radar separation standard. The terminal separation can be reduced from 3 nmi to about 1 nmi, without increasing the collision risk. In the absence of SA the separation standards can be even further reduced.

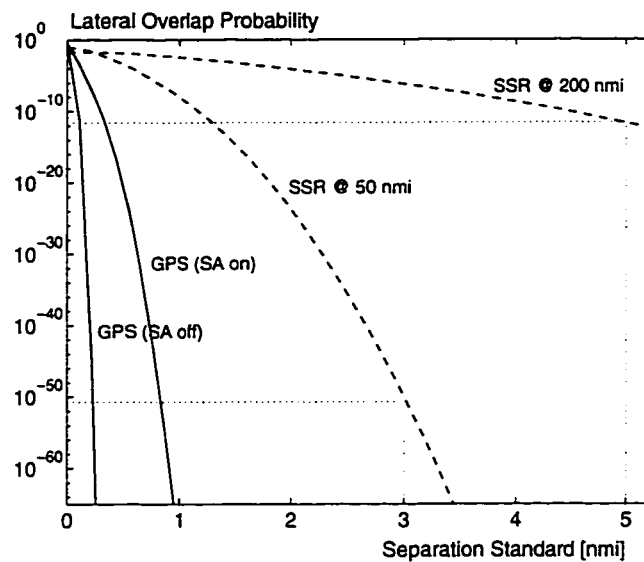


Figure 5.2: Probability of Unobserved Close Approach

Using Secondary Surveillance Radar at close or maximal range, and GPS-based surveillance with SA on or off.

Note that these results hold only for the case where both aircraft use GPS to report their position. In case of gradual transition from radar-based surveillance to ADS, there is some probability that at least one of the aircraft involved is tracked by radar. Figure 5.3 shows the separation standard that keeps the current probability of unobserved close approach, as a function of the fleet fraction which uses GPS.

It seems that the benefits of GPS-based surveillance do not occur until most of the fleet is equipped, and GPS usage might have to be enforced in certain regions. Otherwise, different standards would have to be applied to aircraft surveyed by radar and to aircraft reporting their GPS-based position.

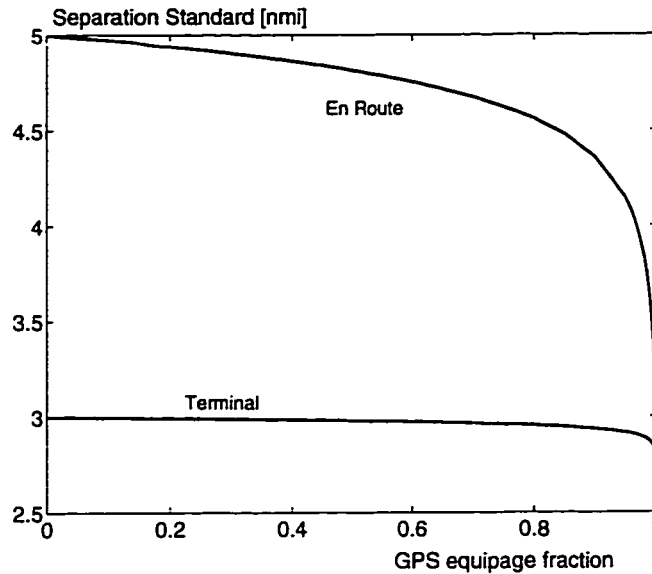


Figure 5.3: GPS Equipage Effect

Separation standard at the current safety level, when only a fraction of the fleet uses GPS, and the rest are surveyed by radar.

The methodology used here to derive the new separation standard is applied in the next section to the required spacing between parallel runways.

5.3 Parallel Runway Separation

During simultaneous approaches to parallel runways under Instrument Meteorological Conditions (IMC), aircraft are required to use the Instrument Landing System (ILS) for lateral guidance. The aircraft intercept the ILS localizer signal 5 to 15 nmi from the runway threshold. Two controllers monitor the approaches, looking at Airport Surveillance Radar (ASR) measurements of each aircraft's lateral deviation with respect to the ILS centerline.

The controllers insure that if either aircraft blunders from a Normal Operating Zone (NOZ) into a 2,000-ft No-Transgression Zone centered between approach paths, then any threatened aircraft on the other approach would be vectored away to a parallel course. The command is given to this aircraft since it is assumed that the conditions leading to the other aircraft's violation of the NOZ may also prevent an adequate turn back maneuver.

The NOZ is sized so that the likelihood of any normally operating aircraft being observed outside of it is very small. The NOZ width depends on the acceptable level of the probability of false alarm, the distribution of the aircraft lateral position deviation from the ILS centerline (total navigation error), and the distribution of errors in the lateral position estimate (surveillance error).

The remainder of the runway spacing provides for safe resolution of the potential conflict. It can be divided into the following components [94]:

Detection Zone (DZ). Allows for the inaccuracy of the surveillance system in detection of the aircraft exactly as it crosses the NOZ boundary. The DZ is sized to provide an acceptable level of the probability of late alarm. Its width depends on the distribution of the surveillance errors, the surveillance update rate, and the specification of the worst case violator (velocity and maximum blunder angle).

Correction Zone (CZ). Allows for the delay between the detection of the NOZ violation and the initiation of the evader's maneuver. The CZ includes also the distance needed during the turn-away maneuver of the threatened aircraft.

Navigation Buffer (NB). Includes a minimum safety distance, and allows for the threatened aircraft to deviate from the ILS localizer centerline.

These components, plus the NOZ, add up to the required runway spacing. Appendix F provides detailed derivation of the runway spacing components, as well as the relevant numerical values. The acceptable false and late alarm probabilities were calibrated to obtain a 4,300-foot runway spacing with the current surveillance system, represented by an ASR-9 radar with a conventional Automated Radar Terminal System (ARTS) display. The total surveillance error in this case is about 5 mrad, and the update interval is 4.8 sec [102].

Figure 5.4 depicts the required runway spacing as a function of the surveillance accuracy and the update interval, for fixed values of the false and late alarm probabilities. GPS accuracy is represented by the Gaussian-mixture distribution described in the previous section (Eq. 5.3), and a digital Final Monitor Aid (FMA) display. This display is part of

the Precision Runway Monitor system developed by the FAA specifically for closely spaced independent parallel approaches [95, 102]. Figure 5.4 shows that by using GPS at an update interval of 1 second, the required runway spacing can be reduced to about 3,400 ft, while keeping the current rate of false and late alarms.

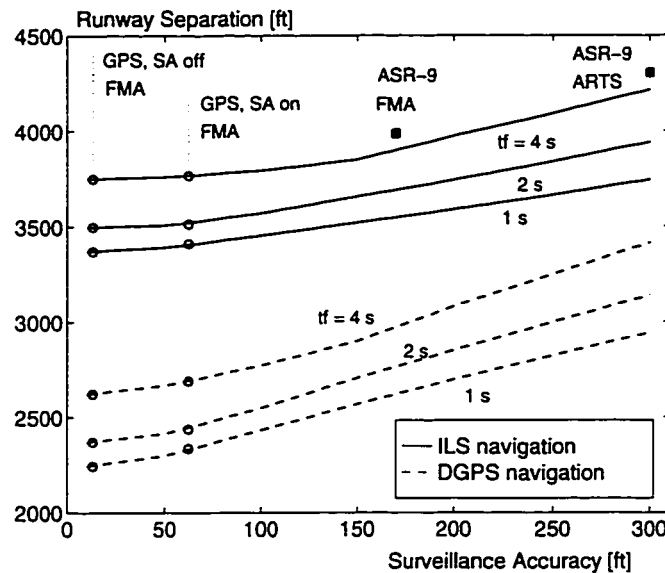


Figure 5.4: **Runway Separation vs. Surveillance Accuracy**

Surveillance accuracy is 1σ at 10 nmi range, for various update periods (t_f). Navigation accuracy is based on using ILS or Differential GPS for lateral guidance.

The improvement in the required runway spacing is smaller than the improvement in the radar separation standard. The latter is determined only by the surveillance accuracy, whereas the required runway separation depends also on other parameters such as the total delay time and the navigation accuracy.

Improving the navigation accuracy can further reduce the required runway spacing. The current spacing is based on the average navigation error when using ILS for lateral guidance. The standard deviation of the course keeping error in this case is estimated as 5 mrad, based on an extensive set of flight tests [96]. Unfortunately, a similar data base for GPS-based guidance does not exist yet.

Preliminary flight test results with aircraft using Differential GPS (DGPS) for lateral

guidance, show a 95% error of 8 meters for B757, and 25 meters for B727, at 2.5 nmi from the runway threshold [103]. Based on this data, we represent the total navigation accuracy of DGPS-based guidance by $1\sigma = 1$ mrad. The effect of the improved navigation accuracy on the required runway spacing is demonstrated by the lower set of curves in figure 5.4.

Below 2,500 feet separation, independent approaches under IMC are prohibited due to wake vortex limitations, and the parallel set of runways is considered as a single runway. In Visual Meteorological Conditions (VMC), however, parallel approaches as close as 750 feet are allowed. The aircraft approach the runways simultaneously, such that neither aircraft can encounter the other's wake. Each aircraft is required to *visually* monitor its position with respect to the other aircraft. In the future, it may be possible for two aircraft equipped with ADS-B to monitor their relative position in a similar way even under IMC, based on the periodical position reports sent by each aircraft.

Providing each pilot with continuous information on the relative location of the other aircraft can transfer the responsibility for issuing an alarm from the controller to the pilot. This could eliminate a major part of the delay time between the blunder detection and the maneuver initiation. The results shown above included 8 seconds for a delay time which combines the controller delay in issuing the alarm and the aircraft delay in starting the avoidance maneuver. The controller delay allows for reaction time, coordination with the other controller and communication with the endangered aircraft. All these elements of the delay time could be eliminated, and the runway spacing could be even further reduced. It is expected therefore that independent approaches under IMC could be allowed with runway spacing smaller than 2,500 feet, provided that pilots are presented with information on the relative location of other aircraft, in a similar way to the information available to them today in VMC.

5.4 Blunder Prediction

In the previous section we assumed that pilots are alerted as soon as a NOZ violation is detected. However, by estimating the aircraft velocity we can predict crossing of the NOZ,

and alert pilots when the *predicted* cross track position is outside the NOZ. This can reduce the probability of late alarm, and reduce or even eliminate the detection zone.

The alert algorithm is studied by using a Monte Carlo simulation of random approaches. The simulation enables us to consider range dependent ILS navigation error and range dependent radar surveillance error, to include a tracking algorithm, and to incorporate in our analysis actual GPS measurement errors (with SA on) and a radio data link model. All these features are missing from the statistical analysis described in the previous section. The random approach simulation is described in Appendix G.2.

5.4.1 Probability of Late Alarm

Given that a blunder is occurring, a late alarm is an alarm issued too late for effective avoidance. For our purposes, we will define the probability of late alarm as the probability that no alarm is given, while the aircraft had already crossed the NOZ boundary:

$$P_{la} = P(z_{\perp} < \text{NOZ} \mid y_{\perp} > \text{NOZ}) \quad (5.5)$$

z_{\perp} is the predicted cross track position, and y_{\perp} is the actual position.

In order to estimate the probability of late alarm, we compute the distribution of the detection lag using the Monte Carlo simulation described previously. The detection lag is the time that passed from the point where the aircraft crossed the NOZ boundary ($y_{\perp} > \text{NOZ}$), to the point where the predicted position crossed the NOZ ($z_{\perp} > \text{NOZ}$). The probability of late alarm is then the positive part of the complimentary cumulative distribution:

$$P_{la} = P(\Delta t > \tau) = 1 - F_{\Delta t}(\tau), \quad \tau > 0 \quad (5.6)$$

where $F_{\Delta t}(\tau)$ is the cumulative distribution of the detection lag.

The probability of late alarm is shown in figure 5.5 for $t_p=0$ (no prediction) and $t_p=2$ sec. When using GPS, several values of the update period are tried. The time axis was multiplied by the blunderer velocity in the direction normal to the runway. In this way the figures represent the probability that the blunderer would travel a certain distance into the no-transgression zone without being detected. We can get the required width of the

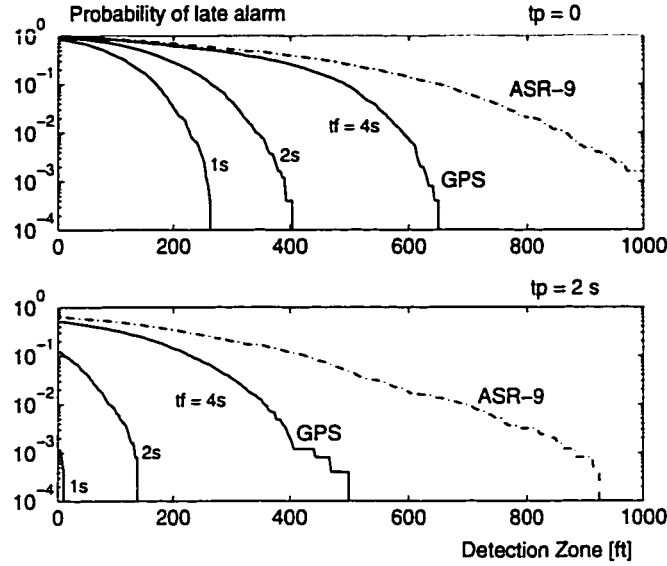


Figure 5.5: Prediction Effect on Late Alarms

The probability of late alarm is shown as a function of the Detection Zone (DZ) size. t_p is the prediction time, and t_f is the update interval.

Detection Zone by fixing the acceptable level of the probability of late alarm and reading the matching distance.

It is clear that certain combinations of update period and prediction time can lead to elimination of the detection zone. However, large prediction times can increase the false alarm rate during normal approaches. This is investigated in the next section.

5.4.2 Probability of False Alarm

The probability of false alarm is the probability that an alarm will be issued during a normal approach when no blunder exists. In order to estimate this probability, we compute the distribution of the predicted cross track position z_{\perp} during a normal approach, using the Monte Carlo simulation described previously. The probability of false alarm for any size of the Normal Operating Zone (NOZ), is the complimentary cumulative distribution of z_{\perp} :

$$P_{fa} = P(z_{\perp} > \text{NOZ}) = 1 - F_z(\text{NOZ}) \quad (5.7)$$

Figure 5.6 shows the probability of false alarm as a function of the NOZ width. The upper set of curves represents the performance of the airport surveillance radar, for various prediction times. Due to the poor quality of the velocity estimate in this case, increasing the prediction time causes an increase in the probability of false alarm.

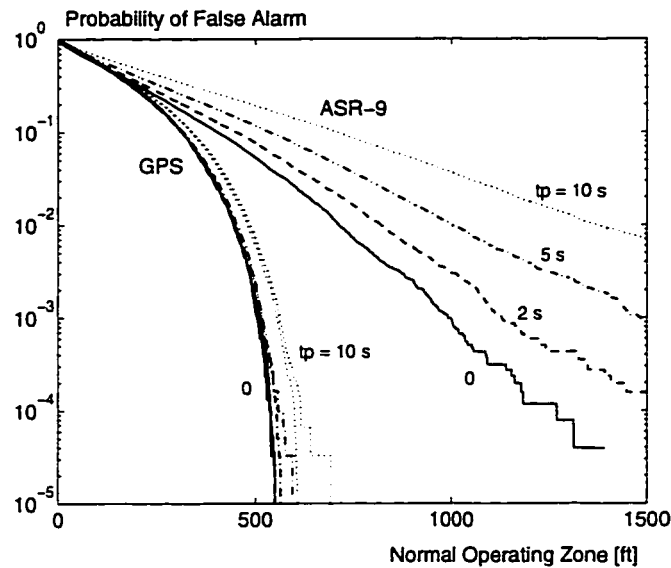


Figure 5.6: Prediction Effect on False Alarms

The probability of false alarm is shown as a function of the Normal Operating Zone (NOZ) size. tp is the prediction time.

The left set of curves represents the performance of GPS-based surveillance. Since the position measurement errors in this case are smaller, the probability of false alarm is lower. Moreover, the high accuracy of the velocity estimate provides a probability of false alarm which is robust to variations in the update period or prediction time.

5.4.3 Effect on Runway Spacing

The minimum width of the NOZ is currently 1,150 ft, based on a required spacing of 4,300 ft and a No Transgression Zone of 2,000 ft centered between approach paths. This value corresponds with $P_{fa}=2.75e-4$, based on figure 5.6 and the curve which represents the performance of ASR-9 with no prediction.

By fixing this value of P_{fa} as the acceptable level of the probability of false alarm, we can get the required size of the NOZ for any prediction time and surveillance system from figure 5.6. The results, depicted in figure 5.7, show that using prediction with the current radar measurements while keeping the same level of false alarm will necessarily require a larger NOZ. However, when using GPS the required NOZ is much smaller due to the increased accuracy of the position measurement. Moreover, the high accuracy of the velocity estimate mitigates the negative effect of the prediction on the probability of false alarm and the required width of the NOZ.

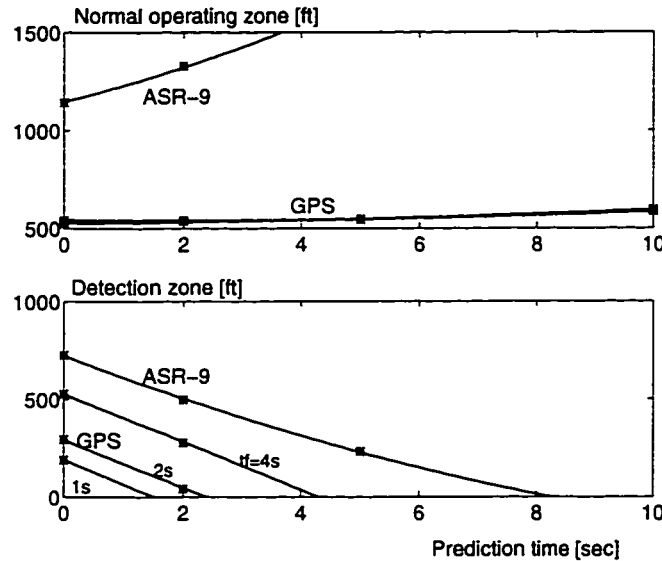


Figure 5.7: Prediction Effect on NOZ and DZ

The width of the Normal Operating Zone which keeps the current value of the probability of false alarm, and the width of the Detection Zone which keeps the current value of the probability of late alarm, are shown as a function of the prediction interval. t_f is the update interval.

In a similar way, we can get the required size of the DZ from figure 5.5, by fixing the acceptable value of the probability of late alarm at $P_{la}=4.72e-2$. This value corresponds with the current DZ width of 725 ft. The effect of the prediction on reducing the DZ width is depicted in figure 5.7. Note that a high enough prediction interval can reduce the required width to zero and eliminate the DZ. Summing the results of figure 5.7 together with the

rest of the runway spacing components, we get the required runway spacing as a function of the prediction interval, as depicted in figure 5.8.

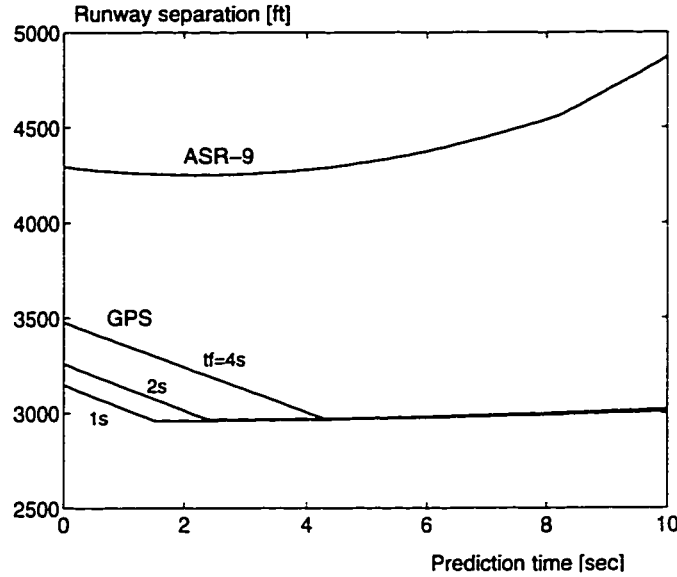


Figure 5.8: **Prediction Effect on Runway Separation**

The required runway spacing which keeps the current probability of false and late alarm is shown as a function of the prediction interval. ILS navigation and GPS with SA on are assumed. t_f is the update interval.

When using radar surveillance, the required runway spacing is dominated by the probability of false alarm. Introducing prediction into the alert algorithms while keeping the acceptable level of the false alarm probability requires a larger separation between runways. Keeping or reducing the runway spacing while introducing prediction might decrease the probability of late alarm, with the penalty of a significant increase in the probability of false alarm. This was observed also in studies of the Precision Runway Monitor [97].

Using GPS to monitor approaching aircraft can reduce the required runway spacing without affecting the false and late alarm rates. The runway spacing can be even further reduced by using prediction as part of the alert algorithm. The prediction reduces the size of the detection zone down to the point where it is completely eliminated. This point provides the minimum runway spacing. The optimal prediction time at this point depends on the update interval t_f , as shown in figure 5.8.

Note that the results shown in this figure for $t_p=0$ are lower than the results presented in figure 5.4 for GPS with SA on. This is because the simulation-based approach used here includes range dependent navigation errors, as well as a GPS tracking filter which improves the accuracy of the velocity estimate. These elements are not modeled in the statistical analysis which was used to create figure 5.4.

5.5 Conclusion

GPS-based surveillance can yield a significant reduction of aircraft separation standards, provided that all aircraft periodically report their GPS-derived position. It can also reduce the required runway spacing for conducting independent parallel approaches under Instrument Meteorological Conditions.

The required runway spacing can be further reduced by using GPS-based guidance instead of ILS, and by introducing prediction into the alert algorithm. The prediction can decrease the probability of late alarm for any surveillance system. However, by using GPS-based surveillance we can insure that the *false* alarm rate would not be increased due to the prediction.

Note also that GPS-based surveillance includes aircraft identities as part of the periodical report. This provides perfect sensor resolution, whereas the limited resolution of current radar systems reduces the ability to resolve conflicts at large range. A GPS-based surveillance system can thus increase the airspace capacity and reduce airport delays, while keeping or increasing the overall safety level.

In addition to the surveillance function of the position reports, they can also be received by other nearby aircraft, thus providing each pilot with a situational awareness which is similar to that achieved in Visual Meteorological Conditions. Appropriate handling of this information could lead to an additional increase in the safety level. This is analyzed in the next chapter, which studies a GPS-based airborne collision avoidance system.

Chapter 6

Airborne Collision Avoidance

6.1 Introduction

An airborne collision avoidance system provides the pilot with information about the relative location of nearby aircraft, and possibly also with recommended collision avoidance maneuvers. The information supplied to the pilot can be divided into three levels:

Proximity warnings are indications on the relative location of nearby aircraft. They are usually presented graphically, on a traffic display.

Traffic advisories are warnings about specific aircraft that pose a threat. They are derived by a collision detection algorithm which identifies those aircraft that are more likely to create a dangerous situation.

Resolution advisories are recommended escape maneuvers that would minimize the collision risk imposed by a specific threat.

In this chapter we demonstrate the possible contribution of a GPS-based collision avoidance system to each one of these information levels. In a GPS-based system every aircraft periodically broadcasts its position as determined by an on-board GPS receiver. The aircraft receives similar data packets from all nearby aircraft, and based on own position tracks the other aircraft, identifies possible threats and issues advisory data.

An overview of the airborne collision avoidance system which is currently used by airline aircraft is provided in the next section. The traffic display of the current system, and a possible traffic display of a GPS-based system are described in section 3. Section 4 studies various collision detection algorithms, and section 5 looks at collision avoidance maneuvers. Section 6 concludes the chapter.

6.2 TCAS Overview

This section provides a brief overview of the current airborne collision avoidance system, known as TCAS (Traffic alert and Collision Avoidance System). A more detailed description of TCAS can be found in [104, 42, 43]. The algorithms and the minimum operational performance standards of TCAS are defined in [105].

6.2.1 Operation

TCAS is an airborne, ground-independent system, which is based on the use of Secondary Surveillance Radar transponders (ATCRBS Mode A/C and Mode S), already installed on all commercial and military aircraft and on most general aviation aircraft.

The TCAS equipped aircraft interrogates these transponders on all nearby aircraft (within a detection range of 30 nmi), at a nominal interval of 1 sec. The transponders respond to the interrogations as they would to a ground-based Secondary Surveillance Radar.

The range to a nearby aircraft is determined by measuring the time elapsed from the interrogation signal to receipt of the reply. If the nearby aircraft is equipped with a Mode C (altitude reporting) or Mode S transponder, altitude information is also received by the TCAS aircraft.

The range measurement and the altitude information are tracked to estimate range rate and vertical speed. These variables, along with a specifically defined protection volume around the TCAS aircraft, are used to determine whether a specific aircraft is a threat. TCAS can not issue advisories regarding aircraft which do not report their altitude (using a Mode A transponder).

TCAS design incorporates a top-mounted directional (multi element) antenna and a bottom-mounted omnidirectional antenna, but rely mainly on the top antenna since the bottom one suffers from multipath. The top antenna indicates the approximate relative bearing to the target. The bearing accuracy is 9° RMS between -10° and $+10^\circ$ elevation, and 15° RMS between 10° and 20° elevation. The bearing measurement is used for directional interrogation and for the traffic display. However, it is not accurate enough for triggering alarms and it is not used in the collision detection and avoidance logic.

6.2.2 Status

There are currently two versions of TCAS in use: TCAS I and TCAS II. If either system predicts that the safe separation between the aircraft will be violated, it issues a traffic advisory (TA), alerting the pilot to acquire the threat aircraft visually.

TCAS II can also issue resolution advisories (RA) when the threat of collision becomes higher. The resolution advisory provided by TCAS II is a recommended escape maneuver in the vertical direction, telling the pilot to either maintain or change altitude so as to avoid the traffic.

TCAS I is intended for installation in general aviation and smaller commuter aircraft. It operates at lower power and shorter range (8 nmi) than TCAS II, which is intended for use in transport category aircraft (large airline aircraft). TCAS II should have been installed by December 30, 1993 on all airline aircraft flying in US airspace and having more than 30 passenger seats. In addition, by February 9, 1995, TCAS I, at a minimum, should have been installed on all commuter airline aircraft having 10 to 30 seats [43].

Neither TCAS I nor II are able to provide resolution advisories in the horizontal plane (course change), a feature planned for TCAS III which is still under development. TCAS III is intended to provide combined lateral and vertical escape maneuvers, based on accurate bearing measurements which will be provided by a large, electronically steerable directional antenna [42].

In general, TCAS is viewed by airline pilots as an essential and important safety tool. However, the major complaint against TCAS is the large false alarm rate. Many false

alarms are reported in the vicinity of busy airports, where aircraft maneuver in close but safe proximity to each other. For example, aircraft on parallel approaches can trigger warnings, even though IFR separation is adequate [106]. Pilots are therefore required to turn off their TCAS below 400 feet [107] and when approaching certain airports, in order to avoid advisories that can be triggered by aircraft in a normal traffic pattern.

False alarms are also generated at altitude during high vertical rate encounters, as when climbing and descending aircraft are converging. TCAS looks only at the vertical rate of closure and has no way of knowing that the pilots are planning to safely level at their assigned altitudes, before their altitudes intersect. Other reported faults of TCAS are the possibility of issuing a ‘descend’ command that would lead the aircraft into the ground, and the possibility of conflicting resolution advisories that might increase the collision risk.

Finally, it should be noted that the TCAS mandate applies to less than 5% of the total number of aircraft in the United States [108]. Many of the non TCAS equipped aircraft have some type of transponder on board, allowing them to be detected by a TCAS equipped aircraft. However, only very few of the non TCAS equipped aircraft have traffic information available to them.

In the following sections we wish to demonstrate how a GPS-based collision avoidance system can alleviate some of the problems mentioned above.

6.3 Traffic Display

The traffic display, also called Cockpit Display of Traffic Information (CDTI) or Proximity Warning Indicator (PWI), provides the pilot with a graphic presentation of the relative location of nearby aircraft. It enhances the pilot’s situational awareness, and assists her in visually acquiring the threat aircraft. It is estimated that the traffic display increases the visual search effectiveness by a factor of eight [109]. The relative bearing information provided by the traffic display was indicated by airline pilots as the most useful component of the information supplied by TCAS [42]. The traffic display is also used by pilots to maintain aircraft separation when flying approaches [106], thus reducing the controllers

workload and increasing the safety of airport operations.

In this section we demonstrate how the information supplied by a GPS-based system can further improve the traffic display and increase its effect on the pilot's situational awareness.

6.3.1 TCAS II Display

Figure 6.1 depicts a typical TCAS II display. The small airplane symbol in the middle of the screen represents own aircraft. Any other transponder equipped aircraft within a selected range (5, 10, 20, or 40 miles) appears as either a diamond-, round-, or square-shaped symbol, indicating increasing threat levels. The selected range in this figure is 5 nmi, and a 2 nmi ring helps the pilot in range estimation. The relative altitude (of altitude-reporting aircraft) is indicated in hundreds of feet near the aircraft symbols. An up or down arrow indicates whether the intruder aircraft is climbing or descending. The shaded regions represent the 95% error in azimuth, assuming all aircraft are between -10° and $+10^\circ$ elevation. These regions do not appear in the actual display.

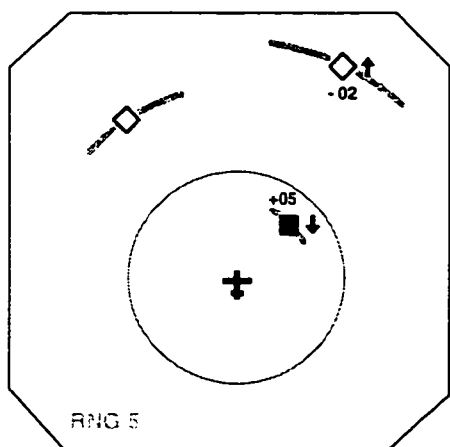


Figure 6.1: TCAS II Traffic Display

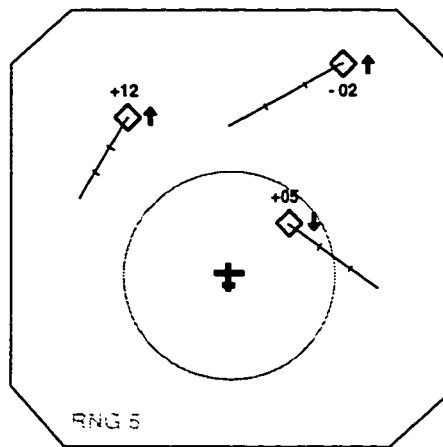


Figure 6.2: GPS-based Traffic Display

6.3.2 GPS-based Traffic Display

The GPS-based collision avoidance system provides full, three-dimensional information about the location of all aircraft. This information can be used to create graphic displays which are very different from the traditional TCAS display. A “glass-cockpit” display [110] which provides a natural perspective view of the outside world could be augmented with symbols that represent other aircraft, as well as as directives for a safe flight path in a form of an imaginary “tunnel-in-the-sky”.

If we keep the current display form, a GPS-based system can enhance it with highly accurate data, including altitude for all aircraft. The large azimuth errors are eliminated, and will not be visible in figure 6.2. Moreover, the accuracy is uniform and does not depend on the elevation angle to the target aircraft.

In addition, with GPS-based information we can compute the velocity vector of each aircraft, and add an estimated future trajectory to the traffic display, as shown in figure 6.2. The estimated future trajectory assumes constant velocity vector during some time interval, for example 30 seconds. The trajectories shown on the display are relative to own location, and they provide the pilot with information about the future relative location of each aircraft. Time marks show the progress of each aircraft, and provide the pilot with a sense about the relative velocity of each aircraft. The color of the trajectory line can be changed to indicate aircraft below and above own altitude.

The information on the relative future location of each aircraft enables the pilot to easily asses the situation, and search visually only for those aircraft that seem to pose a threat. This new feature is expected to further increase the visual search effectiveness, and to enhance the pilot’s situational awareness.

Note that the aircraft that was marked by TCAS as a threat in figure 6.1 (the square-shaped symbol) even though it was diverging, is not marked as a threat by the GPS-based system. This is due to better collision detection algorithms that are available only to a GPS-based system. Such algorithms are described in the next section.

6.4 Collision Detection

A collision detection algorithm is required to detect a possible violation of the minimum safety distance between own aircraft and an intruder, during some time interval:

$$R(t) < R_{min}, \quad 0 < t < t_w$$

where R_{min} is the minimum safety distance, and t_w is the required warning time. t_w should allow enough time for pilot and aircraft delay and for avoidance maneuver.

This test is usually accomplished by comparing the predicted separation with a range threshold:

$$R_e(t_p) < D_m \quad (6.1)$$

where R_e is the estimated range, $t_p \geq t_w$ is the prediction time, and D_m is the range threshold. It is assumed that this test is performed every computation cycle, and that violations of the safe separation which occur prior to t_p should have been detected in the previous cycle.

The estimation of the future separation is based on various measurements, and on some assumptions on the aircraft motion. The range threshold D_m and the prediction time t_p are supposed to compensate for the measurement errors and for the deviations of the aircraft from their assumed motion:

$$D_m = R_{min} + \Delta_p(t_p) + \Delta_m(t_p)$$

where Δ_p is the maximum prediction error due to aircraft motion, and Δ_m is the maximum prediction error due to non-perfect measurements [30].

6.4.1 Basic Algorithms

The various algorithms for collision detection differ in the assumptions they make on the aircraft motion. We can identify three possible sets of assumptions:

1. Constant velocity collision course.

2. Constant aircraft velocity.
3. Bounded turn rate at constant speed.

A collision detection algorithm which is based on the first set of assumptions requires only range measurements. This algorithm is therefore the basis of the TCAS collision detection logic. Algorithms which are based on the other assumptions require full three-dimensional position measurements of both aircraft and can not be done with TCAS. These algorithms were usually associated with ground-based ATC systems, but now can be used with an airborne system which is provided with the required three-dimensional information. The various algorithms are discussed now in detail.

Constant velocity collision course

On a constant velocity collision course, the range rate \dot{R} is constant. Based on that, the range test (Eq. 6.1) is

$$R_e(t_p) = R_o + \dot{R}_o t_p < D_m \quad (6.2)$$

where R_o and \dot{R}_o are the current range and range rate (both scalars). Rearranging, we get:

$$\frac{R_o - D_m}{-\dot{R}_o} < t_p \quad (6.3)$$

This test is known as the Modified TAU criterion, and was the basis of early TCAS algorithms [31]. In the TCAS implementation, the range threshold D_m provides protection only against relative acceleration of the aircraft:

$$D_m = \frac{1}{2} a_r t_p^2 \quad (6.4)$$

It also ensures that the aircraft will not drift closer than that distance without receiving an alarm. Note that D_m does not include any protection against measurement errors.

The value of the relative acceleration used in TCAS is $a_r = 1/3g$, and the value of the prediction time t_p varies with altitude. Between 10 Kft and 20 Kft, $t_p = 30$ seconds, and the appropriate range threshold is $D_m = 0.8$ nmi. This value of t_p is used in the computation of

resolution advisories (RA). Traffic advisories (TA) will be issued 15 seconds earlier, using the same range test with $t_p = 45$ seconds.

The range test (Eq. 6.3) defines an imaginary protection volume around own aircraft. Whenever a threat penetrates this volume an alarm is issued. The protection volume is best viewed in the collision plane [31], which is defined by the range vector \bar{R} and the relative velocity vector \bar{V}_R . A set of Cartesian axes is chosen with own aircraft at the origin, and the x -axis aligned parallel to the \bar{V}_R (see figure 6.3).

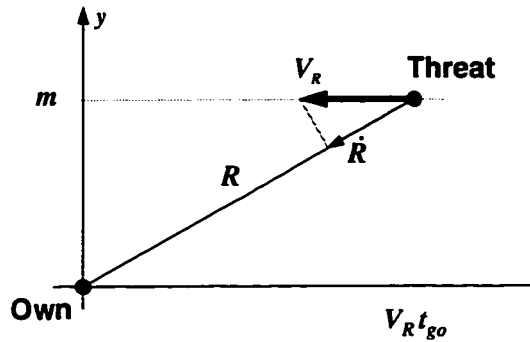
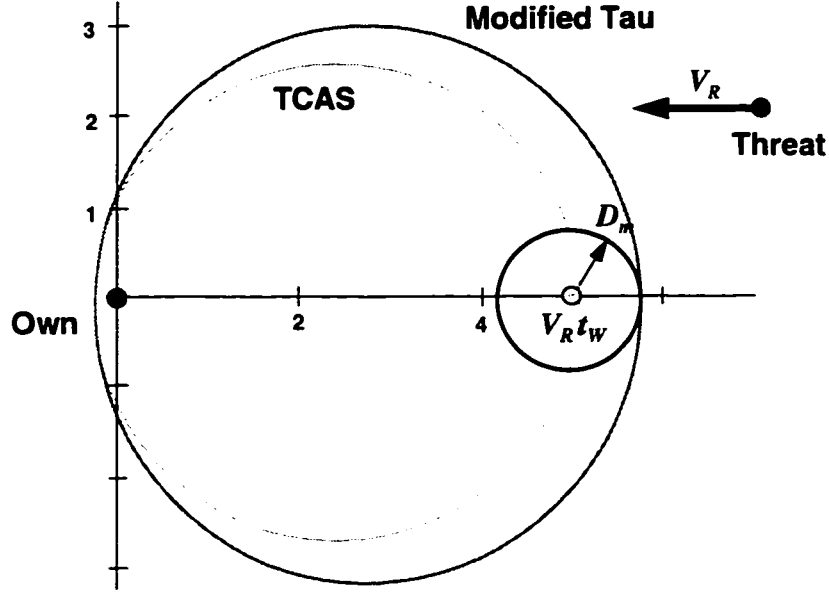


Figure 6.3: Collision Plane

If the velocity vectors remain constant, the collision plane orientation is fixed, and a threat will move in the collision plane on a straight line, parallel to the x axis. The y coordinate of the threat is therefore the range at the closest point of approach (CPA), or the miss distance, and the x coordinate is the time of flight to the CPA, multiplied by the closing velocity.

Figure 6.4 compares protection volumes of several collision detection algorithms, for $V_R = 600$ knots. The protection volume defined by equation 6.3 is the outer circle in this figure. The current version of TCAS varies the distance threshold with range [33]:

$$\frac{R_o - \frac{D_m}{R_o}}{-\dot{R}_o} < t_p \quad (6.5)$$

Figure 6.4: **Protection Volumes**

Calculated for $V_R=600$ knot, $t_p=30$ seconds and $a_r=1/3g$. The appropriate D_m is 0.8 nmi. The axes are in nmi.

The effect of this modification is to reduce slightly the size of the protection volume, as shown in figure 6.4.

Constant aircraft velocity

When aircraft move in constant velocity, their relative velocity vector is constant. The range test in this case is

$$R_e(t_p) = \|\bar{R}_o + \bar{V}_R t_p\| < D_m \quad (6.6)$$

where \bar{R}_o is the current range vector, and \bar{V}_R is the relative velocity vector

$$\bar{V}_R = \bar{V}_{intruder} - \bar{V}_{own} \quad (6.7)$$

This test is identical to the standard ground-based collision detection algorithm [35, 111], which is based on three-dimensional positioning information and looks for overlap of cylindrical volumes of airspace, constructed about the predicted location of each aircraft. The same approach was suggested also for GPS-based airborne formation control [74].

The protection volume in this case is a circle with radius D_m , centered at $[V_R t_p, 0]$ on the collision plane. Figure 6.4 depicts this protection volume together with the protection volume generated by TCAS. The figure shows that TCAS can issue alarms in cases where the miss distance is as large as 3 nmi, whereas the constant velocity range test (Eq. 6.6) will not issue alarms when the miss distance is greater than D_m .

Alarms that are generated when the miss distance is greater than D_m can be considered as false alarms. Figure 6.4 clearly shows the large reduction in the probability of false alarm that can be realized when using a collision detection algorithm which is based on three-dimensional positioning information.

Constant velocity Miss/Tgo

By assuming constant velocity motion and using three-dimensional positioning information, we can get directly the location of any threat on the collision plane, and construct protection volumes with arbitrary shape.

The x coordinate on the collision plane is proportional to t_{go} , which is the time to the point of closest approach:

$$t_{go} = \frac{\bar{R} \cdot \bar{1}_{V_R}}{V_R} \quad (6.8)$$

where $\bar{1}_{V_R}$ is a unit vector in the direction of \bar{V}_R . The y coordinate is the range at the CPA, or the minimum miss distance. It is given by the size of the miss distance vector:

$$\bar{m} = \bar{1}_{V_R} \times (\bar{R} \times \bar{1}_{V_R}) = \bar{R} + \bar{V}_R t_{go} \quad (6.9)$$

The conditions

$$m < D_m \quad \text{and} \quad t_{go} < t_p \quad (6.10)$$

are sufficient to declare a threat when the aircraft move in constant velocity. The protection volume defined by these conditions is a line on the collision plane, stretched between the points $[V_R t_p, -D_m]$ and $[V_R t_p, D_m]$. If the assumption of constant velocity is kept, a collision detection algorithm which is based on this protection volume will provide timely alarms exactly t_p seconds before CPA. No alarms will be issued if the miss distance is greater than D_m .

However, if even one of the aircraft maneuvers, the conditions (6.10) are not sufficient any more, and alarms which are based on these conditions alone will be late in most cases, due to the poor estimation of t_{go} . Nevertheless, we can make use of the observation that the miss distance is constant if the aircraft move in constant velocity. When the derivative of the miss distance is negative, we assume that at least one of the aircraft involved is maneuvering so as to decrease the miss distance. We then estimate the time it would take the miss distance to reach a certain minimum value. If this time is within pre defined limits, an alarm is issued even if the current miss distance is greater than D_m . If the miss distance is increasing, we assume that the aircraft are maneuvering away from the collision course, and the size of D_m can be safely decreased in this case.

The complete algorithm (extended to three dimensions) and a numerical evaluation of its performance will be described below, in section 6.4.2.

Bounded turn rate at constant speed

Assume that the aircraft motion during the prediction interval consists of a coordinated turn (constant speed and turn rate), followed by a straight line path. The aircraft location at the end of the prediction interval is given by

$$x = x_o + \frac{V}{\omega} [\sin(\gamma_o + \omega t_1) - \sin \gamma_o] + V(t_p - t_1) \cos(\gamma_o + \omega t_1) \quad (6.11)$$

$$y = y_o - \frac{V}{\omega} [\cos(\gamma_o + \omega t_1) - \cos \gamma_o] + V(t_p - t_1) \sin(\gamma_o + \omega t_1) \quad (6.12)$$

where x_o , y_o and γ_o are the current location and heading. The aircraft speed is V , ω is the turn rate, $|\omega| < \omega_{max}$, and t_1 is the switching time from the turn phase of the flight to the straight line phase, $0 < t_1 < t_p$.

If we further assume that the aircraft is turning at the maximum turn rate $\omega = \pm\omega_{max}$, equations 6.11 and 6.12 define the boundary of the reachability region, which is the set of all points that can be reached by the aircraft during the prediction interval. A possible collision detection algorithm can look for overlap of the reachability regions attached to each aircraft [112, 36] (see figure 6.5).

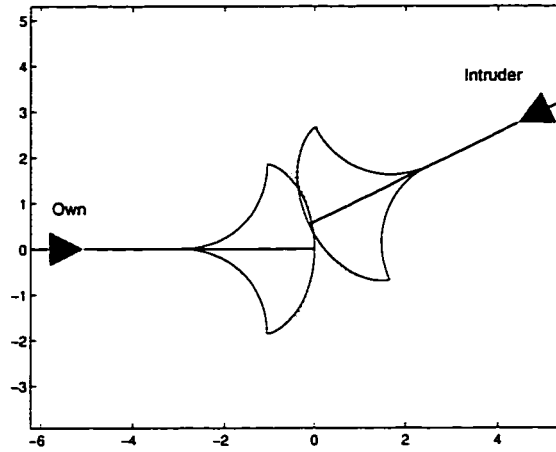


Figure 6.5: **Reachability Regions**

Based on 350 knot velocity, $3^\circ/\text{sec}$ maximum turn rate, and 30 seconds prediction time. The axes are in nmi.

This can be done by solving for the switching times that will satisfy intersection of the boundaries, or by looking for the switching times that will minimize the distance between the two reachability regions. The resulting equations in both cases are rather complicated, and their real time solution might be time consuming. The solution suggested by Dear and Sherif [113, 114] is based on checking the projections of the reachability regions on a set of Cartesian axes. It is easy to show that this algorithm will generate unacceptable alarms in certain geometries, where the reachability regions do not overlap, but their projections do.

In order to evaluate the performance of a reachability-based collision detection algorithm, we approximate the reachability region by a circular wedge (see figure 6.5). The wedge radius is Vt_p and it is limited by the angles

$$\gamma_o \pm \tan^{-1}\left(\frac{1 - \cos(\omega_{max}t_p)}{\sin(\omega_{max}t_p)}\right)$$

The test for overlap of two circular wedges is relatively simple, and it provides us with a good approximation for the performance of this algorithm.

6.4.2 Analysis

The collision detection algorithms described previously are evaluated by a Monte-Carlo simulation of random encounters between pairs of aircraft. The aircraft parameters (velocity, maneuver timing and capability, vertical rate etc.) are randomly selected to represent a realistic distribution of encounters. The encounter geometry is set such that the final miss distance with no avoidance maneuvers is uniformly distributed. The simulation and the relevant parameters will be described in detail in Appendix G.3. The algorithm evaluation is based on the following two variables:

- The probability of false alarm $P_{fa}(\rho)$, defined as the probability that an alarm was given, and the miss distance was greater than ρ .
- The probability of late alarm $P_{la}(\tau)$, defined as the probability that an alarm was given less than τ seconds before the actual CPA.

The probability of false alarm is obtained by integrating the distribution of the miss distance in the cases where an alarm was given, and normalizing by the total number of runs. The probability of late alarm is obtained by integrating the distribution of the time interval between the alarm moment and the CPA, and normalizing by the number of alarms.

Note the difference between the two definitions. The probability of false alarm is the total probability of getting an alarm *and* having a large miss distance. The probability of late alarm is the probability that an alarm is late, *given* that an alarm was issued. This definition of P_{la} prevents a biased representation of the risk associated with late alarms, when a certain algorithm reduces the overall number of alarms but issues them later than acceptable.

Planar encounters

Figure 6.6 depicts the probability of false alarm as function of the miss distance, for the collision detection algorithms described in the previous section. The environment modeled in this case describes planar encounters with constant velocity aircraft. The only randomness is in the encounter geometry and the aircraft speeds. There are no measurement errors, nor wind disturbances.

The reachability-based algorithm yields the largest number of false alarms. The constant velocity range test and the miss/Tgo algorithm provide almost similar false alarm probabilities, both lower than the false alarm probability of the TCAS algorithm. As expected, no alarms are generated by these algorithms when the miss distance is greater than D_m , here equal to 0.8 nmi.

The probability of late alarm for the same environment is depicted in figure 6.7, as a function of the time to CPA. The probability of late alarm is higher for TCAS, and it is very low for the constant velocity range test and the miss/Tgo algorithm. Both provide timely alarms, exactly t_p seconds before CPA. Here t_p is equal to 30 seconds.

Figures 6.6 and 6.7 show that algorithms which are based on the constant velocity assumption and use three dimensional positioning information can significantly reduce both the probability of false alarm and the probability of late alarm, provided that the constant velocity assumption is indeed being kept.

The effect of random aircraft maneuvers on the probability of false alarm is shown in figure 6.8. The aircraft maneuver can vary in magnitude and duration, as described in Appendix G.3. The probability of late alarm for the same environment is depicted in figure 6.9. The reachability-based algorithm provides the highest number of false alarms and the lowest number of late alarms. This demonstrates the basic trend in collision detection algorithms: a large protection volume can decrease the probability of late alarm, but would increase the probability of false alarm.

The constant velocity range test shows a relatively large number of late alarms. It appears that testing for $R(t_p) < D_m$ can miss many encounters in which at least one of

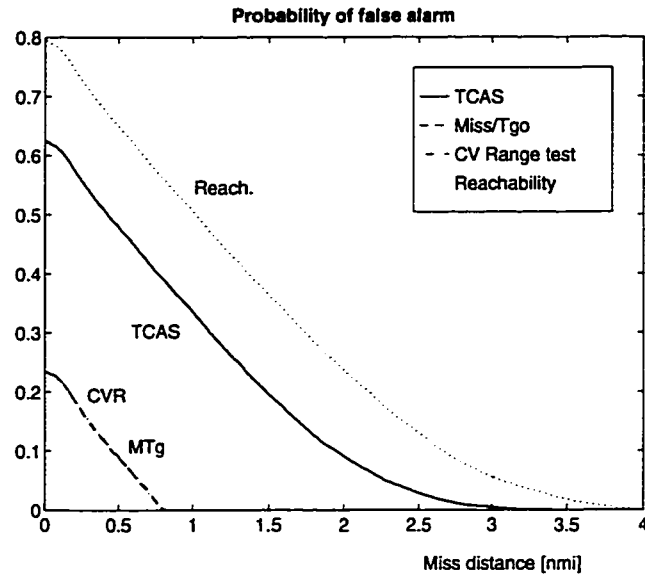


Figure 6.6: Probability of False Alarm in Constant Velocity, Planar Encounters

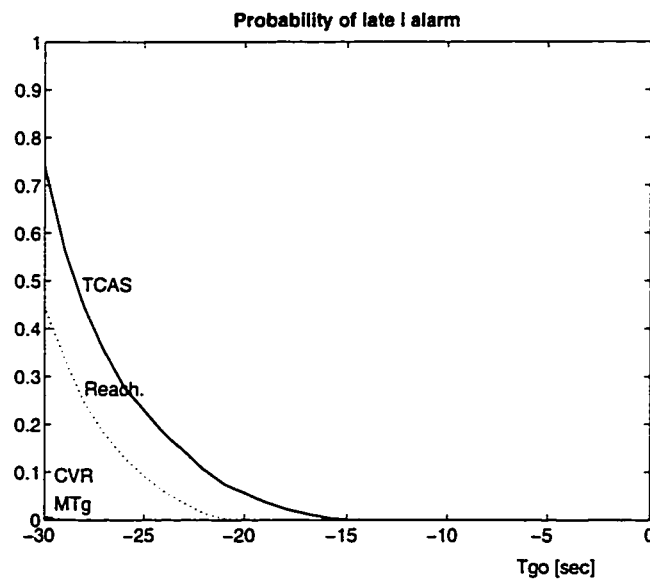


Figure 6.7: Probability of Late Alarm in Constant Velocity, Planar Encounters

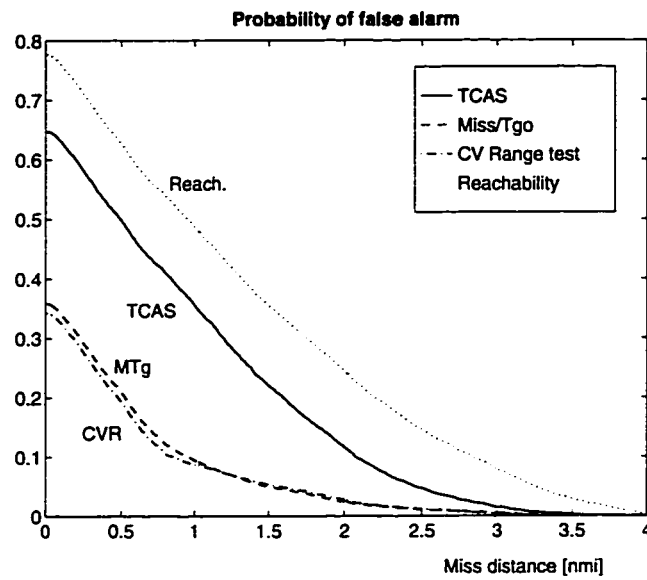


Figure 6.8: Probability of False Alarm in Planar Encounters

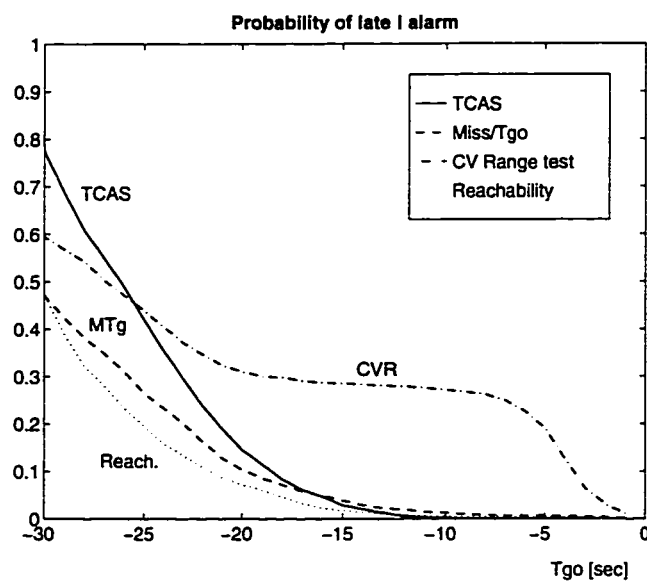


Figure 6.9: Probability of Late Alarm in Planar Encounters

the aircraft is maneuvering. In those cases the projected range might be larger than the threshold, while the current range is very small. The algorithm declares an alarm in these cases only when the actual range is smaller than the threshold. This occurs immediately before the CPA, and does not provide enough time for avoidance maneuver. The threshold size D_m can be increased to alleviate this problem, but this would increase the probability of false alarm.

The miss/Tgo algorithm provides the best combination of low false alarm rate and low late alarm rate. We will now examine its performance in a more realistic environment.

3-D encounters

The collision detection algorithms and the analysis described previously assumed that both aircraft move in the same horizontal plane. We will now present an extension of the algorithms to the general 3-D case, and then analyze their performance.

TCAS logic provides an alarm if both a range threshold and an altitude threshold are crossed. The range threshold is crossed if either the current range is too small ($R_o < D_m$) or the approximate time to the CPA is too small (Eq. 6.5). The altitude threshold is crossed if either the time to coaltitude or the altitude separation are too low [104].

The miss/Tgo logic starts with estimating the time to CPA and the miss distance (Equations 6.8 and 6.9). Next, the miss distance derivative is calculated:

$$\dot{m} = (m_o - m_{-1})/T \quad (6.13)$$

where m_o is the size of the current miss distance vector, m_{-1} is the miss from the previous computation cycle, and T is the computation time step. If the miss distance is decreasing, we estimate the time it would take it to reach a minimum value m_{min} :

$$t_n = \begin{cases} (m_{min} - m_o)/\dot{m} & \text{if } \dot{m} < -\dot{m}_{thr} \\ 0 & \text{otherwise} \end{cases} \quad (6.14)$$

The threshold \dot{m}_{thr} protects against variations in the miss distance due to measurement errors and small random aircraft accelerations. The algorithm issues an alarm if the following

set of conditions is true:

$$t_{go} < t_p \text{ and } \left[\begin{array}{l} \dot{m} < \dot{m}_{thr} \text{ and } |m_z| < A_{lim} \text{ and } [m_{xy} < D_m \text{ or } t_{min} < t_n < t_{max}] \\ \text{or} \\ m_{xy} < D_{m,1} \text{ and } m_z < A_{lim,1} \end{array} \right] \quad (6.15)$$

m_z and m_{xy} are the vertical and horizontal components of the miss distance vector \bar{m} . The thresholds $D_m=0.8$ nmi and $A_{lim}=750$ feet are the parameters used by TCAS II, and we keep them for the sake of fair comparison between the algorithms. $D_{m,1}=0.1$ nmi and $A_{lim,1}=500$ feet are the reduced thresholds for the case of increasing miss distance. The other parameters are: $m_{min}=0$, $\dot{m}_{thr}=0.01$ nmi/sec, $t_p=35$ seconds, $t_{min}=10$ seconds and $t_{max}=25$ seconds. These parameters were optimized for the environment modeled in the simulation. However, the performance of this algorithm was shown to be insensitive to reasonable variations in these parameters.

The environment modeled in the simulation allows the aircraft to climb or descend, according to the distribution detailed in Appendix G.3. The aircraft are subjected to random wind disturbances, modeled by a first order Gauss-Markov process.

Figures 6.10 and 6.11 show the probability of false alarm and the probability of late alarm for the TCAS algorithm and the miss/Tgo algorithm. The TCAS algorithm uses perfect measurements, whereas the miss/Tgo algorithm uses position measurements which are corrupted by actual GPS measurement errors. We assume that own position measurements are available every computation cycle (1 second interval), whereas the intruder's position measurements are transmitted every t_f seconds, and are received with a certain probability which models the interference in the radio data link (see Appendix G.3 for details).

Figures 6.10 and 6.11 depict the performance of the miss/Tgo algorithm for $t_f=1, 2$ and 5 seconds. The figures show that the probabilities of false and late alarm caused by the miss/Tgo algorithm with GPS measurement errors are lower than the probabilities caused by the TCAS algorithm with no measurement errors, provided that the update rate is smaller than 5 seconds.

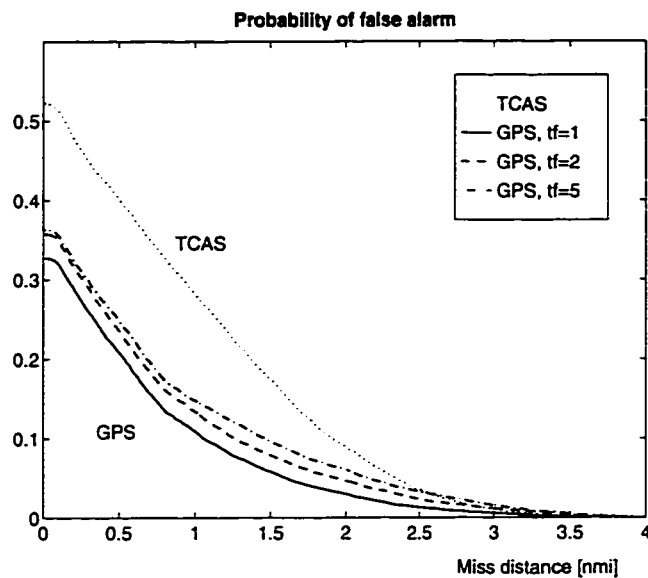


Figure 6.10: Probability of False Alarm, 3-D Encounters

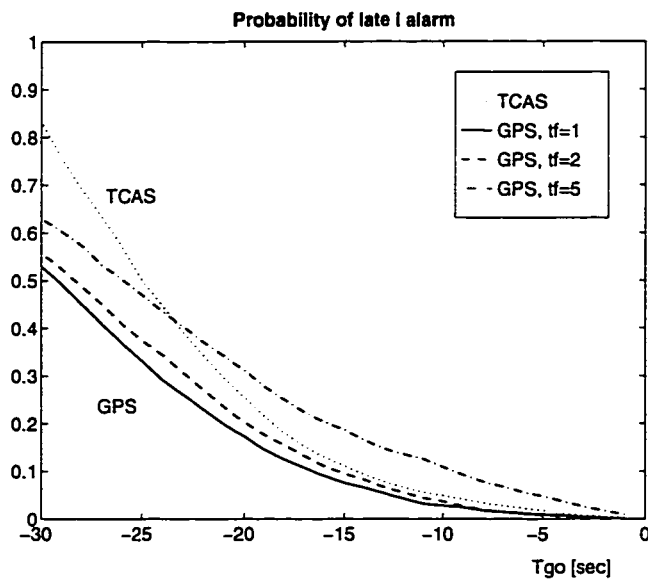


Figure 6.11: Probability of Late Alarm, 3-D Encounters

Note that this improvement in the false alarm rate can not be realized just by adding bearing measurement to the current range-only measurement, unless the aircraft follow only straight line paths [115, 116]. If this is the case, the miss/Tgo algorithm can provide perfect performance with zero false alarms, as demonstrated in figure 6.6. The less impressive performance shown in figure 6.10 is due to the lack of knowledge on future maneuvers of both aircraft. This is the major limitation on any collision detection algorithm.

6.5 Collision Avoidance

Once a conflict is detected, the airborne collision avoidance system should alarm the pilot and provide him with directives for maneuver that avoids the incoming traffic. The escape maneuver is designed so that sufficient separation is generated if only one of the aircraft follows the advisory [117]. The maneuver is accomplished by acceleration which can be applied in the following ways:

- Longitudinal acceleration (speed change) - too small to be effective, unless it acts over very long periods of time. It is therefore not very useful for collision avoidance.
- Normal acceleration in the vertical direction (climb / descend) - natural for aircraft initially in level flight or normal ascent or descent. Can be applied relatively quickly since very little attitude change is required. The limiting factor on the vertical displacement is the allowable rate of climb or descent, rather than acceleration.
- Lateral acceleration - requires attitude change (roll) which delays the maneuver start point. Level turns are therefore more effective than vertical acceleration only if escape time exceeds 30 sec [29]. The displacement produced by the lateral maneuver does not translate directly to miss distance, because of possible conflicting lateral acceleration of the intruder.

TCAS II provides only vertical maneuver directives. Its logic estimates the intruder's altitude at the CPA, assuming that the intruder will keep its current vertical rate, and that the time to CPA is given by equation 6.5. Note that this equation estimates the time to

CPA for constant velocity aircraft, and the actual time to CPA would be different due to the avoidance maneuver.

Own aircraft's altitude at the CPA is predicted for standard vertical rate of 1500 ft/min, both up and down. TCAS allows 5 seconds for pilot response, and assumes vertical acceleration of 0.25g. The TCAS logic then selects the maneuver sense that provides maximum vertical separation. The selection is communicated with the intruder by using the Mode S data link. This ensures that resolution advisories between two conflicting TCAS-equipped aircraft will be coordinated in opposite fashion.

Some of the options for a new collision avoidance scheme which relies on full three-dimensional information are:

- Compute $R(t_{go})$ for various vertical and lateral maneuver combinations, assuming that the intruder moves at constant velocity. Select the maneuver combination that maximizes $R(t_{go})$.
- Solve for the maneuver which maximizes the miss distance, for any permissible maneuver of the intruder.

The first option is simply a three dimensional extension of the TCAS logic, where t_{go} is obtained from equation 6.8. We will check out all possible combinations of {climb, descend, maintain vertical rate} and {turn left, turn right, keep current heading}. The modeling equations in the collision avoidance logic assume that the vertical maneuver consists of 5 seconds delay, and a 0.25g acceleration to +1500 ft/min or -1500 ft/min. The modeling of the horizontal maneuver assumes a 10 seconds delay, and 0.5g acceleration to 30° heading change [34]. This approximates a 6°/sec roll rate to 30° bank. When checking this algorithm in the Monte Carlo simulation, we assumed that the actual aircraft motion is described by a set of random variables, with mean equal to the parameters mentioned above, and distribution as described in Appendix G.3.

The second, more general option requires the solution of a pursuit - evasion differential game between the aircraft. The equations of motion should take into account the delay in

response to a maneuver command, as well as the constraints on the aircraft acceleration and vertical speed.

The solution of such a game is beyond the scope of this work. However, we can use a less restricting set of assumptions to obtain a sub-optimal avoidance strategy. If we assume that both aircraft can apply instantaneous, unlimited acceleration in any direction in space, then the optimal avoidance law would be to apply acceleration in the direction opposite to the miss distance vector [118]. This acceleration should provide the maximum miss distance against the worst possible intruder acceleration.

To apply this avoidance law, we can command the aircraft to climb or descend according to the sign of the vertical component of the miss distance vector:

$$\dot{h}_{com} = -1500 \text{ ft/min} \cdot \text{sign } m_z \quad (6.16)$$

The aircraft will be required to turn to the left or to the right according to the sign of the angle between the horizontal projections of the miss distance vector and the velocity vector:

$$\gamma_{com} = 30^\circ \cdot \text{sign } n_z, \quad \bar{n} \triangleq \bar{m} \times \bar{l}_V \quad (6.17)$$

where γ_{com} is the required heading change and \bar{l}_V is a unit vector in the direction of own velocity vector.

Our simulation studies showed that the vertical part of this algorithm does not perform well in cases of high initial vertical rate. For example, if the aircraft is already climbing at a vertical rate which is close to the limit of 1500 ft/min, a descend command might be better than a climb command even if the direction of the miss distance vector points otherwise. We suggest therefore to combine the horizontal part of this algorithm with a vertical modeling of the aircraft path, similar to the TCAS logic.

We found out that this strategy yields almost identical results to those obtained when evaluating all possible maneuver combinations. Using the miss distance vector as a pointer to the direction of avoidance has several advantages: first, it is much less computationally intensive than the modeling of all possible maneuver combinations. Furthermore, it reduces the need for aircraft to aircraft coordination. If both aircraft use the same algorithm, the miss distance vector is guaranteed by its nature to provide opposite maneuver commands.

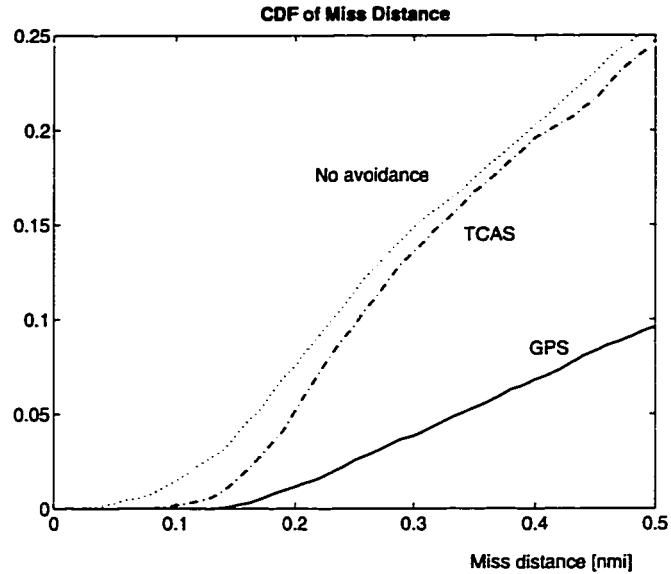


Figure 6.12: CDF of Miss Distance

Figure 6.12 shows the cumulative distribution of the miss distance with and without the avoidance maneuver. The cumulative distribution is the probability that the miss distance is smaller than x . The distribution without avoidance is determined by the environment modeled in the simulation. The distribution for the GPS-based collision avoidance shows clearly the effectiveness of this scheme when compared to TCAS.

A more graphic way to present this result is shown in figure 6.13. This figure shows the spatial distribution of the CPA with and without avoidance. Both TCAS and the GPS-based algorithm use the same basic parameters for determining a risk: a horizontal distance of 0.8 nmi, and a vertical distance of 750 ft. However, only the GPS-based algorithm succeeds in moving the CPA outside of this area, without calling for unnecessary maneuvers.

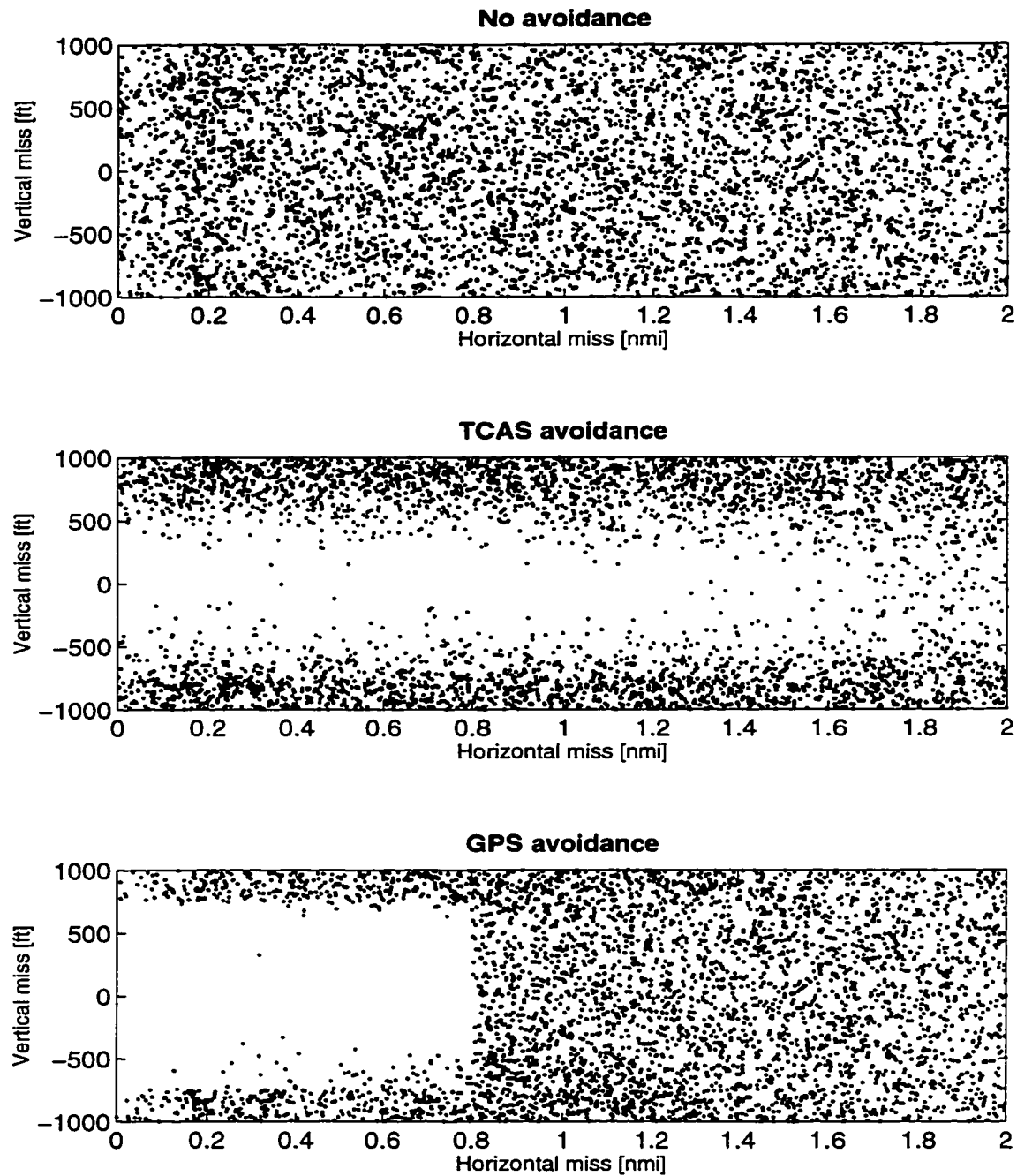


Figure 6.13: Distribution of the Closest Point of Approach (CPA) Distance

6.6 Conclusion

The three-dimensional positioning information provided by GPS, coupled with the appropriate algorithms, can significantly enhance the performance of the current airborne collision avoidance system. The algorithms developed here are based on the miss distance vector: its size and rate of change can determine whether a collision is likely, and it is pointing to the direction of the recommended escape maneuver. These algorithms yielded better performance than traditional methods which look at the reachability regions of the aircraft or at their predicted range.

The GPS-based system can thus issue highly effective avoidance commands, while lowering both the probability of false alarm and the probability of late alarm. Furthermore, a GPS-based traffic display could provide General Aviation aircraft with an affordable collision detection system, even without the additional features of traffic and resolution advisories.

Such a traffic display could also be used to reduce separation standards between aircraft, by providing each pilot with information on nearby traffic. This information, currently available only under Visual Meteorological Conditions, could be used for example to reduce the required spacing between parallel runways which allows independent approaches under Instrument Meteorological Conditions. The responsibility for issuing an alarm would be transferred to the pilot, but the delay associated with the controllers reaction and communication would be eliminated, thus reducing the required separation.

Chapter 7

Conclusion

The growth pace of air travel, both international and domestic, is so fast that it is outstripping the capacities of runways and air traffic control systems all over the world. Consequently, the jet age could become one of congestion, delays, higher costs and possibly diminished safety. It is the combination of two technologies, namely satellite navigation and digital communications that can be used to alleviate many of these problems.

As was shown in this dissertation, periodic transmissions of aircraft position, derived by an on-board GPS receiver could replace the traditional Air Traffic Control (ATC) surveillance methods. This technique can provide ATC with highly accurate surveillance information, even in areas which are not covered today by radar. It has the potential to offer increased safety and capacity, and to allow more efficient operation of aircraft at a reduced cost.

The contributions of this work to the understanding of a GPS-based surveillance system can be summarized in two areas:

- Analysis of basic relationships and requirements, including derivation of appropriate algorithms.
- Evaluation of possible benefits and effects on certain aircraft operations.

As part of the first area, I have derived a basic framework for analysis of spatial Time

Division Multiple Access (TDMA) protocols, where messages are sent periodically by a large number of aircraft distributed on a plane. The main result of this analysis is the relationship between the channel capacity and the detection range, for both random and organized protocols, under various models for signal capture. In addition, I have examined several self-organized communication protocols using a detailed simulation of communication in random air traffic. This analysis framework was used to evaluate the maximum possible capacity of several suggested communication architectures. It was shown that a “random reporting” protocol at the Mode-S frequency is a superior design to a perfectly organized protocol at a VHF frequency, due to the higher capacity of the higher frequency Mode-S channel, and the reduced complexity of the random protocol.

The position reports should be received and tracked by the ground-based ATC center. I have designed an adaptive tracking filter, specifically matched to track GPS position reports received through an imperfect radio data link. Satellite constellation changes and message interference in the radio channel were shown to be important factors in the filter design and evaluation procedure. This work also provided a general solution for optimal tracking filter design in systems with high order correlated measurement noise, including a consistent initialization procedure. In addition, I have developed new algorithms for aircraft collision detection and avoidance, based on the miss distance vector. These algorithms realize the full potential of the three dimensional position and velocity information provided by GPS.

As part of the *evaluation* area of this work, I have demonstrated the significant improvement in tracking accuracy that can be achieved by a GPS-based surveillance system with the appropriate tracking algorithm, as compared to the tracking accuracy of modern ATC radar trackers. The tracking accuracy was estimated by using actual GPS measurement errors, combined with simulated aircraft motion on several representative trajectories.

I have shown that GPS-based surveillance can yield a significant reduction of aircraft separation standards in the domestic airspace. GPS-based surveillance can also reduce the required runway spacing for conducting independent parallel approaches under Instrument Meteorological Conditions. It was also shown that blunder prediction, based on a GPS-derived velocity vector, can further reduce the required runway spacing, without increasing

the false alarm rate. This study called for accurate statistical representation of GPS position measurement errors, achieved here by a Gaussian-mixture distribution function.

In addition, it was verified that a GPS-based collision avoidance system can issue highly effective avoidance commands, while lowering both the probability of false alarm and the probability of late alarm. The performance of this system was evaluated through an extensive simulation of a free-flight environment.

Recommendations for Future Research

Following are several suggestions for future areas of work on GPS-based aircraft surveillance and collision avoidance.

- *Adaptive reporting rate*

The aircraft reporting rate, considered in this work to be constant, could be made adaptive to the number of nearby aircraft, collision danger or aircraft flight phase (e.g. constant velocity, maneuvering, or approach). This has the potential to increase the channel capacity of any communication protocol, at a price of increased transceiver complexity.

- *Aircraft-matched tracking filter*

The traditional location of the tracking filter is on the ground, where the current position sensor - the radar - is located. However, when using an airborne sensor, each aircraft can track its own position and broadcast its estimated or predicted state. This will enable each aircraft to use a filter that matches its GPS receiver and flight control characteristics. It will reduce the computational load at the ATC center and will eliminate the tracking errors caused by the data link.

- *3-D separation standards*

The only separation standards considered in this were lateral. A GPS-based surveillance system has the capacity to reduce also vertical and in-trail separation, thus further increasing air space capacity. This calls for more research on the behavior

of wake vortices to obviate the worst-case assumptions which generate the current conservative spacing between aircraft.

- *TCAS effect on separation standards*

Additional reduction in separation standards could be achieved through the use of a TCAS-like display to provide each pilot with information on nearby traffic, similar to the information available in VFR conditions. A GPS-based TCAS could also be used to detect windshear in the approach path, and report its location to the following aircraft.

- *Statistical collision detection*

The collision detection algorithm described here is deterministic: it compares a projected range or miss distance to a certain threshold. The projected range is based on some deterministic assumption on the aircraft future motion. Another possible collision detection algorithm could calculate the *probability* that the miss distance would be smaller than some safety distance, and alert the pilot accordingly. The aircraft future motion could be described in this case by some probabilistic model, such as a Markov chain.

- *Performance standards*

This work was considered only with the *accuracy* of the new surveillance system. The integrity, availability and continuity of the total surveillance system should also be defined and analyzed, and the additional steps which may be required to achieve an acceptable level of performance should be identified. In addition, the increased coupling between navigation and surveillance should be considered in the overall safety of the air space system.

Appendix A

ADS Message Format and Reporting Rate

This appendix describes the message format and reporting rate of ADS and several versions of ADS-B.

A.1 ADS

The ICAO FANS committee has defined three ADS message formats [1, 28]. The *basic* report provides surveillance data represented by current aircraft latitude, longitude, altitude and time. The basic report includes also the ICAO identification of the aircraft (i.e., the flight ID for commercial aircraft and the tail number for general aviation aircraft [12]), and a Figure of Merit which provides information on the characteristics of the navigation system employed to generate the position report.

The *extended* ADS report will consist mainly of intent and performance data. The intent data is a report of the next two waypoints, extracted from the aircraft's Flight Management System. Performance data will include the current heading, ground speed and vertical speed. The third message format is the *associated* ADS report, which consists of meteorological data, including wind velocity and temperature.

Basic ADS report:

<i>Data Elements</i>	<i>Bits</i>	<i>Resolution</i>
Latitude/longitude	42	0.0125 arc min
Altitude	16	8 ft
Time	15	0.125 sec
Figure of Merit	7	
ADS capability	16	
ICAO aircraft ID	48	8 × 6-bit char.

Extended ADS report:

<i>Data Elements</i>	<i>Bits</i>	<i>Resolution</i>
Next waypoint	42	0.0125 arc min
Estimated altitude at next waypoint	16	8 ft
Next+1 waypoint	42	0.0125 arc min
Estimated altitude at (next+1) waypoint	16	8 ft
Track/Heading	13	0.1°
IAS/Mach	14	0.5 kt / 0.001
Vertical rate	12	0.08 m/s

Associated ADS report:

<i>Data Elements</i>	<i>Bits</i>	<i>Resolution</i>
Wind speed	9	1 knot
Wind direction	9	0.7°
Temperature	12	0.25°C

Table A.1: ADS message formats

The extended and associated reports will be available on request only, whereas the basic report will be sent automatically at the required reporting rate. The FANS committee suggested that the nominal reporting rate in oceanic and remote areas should be every five minutes [45]. This would be increased to every 30 seconds in cases where two aircraft are closer together. In the domestic airspace, the reporting rate is expected to approximate radar scan rate, which is typically 12 seconds for en-route traffic and 4.8 seconds in terminal airspace. Aircraft flying through sparsely occupied airspace will probably be asked to report less frequently.

A.2 GNSS Transponder

A system designed and tested by the Swedish Civil Aviation Administration [5-8] proposes a 256-bit autonomous position report, organized as follows:

Autonomous position report:

<i>Data Elements</i>	<i>Bits</i>	<i>Resolution</i>
Synchronization preamble	40	
Start frames	16	
Message type	8	
ICAO aircraft ID	48	8 × 6-bit char.
Latitude	24	1/1000 min.
Longitude	25	1/1000 min.
Speed	11	2 knots
Heading	12	0.1°
Altitude	12	16 ft
Time mark	6	1 sec
Climb/descend	2	
Communication status	12	
Check sums	16	
Stop frame	8	
Pause	16	

Table A.2: GNSS transponder message format

One of the fields in this message (the 12-bit communication status field) includes information on the future time slot selection of the aircraft, as well as indication whether the GPS receiver which was used to generate the position report is differentially assisted. The nominal reporting rate of the autonomous position report is once per minute.

A.3 ADS Mode-S (GPS Squitter)

This approach, proposed by MIT's Lincoln Laboratory [9-13], is based on using a modified Mode-S transponder to broadcast aircraft identity and position. The message format is limited therefore by the Mode-S message protocol, which defines a 112-bit "extended squitter", out of which only 56 bits are allotted for the actual message.

Two types of messages were proposed for an airborne user, one for surveillance and one for flight identification. The airborne position format contains the aircraft surveillance data, as well as a 5-bit message type/Figure of Merit field which describes the accuracy of the position reports. The identification message provides the 48-bit ICAO identification of the aircraft. Note that both the position format and the identification format contain the aircraft 24-bit Mode-S address as part of the basic squitter format. The surveillance message is sent once every 0.5 sec., and the identification message is sent once every 5 sec.

Extended Mode-S squitter format:

<i>Data Elements</i>	<i>Bits</i>
Control	8
Mode-S address	24
Message	56
Parity	24

Identification message:

<i>Data Elements</i>	<i>Bits</i>	<i>Resolution</i>
Message type	5	
Spare	3	
ICAO aircraft ID	48	8 × 6-bit char.

Airborne position message:

<i>Data Elements</i>	<i>Bits</i>	<i>Resolution</i>
Message type/Figure of Merit	5	
Status	2	
Spare	2	
Turn indicator	1	
Baro. altitude	11	25 ft
Time	1	1 sec
Latitude	17	5.2 m
Longitude	17	5.3 m – 18.4 m

Table A.3: ADS Mode-S message format

A.4 ADS-B Extended Squitter

The message format for ADS-B is currently under development by the Radio Technical Commission for Aviation (RTCA) Special Committee 186, as well as the ICAO Secondary Surveillance Radar Improvements and Collision Avoidance Systems (SICAS) panel.

The format currently suggested by RTCA SC-186 [119] is based on the Mode-S extended squitter format, and is therefore also limited by the Mode-S message protocol, as described in the previous section. Following the basic messages defined by Lincoln Laboratory, SC-186 adopted the identification message and the airborne position message with slight modifications, and added a “trend squitter” which provides information on the aircraft velocity vector.

ID Squitter:

<i>Data Elements</i>	<i>Bits</i>
Message type	5
Aircraft Category	3
ICAO aircraft ID	48

Airborne squitter:

<i>Data Elements</i>	<i>Bits</i>	<i>Resolution</i>
Message type	5	
Surveillance status	2	
Broadcast only bit	1	
Altitude	12	
Unassigned	1	
CPR encoding type	1	
Latitude	17	5.2 m
Longitude	17	5.3 m – 18.4 m

Table A.4: ADS-B message format (RTCA SC-186)

Trend squitter:

<i>Data Elements</i>	<i>Bits</i>	<i>Resolution</i>
Message type	5	
Subtype code	3	
Synch bit	1	
Track angle sign	1	
Track angle	11	0.088°
Ground speed	12	0.25 knots
Turn rate sign	1	
Turn rate	6	0.242°/sec
Vertical rate sign	1	
Vertical rate	9	32 ft/min
Unassigned	6	

Table A.5: ADS-B message format (RTCA SC-186) - cont.

Note that the identification message includes information on the aircraft weight category in addition to the flight ID. The identification message will be sent once every 5 seconds. The airborne and trend squitters will be sent independently twice per second each.

Appendix B

Probability of Clear Reception

In this appendix we derive exact expressions for the probability of clear reception under random access protocols. We consider M aircraft, uniformly distributed over large area A . All aircraft generate short messages periodically, once every t_f seconds. Each message is t_m seconds long. An aircraft can receive messages sent by other aircraft, only if they are within its detection range R . The detection range is identical for all aircraft.

Initially, we assume that whenever two or more messages overlap at a receiver, all are lost and can not be received correctly by this receiver. The channel is assumed to be noiseless, such that errors caused by random noise are neglected in comparison with errors caused by messages overlap [52]. The only activity in the channel is due to the periodical reports generated by the aircraft.

B.1 Random Channel

Assume that all aircraft select a random transmission start time between 0 and t_f . A specific message, sent from \mathbf{P} to \mathbf{Q} , is received correctly if no other messages arrive at \mathbf{Q} during the vulnerable period for \mathbf{P} 's message. The vulnerable period starts one message length before \mathbf{P} 's message arrives, and lasts until its end. Hence, the length of the vulnerable period is $2t_m$, and the probability that any message arrives at \mathbf{Q} during this period is $2t_m/t_f$. Let A_k denote the event that there are k aircraft in the detection range of \mathbf{Q} , excluding \mathbf{P} and

Q. The probability of this event is

$$P(A_k) = \binom{M-2}{k} p^k (1-p)^{M-2-k} \quad k = 0, 1 \dots M-2 \quad (\text{B.1})$$

where p is the probability that any aircraft is within range:

$$p = \frac{\pi R^2}{A} \quad (\text{B.2})$$

The message sent by **P** will be received correctly by **Q**, if it does not overlap with any of the messages transmitted by the aircraft in range, including **Q** itself

$$P(\mathbf{P} \rightarrow \mathbf{Q} | A_k) = (1 - \frac{2t_m}{t_f})^{k+1} \quad (\text{B.3})$$

The total probability of clear reception is therefore:

$$P_r = \sum_{k=0}^{M-2} \binom{M-2}{k} p^k (1-p)^{M-2-k} (1 - \frac{2t_m}{t_f})^{k+1} \quad (\text{B.4})$$

Expanding and rearranging, we get:

$$P_r = (1 - \frac{2t_m}{t_f}) (1 - \frac{2t_m}{t_f} p)^{M-2} \quad (\text{B.5})$$

Note that the probability of clear reception in a random channel is independent of the range between the transmitter and the receiver, as long as this range is smaller than the detection range.

B.2 Random Slot Selection

Assume that all aircraft share a common time base. The time axis can thus be divided into slots, which are organized into frames with s slots in each frame. This is a traditional TDMA protocol [120]. Aircraft select at random one transmission slot each frame, and broadcast their message at slot beginning. Messages transmitted at slot beginning are received some time later, due to propagation delay. In order to assure that messages are sent and received at the same time slot, the message is padded with a propagation delay guard band. The

guard band is sized according to the maximum expected propagation delay, determined by the detection range R :

$$t_d = R/c \quad (\text{B.6})$$

where c is the speed of light. The slot size is therefore $t_s = t_m + t_d$ and the number of slots in a frame is $s = t_f/t_s$.

A specific message sent from **P** to **Q** over range r , will arrive at **Q** after r/c seconds. Other messages can interfere with this message, if they arrive at **Q** within $[r/c - t_m, r/c + t_m]$, measured from the slot beginning. These messages can be sent only by aircraft that use the same time slot as **P** does, and are located at range ρ from **Q**, where $r - ct_m \leq \rho \leq r + ct_m$. We can define the interference region as a ring, bounded by r_1 and r_2 :

$$\begin{aligned} r_1 &= \max(0, r - ct_m) \\ r_2 &= \min(R, r + ct_m) \end{aligned} \quad (\text{B.7})$$

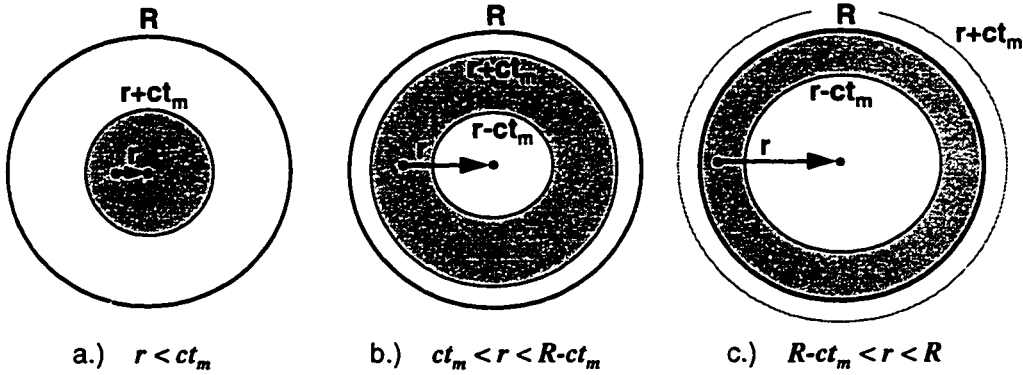


Figure B.1: Interference Region in a Slotted Channel

The interference region is depicted in figure B.1. The probability that any aircraft is inside this region is:

$$p(r) = \frac{\pi(r_2^2 - r_1^2)}{A} \quad (\text{B.8})$$

and the probability that any aircraft is using the same time slot as the transmitter is simply $1/s$. Following the derivation in the previous section, the probability that the message sent by **P** will arrive to **Q** without interference from any other aircraft, is

$$(1 - \frac{p(r)}{s})^{M-2}$$

We should also consider the possibility that both **P** and **Q** are using the same time slot. In this case, the two messages would overlap only when the distance between **P** and **Q** is less than ct_m . The probability of clear reception from a specific aircraft at range r is therefore:

$$P_r(r) = (1 - \frac{p_d(r)}{s})(1 - \frac{p(r)}{s})^{M-2} \quad (\text{B.9})$$

where

$$p_d(r) = \begin{cases} 1 & r \leq ct_m \\ 0 & r > ct_m \end{cases} \quad (\text{B.10})$$

and $p(r)$ is given by equation B.8. The probability of clear reception from a *specific* aircraft at distance r depends on the area of the interference region, and therefore varies with r . In order to get the channel capacity, we are interested in the average probability of clear reception from *any* aircraft within the detection range. Assuming that aircraft are uniformly distributed on a plane, the distribution function of the number of aircraft in radius r is

$$f(r) = \frac{2r}{R^2} \quad (\text{B.11})$$

The average probability of clear reception is then given by

$$P_r = \int_0^R P_r(r) f(r) dr \quad (\text{B.12})$$

The integral obtained after substituting $P_r(r)$ from (B.9) into (B.12) can not be evaluated analytically. In order to get an expression for the average probability without using $P_r(r)$, we look for the joint probability

$$P_o = P[r, \rho | 0 < r \leq R, r_1 < \rho \leq r_2]$$

where r and ρ are linearly distributed between 0 and R according to (B.11), and r_1 and r_2 are given by (B.7). This is the average overlap probability of a message from an aircraft

at range r , with a message from an aircraft at range ρ , given that both use the same time slot, and both are within the detection range of the receiver.

When the detection range is smaller than ct_m , all aircraft within the detection range of the receiver are also inside the interference region, and $P_o = 1$. When the detection range is larger than ct_m , some of the aircraft in range might be outside the interference region. The overlap probability is evaluated by integrating the density functions of r and ρ over the area of the interference region:

$$\begin{aligned} P_o &= \int_0^{ct_m} \frac{2r}{R^2} \int_0^{r+ct_m} \frac{2\rho}{R^2} d\rho dr + \int_{ct_m}^{R-ct_m} \frac{2r}{R^2} \int_{r-ct_m}^{r+ct_m} \frac{2\rho}{R^2} d\rho dr + \int_{R-ct_m}^R \frac{2r}{R^2} \int_{r-ct_m}^R \frac{2\rho}{R^2} d\rho dr \\ &= \frac{1}{3} \left(\frac{ct_m}{R} \right)^4 - 2 \left(\frac{ct_m}{R} \right)^2 + \frac{8}{3} \frac{ct_m}{R} \end{aligned}$$

The integration boundaries were set according to the possible values of r and ρ , depicted in figure B.1 for $R > 2ct_m$. Although the integration boundaries are different for $ct_m < R \leq 2ct_m$, the expressions obtained after the integration are the same. We substitute the propagation delay guard band $t_d = R/c$, and remove the conditions that the interfering aircraft are in range of the receiver, and are using the same time slot. The average probability of interference from any other aircraft is then:

$$\frac{1}{s} \frac{\pi R^2}{A} P_o$$

where

$$P_o = \begin{cases} 1 & R \leq ct_m \\ \frac{1}{3} (t_m/t_d)^4 - 2(t_m/t_d)^2 + \frac{8}{3} (t_m/t_d) & R > ct_m \end{cases} \quad (\text{B.13})$$

The overlap probability P_o can be interpreted in the following way: When $R \leq ct_m$, the message length is larger than the propagation delay guard band ($t_m \geq t_d$). In this case, all the messages transmitted at the same time slot overlap. When the message length is smaller than the propagation delay guard band, several messages can be received at the same time slot without interference [19]. The overlap probability P_o is smaller than one in this case, and is a function of the ratio t_m/t_d .

We should also consider the possibility of direct transmitter-receiver interference, where a message from an aircraft in range arrives at the receiver during the transmission period

of the receiver itself. The average probability of this event is

$$P_d = \begin{cases} 1 & t_m \geq t_d \\ (t_m/t_d)^2 & t_m < t_d \end{cases} \quad (\text{B.14})$$

given that both aircraft use the same time slot. Collecting all terms, we get the average probability of clear reception from any aircraft in range:

$$P_r = (1 - \frac{P_d}{s})(1 - p\frac{P_o}{s})^{M-2} \quad (\text{B.15})$$

where P_o is given by (B.13), and $p = \pi R^2/A$.

Figure 3.1 depicts the average probability of clear reception in a random channel (Equation B.5) and a slotted channel, as function of the detection range. The probability in the slotted channel was obtained by using (B.15). This curve matches perfectly the curve obtained by numerical integration of the range-dependent probability according to (B.12).

B.3 Capture Effects

Many receivers can correctly receive the strongest of several interfering signals, if the received power of the next to strongest is down by several dB. This “capture” effect can be modeled by using a distance measure [121, 53, 122]: an aircraft will correctly receive a message from another aircraft at distance $r \leq R$, if this message does not overlap with any of the messages sent by aircraft within distance αr , where:

$$\alpha = 10^{CR/20}, \quad \alpha \geq 1 \quad (\text{B.16})$$

CR is the capture ratio, defined as the received power ratio of two interfering signals:

$$CR = 10 \log \frac{P_1}{P_2}, \quad P_1 > P_2 \quad (\text{B.17})$$

It is assumed here that, in this radio environment, signal propagation path loss is proportional to the square of the distance from the source. For other propagation loss models and definitions of the capture condition, see [123].

Random channel

In a random channel, the possible location of aircraft that can interfere with a message sent from distance r , is a circle with radius

$$r_2 = \min(R, \alpha r) \quad (\text{B.18})$$

The interference region in this case is depicted in figure B.2.

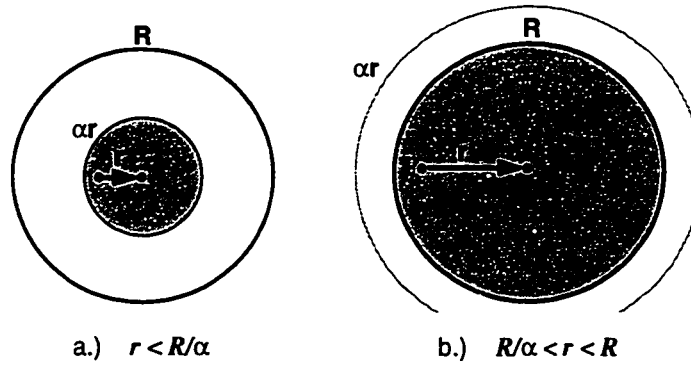


Figure B.2: Interference Region with Capture

Following the previous derivation for the “no capture” case, the probability of clear reception from an aircraft at distance r is:

$$P_r(r) = \left(1 - \frac{2t_m}{t_f}\right) \left(1 - p(r) \frac{2t_m}{t_f}\right)^{M-2} \quad (\text{B.19})$$

where

$$p(r) = \frac{\pi r^2}{A}$$

Note that the probability of clear reception in a random channel depends now on the distance between the receiver and the transmitter.

Slotted channel

In a slotted channel, the interference region is a ring bounded by

$$\begin{aligned} r_1 &= \max(0, r - ct_m) \\ r_2 &= \min(R, r + ct_m, \alpha r) \end{aligned} \quad (\text{B.20})$$

Graphically, this interference region can be presented by overlaying all possible combinations from figures B.1 and B.2. The probability of clear reception from an aircraft at distance r is

$$P_r(r) = (1 - \frac{p_d(r)}{s})(1 - \frac{p(r)}{s})^{M-2} \quad (\text{B.21})$$

where

$$p_d(r) = \begin{cases} 1 & r \leq ct_m \\ 0 & r > ct_m \end{cases}$$

and

$$p(r) = \frac{\pi(r_2^2 - r_1^2)}{A}$$

Exponential approximation

When $t_m \ll t_f$ and M is large, we can write

$$P_r(r) = \exp(-p_a(r)\frac{N}{s}) \quad (\text{B.22})$$

where p_a is the interference region ratio:

$$p_a(r) = \begin{cases} (\alpha r/R)^2 & 0 < r \leq R/\alpha \\ 1 & R/\alpha > r \leq R \end{cases} \quad (\text{B.23})$$

s is the number of time slots in a frame:

$$s = \begin{cases} t_f/2t_m & \text{Random Channel} \\ t_f/(t_m + t_d) & \text{Slotted Channel, } t_m \geq t_d \end{cases} \quad (\text{B.24})$$

and $N = M\pi R^2/A$ is the average number of aircraft in the detection range. The average probability of clear reception from *any* aircraft within the detection range is obtained by integrating $P_r(r)$:

$$P_r = \int_0^R P_r(r) f(r) dr \quad (\text{B.25})$$

where $f(r) = 2r/R^2$ is the distribution function of the number of aircraft in radius r . Defining $\beta = 1/\alpha^2$, we get:

$$P_r = \frac{\beta}{N/s} + (1 - \beta - \frac{\beta}{N/s}) \exp(-\frac{N}{s}) \quad (\text{B.26})$$

This expression is similar to the one obtained by Roberts [54] for the ALOHA computer network.

In case of no capture, $\alpha \rightarrow \infty$, $\beta \rightarrow 0$, and $P_r = \exp(-N/s)$ as was obtained in the previous sections. Perfect, or “full” capture is obtained when $\beta = 1$. In this case one packet always survives a collision, for any value of N [122].

Appendix C

Aircraft Traffic Density

The requirement for successful surveillance in a maximum traffic density of 0.3 aircraft per square nmi is based on the Minimum Operational Performance Standards of the current airborne Traffic alert and Collision Avoidance System (TCAS), as defined by RTCA [105]. The “0.3” figure represents a worst case scenario of traffic density in a crowded terminal airspace. However, even in crowded regions it can not be applied over a range larger than a few miles, as will be shown below.

TCAS required performance is stated in terms of probability of success for a target of interest in a given traffic density. For purposes of TCAS performance characterization, traffic density was defined as being constant within a given radius of uniform density, and falling off beyond. Specifically, the traffic count within a circle of radius R was assumed to be proportional to R^2 within the radius R_o , and to increase linearly beyond:

$$N(R) = \begin{cases} \sigma_o \pi R^2 & R \leq R_o \\ N(R_o)R/R_o = \sigma_o \pi R R_o & R > R_o \end{cases} \quad (\text{C.1})$$

The values presented as a design goal for TCAS are $\sigma_o = 0.3$ aircraft per square nmi, and $R_o = 5$ nmi. The traffic count according to this model is shown in figure C.1. Also shown in this figure is the effect of assuming a uniform traffic density of 0.3 aircraft per square nmi over a range larger than 5 nmi.

In order to compare these values with actual traffic densities, we define the average

traffic density as the ratio of the traffic count within a circle of radius R with the area of this circle¹:

$$\bar{\sigma} = \frac{N(R)}{\pi R^2} = \begin{cases} \sigma_o & R \leq R_o \\ \sigma_o R_o / R & R > R_o \end{cases} \quad (\text{C.2})$$

Figure C.2 depicts the average traffic density according to the TCAS model (Eq. C.2), and three points which represent the average traffic density in the San Francisco bay area, during a “busy” 10 minutes period in 1994. These points are based on radar returns from the Oakland radar site, as provided by the National Transport Analysis Program (NTAP) and analyzed by G. H. Elkaim [124]. This data clearly shows that regions of high traffic density do exist, but only over very short range. We can expect therefore that even in busier regions with higher traffic density, the high density will not be uniform over a range greater than a few miles.

¹Note that this average density does not agree with the mathematical definition of density, which should be assumed constant only over a thin ring between r and $r + dr$. The traffic count in this case should be integrated: $N(R) = \int_0^R \sigma(r) 2\pi r dr$, and the appropriate density which would yield the traffic count in Eq. C.1 is: $\sigma(R) = \sigma_o$ for $R \leq R_o$ and $\sigma(R) = \sigma_o R_o / 2R$ for $R > R_o$.

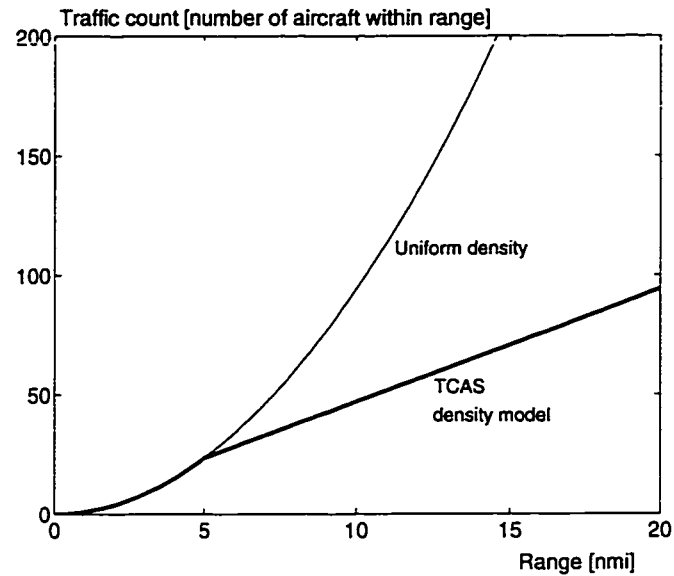


Figure C.1: Traffic Count

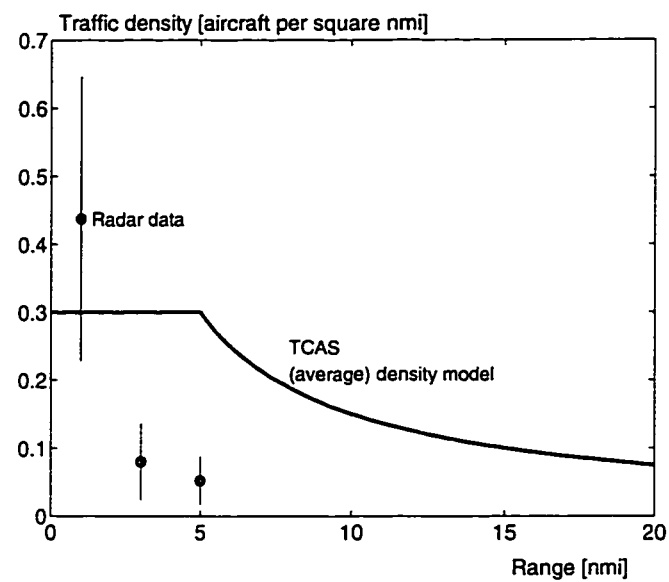


Figure C.2: Average Traffic Density

The average density is the ratio of the traffic count within a circle of radius R with the area of this circle. This should be compared with the average traffic density from radar data (circles with error bars) at the San Francisco bay area. The error bars represent the 1σ computation error.

Appendix D

Correlation Functions

In this appendix we derive the position and velocity correlation functions of several Gauss-Markov processes. These correlation functions were used in identification of a model for GPS measurement errors.

D.1 Theory

Consider a continuous linear Markov process

$$\dot{x} = A(t)x + B(t)w(t) \quad (\text{D.1})$$

where $w(t)$ is zero mean white noise, with spectral density Q

$$w \sim N(0, Q)$$

If the process is time-invariant and stable, the autocorrelation matrix of $x(t)$ is [125]:

$$C(\tau) = \Phi(\tau)X_{ss} \quad \text{for } \tau > 0 \quad (\text{D.2})$$

where $\Phi(\tau)$ is the state transition matrix

$$\Phi(\tau) = \exp(A\tau) \quad (\text{D.3})$$

and X_{ss} is the steady state covariance matrix of $x(t)$, described by the Lyapunov equation:

$$AX_{ss} + X_{ss}A^T + BQB^T = 0 \quad (\text{D.4})$$

In the following examples, the position and velocity are the first and second elements in $x(t)$, respectively. The position autocorrelation is then $\phi_{xx} = C_{(1,1)}$, the velocity autocorrelation is $\phi_{vv} = C_{(2,2)}$, and their cross-correlation is $\phi_{xv} = C_{(1,2)}$. All the correlation functions are given for $\tau > 0$ only.

D.2 Examples

1. A 1st order Gauss Markov process:

$$\dot{x} + \beta x = \beta w, \quad w \sim N(0, Q)$$

$$\phi_{xx}(\tau) = \frac{Q\beta}{2} e^{-\beta\tau} \quad (\text{D.5})$$

2. A simple (critically damped, $\zeta = 1$) 2nd order Gauss Markov process [75]:

$$\ddot{x} + 2\beta\dot{x} + \beta^2 x = \beta^2 w, \quad w \sim N(0, Q)$$

$$A = \begin{bmatrix} 0 & 1 \\ -\beta^2 & -2\beta \end{bmatrix} \quad B = \begin{bmatrix} 0 \\ \beta^2 \end{bmatrix}$$

$$\phi_{xx}(\tau) = \frac{Q\beta}{4} e^{-\beta\tau} (1 + \beta\tau) \quad (\text{D.6})$$

$$\phi_{vv}(\tau) = \frac{Q\beta^3}{4} e^{-\beta\tau} (1 - \beta\tau) \quad (\text{D.7})$$

$$\phi_{xv}(\tau) = \frac{Q\beta^3\tau}{4} e^{-\beta\tau} \quad (\text{D.8})$$

For the correlation matrix of a general 2nd order Gauss Markov (under damped, $\zeta < 1$), see [125].

3. A simple 3rd order process:

$$A = \begin{bmatrix} 0 & 1 & 0 \\ 0 & 0 & 1 \\ -\beta^3 & -3\beta^2 & -3\beta \end{bmatrix} \quad B = \begin{bmatrix} 0 \\ 0 \\ \beta^3 \end{bmatrix}$$

$$\phi_{xx}(\tau) = \frac{Q\beta}{16}e^{-\beta\tau}(3 + 3\beta\tau + \beta^2\tau^2) \quad (\text{D.9})$$

$$\phi_{vv}(\tau) = \frac{Q\beta^3}{16}e^{-\beta\tau}(1 + \beta\tau - \beta^2\tau^2) \quad (\text{D.10})$$

$$\phi_{xv}(\tau) = \frac{Q\beta^3\tau}{16}e^{-\beta\tau}(1 + \beta\tau) \quad (\text{D.11})$$

4. A simple 4th order process:

$$A = \begin{bmatrix} 0 & 1 & 0 & 0 \\ 0 & 0 & 1 & 0 \\ 0 & 0 & 0 & 1 \\ -\beta^4 & -4\beta^3 & -6\beta^2 & -4b \end{bmatrix} \quad B = \begin{bmatrix} 0 \\ 0 \\ 0 \\ \beta^4 \end{bmatrix}$$

$$\phi_{xx}(\tau) = \frac{Q\beta}{96}e^{-\beta\tau}(15 + 15\beta\tau + 6\beta^2\tau^2 + \beta^3\tau^3) \quad (\text{D.12})$$

$$\phi_{vv}(\tau) = \frac{Q\beta^3}{96}e^{-\beta\tau}(3 + 3\beta\tau - \beta^3\tau^3) \quad (\text{D.13})$$

$$\phi_{xv}(\tau) = \frac{Q\beta^3\tau}{96}e^{-\beta\tau}(3 + 3\beta\tau + \beta^2\tau^2) \quad (\text{D.14})$$

5. A general underdamped 3rd order process:

$$A = \begin{bmatrix} 0 & 1 & 0 \\ 0 & 0 & 1 \\ -a\omega^2 & -\omega^2 - 2a\omega\zeta & -a - 2\omega\zeta \end{bmatrix} \quad B = \begin{bmatrix} 0 \\ 0 \\ a\omega^2 \end{bmatrix}$$

$$\begin{aligned} \phi_{xx}(\tau) = & \frac{Qa\omega}{4b\zeta[(a^2 + \omega^2)^2 - (2a\omega\zeta)^2]} \left[2b\omega^3\zeta e^{-a\tau} + \right. \\ & \left. + ae^{-\omega\zeta\tau} \left(b \cos b\tau(a^2 + \omega^2 - 4\omega^2\zeta^2) + \omega\zeta \sin b\tau(a^2 + 3\omega^2 - 4\omega^2\zeta^2) \right) \right] \end{aligned} \quad (\text{D.15})$$

$$\begin{aligned} \phi_{vv}(\tau) = & \frac{Qa^2\omega^3}{4b\zeta[(a^2 + \omega^2)^2 - (2a\omega\zeta)^2]} \left[-2ab\omega\zeta e^{-a\tau} + \right. \\ & \left. + e^{-\omega\zeta\tau} \left(b \cos b\tau(a^2 + \omega^2) + \omega\zeta \sin b\tau(-a^2 + \omega^2) \right) \right] \end{aligned} \quad (\text{D.16})$$

$$\begin{aligned} \phi_{xv}(\tau) = & \frac{Qa^2\omega^3}{4b\zeta[(a^2 + \omega^2)^2 - (2a\omega\zeta)^2]} \left[2b\omega\zeta e^{-a\tau} + \right. \\ & \left. + e^{-\omega\zeta\tau} \left(-2b\omega\zeta \cos b\tau + \sin b\tau(a^2 + \omega^2 - 2\omega^2\zeta^2) \right) \right] \end{aligned} \quad (\text{D.17})$$

where $b \triangleq \omega\sqrt{1 - \zeta^2}$.

Appendix E

Correlated Measurement Noise

In this appendix we derive an optimal, reduced order tracking filter for a linear, time invariant system with high order correlated measurement noise. This appendix is an abridged version of [126], which provides also some background information and additional discussion.

E.1 Reduced Order Model

State space partition

The following linear time invariant system can be used as a dynamic model for tracking with correlated measurement noise:

$$x(k+1) = \Phi x(k) + w(k) \quad (\text{E.1})$$

$$e(k+1) = \Psi e(k) + v(k) \quad (\text{E.2})$$

where $x \in \mathcal{R}^{n_x}$ is the target state vector, $e \in \mathcal{R}^{n_e}$ is the state vector of the measurement error model, and w and v are independent, zero mean white noise vectors with covariance matrices

$$E[w(j)w^T(k)] = W\delta_{jk} \quad E[v(j)v^T(k)] = V\delta_{jk} \quad E[w(j)v^T(k)] = 0 \quad (\text{E.3})$$

The measurement vector $z \in \mathcal{R}^{n_z}$ is a linear combination of x and e :

$$z(k) = Cx(k) + De(k)$$

In tracking filters, the state vector x describes the target position, velocity and in some cases, acceleration. The matrix C extracts the measured elements of x , for example position only, or position and velocity. The matrix D extracts those elements of e which appear as measurement errors.

It is convenient to arrange the target state vector and the error model state vector such that their measured elements are grouped together. We can now rewrite the measurement equation:

$$z(k) = x_a(k) + e_a(k) \quad (\text{E.4})$$

where $x_a \in \mathcal{R}^{n_z}$ and $e_a \in \mathcal{R}^{n_z}$ are the measured elements of x and e . We have actually formed a partition of the state vectors:

$$x = \left[\begin{array}{c} x_a \\ x_b \end{array} \right] \begin{array}{l} \} n_z \\ \} n_x - n_z \end{array} \quad e = \left[\begin{array}{c} e_a \\ e_b \end{array} \right] \begin{array}{l} \} n_z \\ \} n_e - n_z \end{array}$$

We can form a similar partition of the transition matrices:

$$\Phi = \left[\begin{array}{c|c} \Phi_a & \Phi_b \\ \hline \Phi_c & \Phi_d \end{array} \right] \begin{array}{l} \} n_z \\ \} n_x - n_z \end{array} \quad \Psi = \left[\begin{array}{c|c} \Psi_a & \Psi_b \\ \hline \Psi_c & \Psi_d \end{array} \right] \begin{array}{l} \} n_z \\ \} n_e - n_z \end{array}$$

$\underbrace{\hspace{1.5cm}}_{n_z} \quad \underbrace{\hspace{1.5cm}}_{n_x - n_z} \qquad \underbrace{\hspace{1.5cm}}_{n_z} \quad \underbrace{\hspace{1.5cm}}_{n_e - n_z}$

The white noise vectors w and v and their covariance matrices are partitioned in the same way:

$$w = \left[\begin{array}{c} w_a \\ w_b \end{array} \right] \begin{array}{l} \} n_z \\ \} n_x - n_z \end{array} \quad v = \left[\begin{array}{c} v_a \\ v_b \end{array} \right] \begin{array}{l} \} n_z \\ \} n_e - n_z \end{array}$$

$$W = \left[\begin{array}{c|c} W_a & W_b \\ \hline W_c & W_d \end{array} \right] \begin{array}{l} \} n_z \\ \} n_x - n_z \end{array} \quad V = \left[\begin{array}{c|c} V_a & V_b \\ \hline V_c & V_d \end{array} \right] \begin{array}{l} \} n_z \\ \} n_e - n_z \end{array}$$

$\underbrace{\hspace{1.5cm}}_{n_z} \quad \underbrace{\hspace{1.5cm}}_{n_x - n_z} \qquad \underbrace{\hspace{1.5cm}}_{n_z} \quad \underbrace{\hspace{1.5cm}}_{n_e - n_z}$

The system can now be described by the following set of equations:

$$x_a(k+1) = \Phi_a x_a(k) + \Phi_b x_b(k) + w_a(k) \quad (\text{E.5})$$

$$x_b(k+1) = \Phi_c x_a(k) + \Phi_d x_b(k) + w_b(k) \quad (\text{E.6})$$

$$e_a(k+1) = \Psi_a e_a(k) + \Psi_b e_b(k) + v_a(k) \quad (\text{E.7})$$

$$e_b(k+1) = \Psi_c e_a(k) + \Psi_d e_b(k) + v_b(k) \quad (\text{E.8})$$

with the measurement

$$z(k) = x_a(k) + e_a(k) \quad (\text{E.9})$$

Reduced model formulation

We define a new measurement vector z_r , which is a linear combination of the current measurement and the measurement at the next time step:

$$z_r(k) \triangleq z(k+1) - \Psi_a z(k) \quad (\text{E.10})$$

where the measurement at the next time step is obtained from (E.5), (E.7) and (E.9):

$$z(k+1) = \Phi_a x_a(k) + \Phi_b x_b(k) + w_a(k) + \Psi_a e_a(k) + \Psi_b e_b(k) + v_a(k) \quad (\text{E.11})$$

We can use the perfect measurement of $z(k)$ at the current time step (E.9) to eliminate the measured part of the error state vector:

$$e_a(k) = z(k) - x_a(k) \quad (\text{E.12})$$

Substituting (E.11) and (E.12) into (E.10) forms a new measurement equation:

$$z_r(k) = [\Phi_a - \Psi_a] x_a(k) + \Phi_b x_b(k) + \Psi_b e_b(k) + w_a(k) + v_a(k) \quad (\text{E.13})$$

Equation (E.12) can also be used to eliminate e_a from the difference equation for e_b :

$$e_b(k+1) = \Psi_c z(k) - \Psi_c x_a(k) + \Psi_d e_b(k) + v_b(k) \quad (\text{E.14})$$

We can now combine x and e_b into a new state vector of dimension $n_r = n_x + n_e - n_z$:

$$x_r = \left[\begin{array}{c} x \\ e_b \end{array} \right] \left. \begin{array}{l} \} n_x \\ \} n_e - n_z \end{array} \right\}$$

The new state vector propagates according to

$$x_r(k+1) = Fx_r(k) + Gu_r(k) + w_r(k) \quad (\text{E.15})$$

where

$$F = \left[\begin{array}{cc|c} \Phi_a & \Phi_b & 0 \\ \Phi_c & \Phi_d & 0 \\ \hline -\Psi_c & 0 & \Psi_d \end{array} \right] \quad G = \left[\begin{array}{c|c} 0 & \\ 0 & \\ \hline \Psi_c & \end{array} \right] \quad (\text{E.16})$$

u_r is a deterministic input, equal to the current measurement:

$$u_r(k) = z(k)$$

and the new noise vector w_r is

$$w_r = \left[\begin{array}{c} w \\ \hline v_b \end{array} \right]$$

w_r is a zero mean white noise vector, with a covariance matrix

$$E[w_r(j)w_r^T(k)] = Q\delta_{jk}, \quad Q = \left[\begin{array}{cc|c} W_a & W_b & 0 \\ W_c & W_d & 0 \\ \hline 0 & 0 & V_d \end{array} \right] \quad (\text{E.17})$$

The new measurement equation is

$$z_r(k) = Hx_r(k) + v_r(k) \quad (\text{E.18})$$

where

$$H = [\Phi_a - \Psi_a \quad \Phi_b \quad \Psi_b] \quad (\text{E.19})$$

The measurement noise v_r , given by

$$v_r(k) = w_a(k) + v_a(k)$$

is a zero mean white noise vector, with a covariance matrix

$$E[v_r(j)v_r^T(k)] = R\delta_{jk}, \quad R = W_a + V_a \quad (\text{E.20})$$

Note that the new process noise and measurement noise are correlated:

$$E[w_r(j)v_r^T(k)] = S\delta_{jk}, \quad S = \begin{bmatrix} W_a \\ W_c \\ \hline V_c \end{bmatrix} \quad (\text{E.21})$$

Equations (E.15) and (E.18) describe a linear, time invariant system, with white process and measurement noise. The system order is $n_x + n_e - n_z$, and it is smaller than the augmented system order, which is $n_x + n_e$. The reduced order system is now in a form suitable for the application of the standard Kalman filter equations, in which the process and measurement errors are presumed white.

E.2 Filter Design

Consider the linear, time invariant system described by equations (E.15) and (E.18):

$$\begin{aligned} x(k+1) &= Fx(k) + Gu(k) + w(k) \\ y(k) &= Hx(k) + v(k) \end{aligned}$$

where w and v are zero mean white noise vectors with covariance matrices

$$E[w(j)w^T(k)] = Q\delta_{jk} \quad E[v(j)v^T(k)] = R\delta_{jk} \quad E[w(j)v^T(k)] = S\delta_{jk}$$

and u is a deterministic input. The optimal state estimator is given by the following Kalman filter equations [78]:

Measurement update:

$$K(k) = \bar{P}(k)H^T[H\bar{P}(k)H^T + R]^{-1} \quad (\text{E.22})$$

$$\hat{x}(k) = \bar{x}(k) + K(k)[y(k) - H\bar{x}(k)] \quad (\text{E.23})$$

$$\hat{P}(k) = \bar{P}(k) - K(k)H\bar{P}(k) \quad (\text{E.24})$$

Time update:

$$\bar{x}(k+1) = F\hat{x}(k) + Gu(k) + \quad (\text{E.25})$$

$$\begin{aligned}
& +S[H\bar{P}(k)H^T + R]^{-1}[y(k) - H\bar{x}(k)] \\
\bar{P}(k+1) &= F\hat{P}(k)F^T + Q + \\
& -S[H\bar{P}(k)H^T + R]^{-1}S^T - FK(k)S^T - SK(k)F^T
\end{aligned} \tag{E.26}$$

where \hat{x} and \hat{P} are the optimal estimate and its covariance matrix, and \bar{x} and \bar{P} are the optimal one step prediction and its covariance matrix. K is the Kalman filter gain matrix. Note the additional terms in the time update phase, due to the correlation between the process and measurement noise.

We can get directly the optimal state prediction, by substituting the measurement update equations into the time update equations. Rearranging, we get:

$$\bar{x}(k+1) = F\bar{x}(k) + Gu(k) + \bar{K}(k)[y(k) - H\bar{x}(k)] \tag{E.27}$$

$$\bar{P}(k+1) = F\bar{P}(k)F^T + Q - \bar{K}(k)[H\bar{P}(k)H^T + R]\bar{K}(k)^T \tag{E.28}$$

where the modified gain matrix is

$$\bar{K}(k) = [F\bar{P}(k)H^T + S][H\bar{P}(k)H^T + R]^{-1} \tag{E.29}$$

In our case, the deterministic input $u(k)$ is equal to the current measurement

$$u(k) \leftarrow z(k)$$

and the measurement $y(k)$ is a linear combination of the current measurement and the measurement at the next time step (E.10):

$$y(k) \leftarrow z(k+1) - \Psi_a z(k)$$

In this way, $\bar{x}(k+1)$ depends on $z(k+1)$, and it is actually the optimal *estimate* of the state, and not the optimal one step prediction. By shifting the time index and changing the notation we get:

$$\hat{x}(k) = F\hat{x}(k-1) + Gz(k-1) + \bar{K}(k-1)[z(k) - \Psi_a z(k-1) - H\hat{x}(k-1)] \tag{E.30}$$

where \bar{K} and \bar{P} are given by (E.29) and (E.28). The dynamic model matrices F , G and H are given by (E.16) and (E.19), and the appropriate covariance matrices Q , R and S are given in (E.17), (E.20) and (E.21). This completes the formulation of the optimal tracking filter.

E.3 Filter Initialization

Rogers [82] suggested to start the filter in its information form. Bryson and Henrikson [79, 86] suggested to initialize the reduced order filter by using the augmented state vector and its associated full order filter for the first time step. However, the common practice in tracking filters is to initialize the filter by using the first two measurements [65]. The initial value of the covariance matrix is then calculated by using the standard deviation of the white measurement error. In the following discussion we extend this approach to vehicle tracking filters with colored measurement noise.

Consider the case where the target is assumed to fly with constant velocity, only its position is measured, and the position error is modeled as a 2nd order Gauss-Markov process. In that case, the dimension of the target model is $n_x = 2$, the dimension of the error model is $n_e = 2$ and the dimension of the measurement vector is $n_z = 1$. The reduced order model has a dimension of $n_r = n_x + n_e - n_z = 3$, and its state vector combines the target position, velocity and velocity error:

$$\mathbf{x}_r = [x_1 \quad x_2 \quad e_2]^T$$

The position measurement is the sum of the true position and the position error:

$$z = x_1 + e_1$$

The initial state estimate $\hat{\mathbf{x}}_r(0)$ can be obtained after the first two measurements:

$$\begin{aligned}\hat{x}_{r,1}(0) &= z(0) \\ \hat{x}_{r,2}(0) &= [z(0) - z(-1)]/T \\ \hat{x}_{r,3}(0) &= 0\end{aligned}$$

where T is the sampling interval. The initial estimation error $\tilde{\mathbf{x}}_r \triangleq \mathbf{x}_r - \hat{\mathbf{x}}_r$ is

$$\begin{aligned}\tilde{x}_{r,1}(0) &= x_1(0) - [x_1(0) + e_1(0)] \\ \tilde{x}_{r,2}(0) &= x_2(0) - [x_1(0) + e_1(0) - x_1(-1) - e_1(-1)]/T \\ \tilde{x}_{r,3}(0) &= e_2(0)\end{aligned}$$

Based on our assumption that the target velocity is constant, we can approximate

$$x_2(0) \cong [x_1(0) - x_1(-1)]/T$$

The initial estimation error is then

$$\begin{aligned}\tilde{x}_{r,1}(0) &= -e_1(0) \\ \tilde{x}_{r,2}(0) &= [-e_1(0) + e_1(-1)]/T \\ \tilde{x}_{r,3}(0) &= e_2(0)\end{aligned}$$

and the corresponding initial covariance matrix is

$$\begin{aligned}\bar{P}(0) = E[\tilde{x}_r(0)\tilde{x}_r^T(0)] = \\ E \begin{bmatrix} e_1^2(0) & e_1(0)[e_1(0) - e_1(-1)]/T & -e_1(0)e_2(0) \\ e_1(0)[e_1(0) - e_1(-1)]/T & [e_1(0) - e_1(-1)]^2/T^2 & e_2(0)[-e_1(0) + e_1(-1)]/T \\ -e_1(0)e_2(0) & e_2(0)[-e_1(0) + e_1(-1)]/T & e_2^2(0) \end{bmatrix} \quad (\text{E.31})\end{aligned}$$

These values can be calculated by using the correlation matrix associated with the error model. For a general 2nd order model we have:

$$C(\tau) = E[e(t)e^T(t + \tau)] = \begin{bmatrix} \phi_{xx}(\tau) & \phi_{xv}(\tau) \\ \phi_{vx}(\tau) & \phi_{vv}(\tau) \end{bmatrix}$$

where ϕ_{xx} is the position error autocorrelation, ϕ_{vv} is the velocity error autocorrelation, and ϕ_{xv} is the crosscorrelation of the position and velocity errors. Referring to the elements of $\bar{P}(0)$, we have:

$$\begin{aligned}E[e_1^2(0)] = E[e_1^2(-1)] &= \phi_{xx}(0) \\ E[e_1(0)e_1(-1)] &= \phi_{xx}(T) \\ E[e_2(0)e_1(0)] &= \phi_{xv}(0) \\ E[e_2(0)e_1(-1)] &= \phi_{xv}(T) \\ E[e_2^2(0)] &= \phi_{vv}(0)\end{aligned}$$

Substituting in (E.31), we get:

$$\bar{P}(0) = \begin{bmatrix} \phi_{xx}(0) & \Delta\phi_{xx} & -\phi_{xv}(0) \\ \Delta\phi_{xx} & 2\Delta\phi_{xx}/T & -\Delta\phi_{xv} \\ -\phi_{xv}(0) & -\Delta\phi_{xv} & \phi_{vv}(0) \end{bmatrix} \quad (\text{E.32})$$

where $\Delta\phi_{xx} \triangleq [\phi_{xx}(0) - \phi_{xx}(T)]/T$ and $\Delta\phi_{xv} \triangleq [\phi_{xv}(0) - \phi_{xv}(T)]/T$. The same procedure can be applied to other target and error models. This method guarantees consistency of the filter initialization, and does not require additional code for the augmented model or the information form.

E.4 Examples

In the following examples we assume that the target moves with constant velocity, subject to zero mean random acceleration. We also assume that the measurement error can be described by a simple 2nd order Gauss Markov process. The treatment of these specific cases can be easily extended to other target and error models, by following the derivations in the previous sections.

Target model

The dimension of a constant velocity target model is $n_x = 2$, and it is given by

$$x(k+1) = \Phi x(k) + w(k), \quad E[w(j)^T w(k)] = W \delta_{jk}$$

The state transition matrix and the maneuver noise covariance matrix are [65]:

$$\Phi = \begin{bmatrix} 1 & T \\ 0 & 1 \end{bmatrix}, \quad W = q_w T \begin{bmatrix} T^2/3 & T/2 \\ T/2 & 1 \end{bmatrix}$$

and q_w is the spectral density of the maneuver noise.

Measurement error model

A simple 2nd order Gauss Markov process can be described by the following differential equation (see Appendix D):

$$\dot{e}(t) = Ae(t) + Bv(t)$$

where

$$A = \begin{bmatrix} 0 & 1 \\ -\beta^2 & -2\beta \end{bmatrix} \quad B = \begin{bmatrix} 0 \\ \beta^2 \end{bmatrix}$$

and v is a zero mean white noise with spectral density q_v . The discretized version of this error model is

$$e(k+1) = \Psi e(k) + v(k), \quad E[v(j)v^T(k)] = V\delta_{jk}$$

where the state transition matrix is given by $\Psi(\tau) = \exp(A\tau)$, and the noise covariance matrix is

$$V = \int_0^T \Psi(\tau) B q_v B^T \Psi^T(\tau) d\tau$$

Position measurement

When only the target position is measured, $n_z = 1$. Following the state space partition rules from section E.1, we obtain the dynamic model matrices:

$$F = \left[\begin{array}{cc|c} 1 & T & 0 \\ 0 & 1 & 0 \\ \hline -\Psi_{2,1} & 0 & \Psi_{2,2} \end{array} \right] \quad G = \left[\begin{array}{c} 0 \\ 0 \\ \hline \Psi_{2,1} \end{array} \right] \quad H = \left[\begin{array}{cc|c} 1 - \Psi_{1,1} & T & \Psi_{1,2} \end{array} \right]$$

and the covariance matrices:

$$Q = \left[\begin{array}{cc|c} W_{1,1} & W_{1,2} & 0 \\ W_{2,1} & W_{2,2} & 0 \\ \hline 0 & 0 & V_{2,2} \end{array} \right] \quad R = W_{1,1} + V_{1,1} \quad S = \left[\begin{array}{c} W_{1,1} \\ W_{2,1} \\ \hline V_{2,1} \end{array} \right]$$

where $(\cdot)_{i,j}$ denotes the $\{i,j\}$ element of (\cdot) . These matrices can now be used in the filter equations (E.28-E.30). As shown in the previous section, the filter is initialized after the

second position measurement:

$$\hat{x}(0) = \begin{bmatrix} z(0) \\ [z(0) - z(-1)]/T \\ 0 \end{bmatrix}$$

Evaluating the correlation functions $\phi_{xx}(\tau)$, $\phi_{vv}(\tau)$ and $\phi_{xv}(\tau)$ (Equations D.6–D.8) at $\tau = 0$ and $\tau = T$, and substituting in (E.32), we get the initial value of the covariance matrix:

$$\bar{P}(0) = \sigma_x^2 \begin{bmatrix} 1 & f_x/T & 0 \\ f_x/T & 2f_x/T^2 & \beta^2 e^{-\beta T} \\ 0 & \beta^2 e^{-\beta T} & \beta^2 \end{bmatrix}$$

where $f_x \triangleq 1 - (1 + \beta T)e^{-\beta T}$. We have used here the identity $\sigma_x^2 = \phi_{xx}(0)$ to normalize $\bar{P}(0)$ by the variance of the position error.

Position and velocity measurement

The additional measurement in this case reduces the filter order to $n_r = 2$. The dynamic model matrices are:

$$F = \Phi \quad G = 0^{2 \times 2} \quad Q = W$$

and the covariance matrices are:

$$H = \Phi - \Psi \quad R = W + V \quad S = W$$

In this case the dimension of the error model is equal to the dimension of the measurement vector. We can therefore follow the basic approach suggested by Bryson and Henrikson [79]. The tracking filter we get is similar to the one obtained by using the matrices defined above and equations (E.28–E.30).

The filter can be initialized after the first measurement:

$$\hat{x}(0) = z(0)$$

with the covariance matrix

$$\bar{P}(0) = \begin{bmatrix} \phi_{xx}(0) & 0 \\ 0 & \phi_{vv}(0) \end{bmatrix} = \sigma_x^2 \begin{bmatrix} 1 & 0 \\ 0 & \beta^2 \end{bmatrix}$$

Appendix F

Runway Spacing Components

This appendix derives the elements for the required runway spacing which allows independent, parallel approaches under IMC. The derivations were adapted from a preliminary work on runway separation done by The MITRE Corporation in 1981 [94].

1. The Normal Operating Zone (NOZ) width is computed such that the probability of detecting a normally operating aircraft outside of it is equal to an acceptable level.

The probability of detecting an aircraft outside the NOZ is:

$$P(\hat{y} > \text{NOZ}) = 1 - F_{\text{Nav+Surv}}(y) \quad (\text{F.1})$$

where \hat{y} is the estimated cross track position, and $F_{\text{Nav+Surv}}(y)$ is the cumulative distribution function of the navigation and surveillance errors, convolved together. The NOZ boundary is then:

$$\text{NOZ} = F_{\text{Nav+Surv}}^{-1}(1 - P_{fa}) \quad (\text{F.2})$$

where F^{-1} is the inverse cumulative distribution function, and P_{fa} is the acceptable probability of false alarm.

2. The Detection Zone (DZ) allows for the inaccuracy of the surveillance system in detection that the aircraft crossed the NOZ boundary. The DZ width provides an acceptable level of the late alarm probability.

The probability that a violating aircraft is not detected after K measurements is:

$$\prod_{n=0}^K F_{Surv}(3\sigma_{Surv} - x - nD) \frac{dx}{D}$$

where F_{Surv} is the cumulative distribution function of the surveillance errors, with standard deviation σ_{Surv} , and D is the distance the aircraft travels between updates, in the direction normal to the runway:

$$D = V_1 t_f \sin \gamma \quad (\text{F.3})$$

V_1 is the violator velocity, t_f is the update period, and γ is the maximum angle of deviation from the ILS centerline (blunder angle).

We assume that the position measurements are uncorrelated, and that the first opportunity for detection outside the NOZ occurs when the aircraft is still $3\sigma_{Surv} - x$ within the NOZ, where $0 < x < D$. We now search for DZ which satisfies

$$P_{la} = \int_0^D \prod_{n=0}^K F_{Surv}(3\sigma_{Surv} - x - nD) \frac{dx}{D} \quad (\text{F.4})$$

where K is the minimum integer such that

$$-3\sigma_{Surv} + x + KD \leq \text{DZ} \quad (\text{F.5})$$

and P_{la} is the acceptable probability of late alarm.

3. The Correction Zone (CZ) accounts for the delay between the detection of the violator and the initiation of the evader's response; as well as the distance that the violator travels until the evader reaches a parallel course, minus the distance needed during the turn-away maneuver by the evader:

$$\text{CZ} = (\text{DEL} + \gamma/\omega) V_1 \sin \gamma - V_2/\omega(1 - \cos \gamma) \quad (\text{F.6})$$

where ω is the aircraft turn rate, and γ/ω is the time required by non blunderer to turn to a parallel course.

4. The Navigation Buffer (NB) accounts for an adequate lateral separation between the aircraft at their point of closest approach, and includes an allowance for the fact that even normally operating aircraft may not be exactly on the ILS localizer:

$$NB = d + N_\sigma \sigma_{Nav} \quad (F.7)$$

where d is the minimum safety distance, σ_{Nav} is the standard deviation of the navigation error, and N_σ is the number of navigation sigmas allowed for the non-blunderer.

Note that in this context only one NOZ is relevant to the process of handling a particular blunder situation. Dividing the runway spacing into two NOZs plus an NTZ is done for the convenience of the controllers. The parameters used to obtain the current separation of 4,300 ft are described in table F.1.

Violator velocity	V_1	150 knot
Evader velocity	V_2	150 knot
Evader turn rate	ω	3° /sec
Maximum blunder angle	γ	30°
Total Delay time	DEL	8 sec
Minimum safety distance	d	200 ft
Navigation buffer	N_σ	2
Navigation accuracy	σ_{Nav}	300 ft
Surveillance accuracy	σ_{Surv}	300 ft
Update interval	t_f	4.8 sec
Probability of false alarm	P_{fa}	3.36e-3
Probability of late alarm	P_{la}	0.1

Table F.1: **Model Parameters for Parallel Runway Separation**

The ILS navigation accuracy is 5 mrad, evaluated at a maximum range of 10 nmi. This is based on actual flight test data described in [96]. The surveillance accuracy is also 5 mrad, evaluated at the same maximum range of 10 nmi. This accuracy and the 4.8-sec update interval represent the performance of an ASR-9 radar and an Automated Radar

Terminal System (ARTS) display [102]. We have calibrated the navigation buffer size and the acceptable level of the false and late alarm probabilities to obtain the current runway spacing of 4,300 ft. All the other parameters are based on [94].

Appendix G

Monte Carlo Simulations

This appendix describes several Monte Carlo simulations that were used throughout this work.

G.1 Random Air Traffic Communication Network

Following is a brief description of the simulation that was used to verify the analytical results for the probability of clear reception in random access protocols, and to analyze the behavior of organized protocols.

Initialization

Aircraft initial position is uniformly distributed over a circular playing area with a 150 nmi radius. Aircraft heading is selected from a uniform distribution in the range $0 \rightarrow 2\pi$. The aircraft velocity is fixed and equal for all aircraft.

Initial time slot selection is uniformly distributed between 0 and $s-1$, where s is the number of available time slots. There is also an option to start the simulation with a perfect time slot combination, such that no transmission conflicts occur in the first time step.

Time propagation

In the case of random reporting and random time slot selection, the aircraft motion has no effect on the probability of clear reception. We can therefore set all aircraft with zero velocity, and re-initialize the simulation after each frame.

In the case of organized protocols, all aircraft follow straight line paths, until leaving the playing area. Whenever an aircraft is leaving, a new aircraft is introduced on the perimeter of the playing area. The entry point and the new heading are selected such that the uniform distribution of the aircraft heading in the playing area would not be distorted [127]. The new aircraft also selects a random time slot, and all the other protocol parameters are re-initialized.

We have used a relatively high velocity of 600 knots for all aircraft, so that transmission conflicts would be generated more frequently. The simulation time step is equal to the slot length. A slot counter, common to all aircraft, is initialized after each frame.

Probability calculation

In order to avoid edge effects, we look only at aircraft located inside an inner region, with a 110 nmi radius. However, all aircraft in the playing area follow the communication protocol rules being tested. In order to calculate the average probability of clear reception, the following procedure is performed each time slot:

For any aircraft i , find its neighbors who use the current time slot.

For any neighbor j , find the arrival time at i of the message sent by j .

For any other neighbor of i , check if its message arrives to i during the vulnerable period for the message sent by j .

If no other messages arrive to i during the vulnerable period, then i can receive j .

Count the number of neighbors each aircraft in the inner circle have, during the whole frame.

Count how many of these neighbors are received without interference. The ratio of these counts is the probability of clear reception. This is averaged over an hour of flight.

G.2 Random Approach Simulation

This section describes a Monte Carlo simulation of random approaches. This simulation was used to study the effect of blunder prediction on the probability of false and late alarms in the approach monitoring alert algorithm.

The simulation starts with an aircraft at a range of 10 nmi, approaching the runway at 150 knot. The cross-track position during a normal approach is synthesized by a sinusoidal model [97]:

$$y_{\perp}(t) = A(t) \sin\left(\frac{2\pi}{T}t + \phi\right) \quad (\text{G.1})$$

where $A(t)$ is the amplitude of the cross-track position:

$$A(t) = \psi_o R(t) = \psi_o (R_o - Vt) \quad (\text{G.2})$$

ψ_o provides a standard deviation of 5 mrad [96]. T is the period and ϕ is the phase. They are represented with uniform distributions: $T \sim \text{U}(100, 140)$ sec, and $\phi \sim \text{U}(0, 2\pi)$ rad.

The blunder maneuver starts at a randomly selected point on a normal approach, up to 2 nmi from the runway. The deviating aircraft starts to turn towards the other runway at a constant turn rate of $3^\circ/\text{sec}$, up to a blunder angle of 30° .

The aircraft position is sampled, and a measurement error is added. Radar surveillance error is assumed white, with a standard deviation of 5 mrad, multiplied by the range to the runway. When using GPS, the measurement error is provided by actual GPS measurement errors, selected from the data base described in the previous chapter. The measurements in this case arrive each update with a certain probability which models the interference in the radio data link. The data link model is identical to the one used in the previous chapter to study GPS-based tracking filters in a future ATC environment (see section 4.5).

The measured position is then fed to a tracking filter. In case of radar-based surveillance, the estimated position and velocity are derived from a simple α - β tracking filter [97], with

$\alpha = 0.8$ and $\beta = 0.53$. In case of GPS-based surveillance, we use the multiple model tracking filter that was developed in the previous chapter.

Finally, the predicted cross track position is computed by a simple linear projection:

$$z_{\perp} = \hat{y}_{\perp} + \hat{v}_{\perp} t_p \quad (\text{G.3})$$

where \hat{y}_{\perp} and \hat{v}_{\perp} are the estimated cross track position and velocity, and t_p is the prediction time.

G.3 Random Encounters in “Free Flight”

The simulation described below was used to analyze several collision detection and avoidance algorithms and compare their performance. The distributions of the aircraft parameters were selected to model a future “Free Flight” environment, where aircraft are free to change their flight direction at any moment.

Aircraft parameters

The simulation determines the relative location of a pair of aircraft at the point of closest approach, such that the horizontal miss distance between the aircraft is uniformly distributed between 0 and 4 nmi, and the vertical miss distance is uniformly distributed between -1000 ft and +1000 ft. The aircraft heading is chosen such that the range rate at this point would be zero, thus ensuring that this point is indeed the CPA. The aircraft equations of motion are then propagated backward in time, until the range between the aircraft is 12 nmi, or the time of flight exceeds 200 seconds.

The velocity of both aircraft is uniformly distributed between 150 and 450 knots. Each aircraft is initially flying a straight line path, and starts turning t_h seconds before CPA, where t_h is uniformly distributed between 10 and 45 seconds. The probability density of the turn rate during the maneuver is shown in figure G.1. The aircraft has a probability P_1 of turning at the maximum turn rate (ω_{max} or $-\omega_{max}$) and a probability P_0 of not turning at all. The aircraft will turn between the limits ω_{max} and $-\omega_{max}$ according to the appropriate

uniform distribution. The values we used are $P_0=0.5$, $P_1=0.2$, and $\omega_{max}= 3^\circ/\text{sec}$. This model has been shown to provide a satisfactory representation of the target's maneuver characteristics [128].

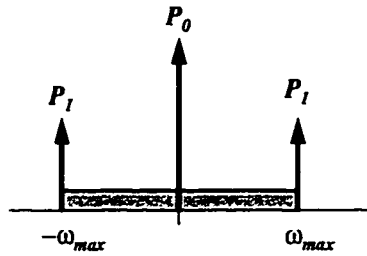


Figure G.1: Distribution of Aircraft Turn Rate

The aircraft vertical speed is distributed in the following way [117]: 60% of the aircraft are level (vertical speed uniformly distributed between -300 fpm and +300 fpm) and the rest climb or descend at a vertical speed which is uniformly distributed between -1500 fpm and +1500 fpm [117]. 65% of the aircraft do not change their vertical speed during the encounter. The rest may change their vertical speed t_v seconds before CPA, where t_v is uniformly distributed between 10 and 55 seconds. The acceleration used when changing the vertical rate is uniformly distributed between 0.125g and 0.25g.

Table G.1 summarizes the parameters used in the simulation, including the parameters describing the aircraft response to a resolution advisory.

Measurements

In addition to the motion described above, both aircraft were subjected to zero mean, exponentially correlated wind disturbances in all directions, with $\sigma_w=0.7$ m/s and $\tau=1$ sec [129]. In order to examine the sensitivity of the algorithm to measurement errors, we have added actual GPS position measurement errors to the simulated location of both aircraft. The measurement errors were selected from the data base described in chapter 4. We assumed that the measurement errors of the two aircraft are uncorrelated.

Velocity	U(150, 450)	knot
Maximum turn rate	3	deg/sec
Probability of straight flight	0.5	
Probability of maximum maneuver	0.2	
Horizontal maneuver switch time	U(10, 45)	sec before CPA
Vertical rate in near-level flight	U(-300, +300)	fpm
Vertical rate in climb/descend	U(-1500, +1500)	fpm
Probability of near-level flight	0.6	
Probability of vertical profile change	0.65	
Vertical maneuver switch time	U(10, 55)	sec before CPA
Vertical acceleration	U(0.125, 0.25)	g
Vertical acceleration in RA	N(0.25, 0.025)	g
Delay in response to vertical RA	U(3, 7)	sec
Horizontal acceleration in RA	N(0.5, 0.05)	g
Delay in response to horizontal RA	U(8, 12)	sec

Table G.1: “Free Flight” Simulation Parameters

Own position measurements were available every computation cycle (1 sec). The intruder’s position was available every t_f seconds, with a certain probability which models the interference in the radio data link. The data link model is identical to the one used in the previous chapters: each aircraft broadcasts a 125 bit message once every t_f seconds, in a 1Mbps bit rate. We assume that there are 100 aircraft in the detection range of own receiver. For comparison, the maximum capacity of a TCAS sensor is 54 transponders within 30 nmi [105]. If $t_f=1$ second, the resulting probability of clear reception is $P_r=0.9753$. As t_f grows, so does P_r , according to Eq. 4.24.

The various algorithms for collision detection and avoidance were included in the simulation exactly as described in the text of Chapter 6, except for the TCAS algorithms. The actual TCAS logic is much more complicated than the basics described in the text, and we have made a special effort to use most of the original TCAS code in our simulation.

Bibliography

- [1] P. L. Massoglia, M. T. Pozeski, and G. T. Germana, "The use of satellite technology for oceanic air traffic control," *Proceedings of the IEEE*, vol. 77, no. 11, pp. 1695–1708, 1989.
- [2] B. Flax, "A minimum rate of position reporting in the future oceanic air traffic control system," in *IEEE PLANS*, pp. 223–230, 1992.
- [3] C. A. Shivley, "Capacity as a consideration for providing aeronautical mobile satellite air traffic services in the U.S. domestic airspace," *IEEE AES Magazine*, pp. 51–58, June 1992.
- [4] G. W. Bartkiewicz and R. L. Berkowitz, "Preliminary requirements for satellite based automatic dependent surveillance (ADS)," in *AIAA/IEEE 12th Digital Avionics Systems Conference*, pp. 209–214, 1993.
- [5] J. Nilsson, "GPS/GLONASS user systems in sweden," *Journal of Navigation*, vol. 45, pp. 258–265, May 1992.
- [6] J. Nilsson and H. Lans, "A GNSS-based time division multiple access data link," *Air Traffic Control Quarterly*, vol. 1, no. 4, pp. 353–363, 1993.
- [7] J. Nilsson, "The GNSS transponder and the time synchronized self organizing TDMA data link," in *AIAA/IEEE 13th Digital Avionics Systems Conference*, pp. 489–497, November 1994.
- [8] J. Nilsson and H. Lans, "The GNSS transponder - a cost-effective worldwide GNSS-based civil aviation CNS/ATM, ATC, ATN data link and collision avoidance system concept," *Journal of Navigation*, vol. 47, pp. 403–426, September 1994.
- [9] V. A. Orlando and G. H. Knittel, "GPS-Squitter: system concept and performance," *Air Traffic Control Quarterly*, vol. 1, no. 4, pp. 303–326, 1993.
- [10] R. E. Boisvert and V. A. Orlando, "ADS-Mode S system overview," in *AIAA/IEEE 12th Digital Avionics Systems Conference*, pp. 104–109, 1993.

- [11] E. T. Bayliss, R. E. Boisvert, and G. H. Knittel, "Demonstration of GPS automatic dependent surveillance of aircraft using spontaneous Mode S beacon reports," in *ION GPS - 93*, pp. 185–197, 1993.
- [12] R. E. Boisvert, K. W. Saunders, M. L. Wood, and V. A. Orlando, "GPS-Squitter experimental results," in *AIAA/IEEE 13th Digital Avionics Systems Conference*, pp. 521–527, November 1994.
- [13] E. T. Bayliss, R. E. Boisvert, M. L. Burrows, and W. H. Harman, "Aircraft surveillance based on GPS position broadcasts from mode s beacon transponders," in *ION GPS - 94*, 1994.
- [14] A. Beining, "Low-cost high tech, now!," *Sport Aviation*, pp. 36–39, February 1993.
- [15] C. Moody and D. Peed, "A system concept for GNSS augmentation data link," *Air Traffic Control Quarterly*, vol. 1, no. 4, pp. 327–352, 1993.
- [16] D. Peed and C. Moody, "A system analysis of a GNSS augmentation data link," in *AIAA/IEEE 13th Digital Avionics Systems Conference*, pp. 483–488, November 1994.
- [17] M. Spellman, "The application of spread spectrum datalinks to GPS-based air traffic navigation, surveillance and control," in *IEEE PLANS '94*, pp. 194–198, 1994.
- [18] C. B. Villani and R. J. Pankiewicz, "A spread spectrum digital data link for aviation," in *AIAA/IEEE 13th Digital Avionics Systems Conference*, pp. 498–503, November 1994.
- [19] S. R. Jones, "Relative capacities of generic ADS protocols," *Air Traffic Control Quarterly*, vol. 1, no. 4, pp. 365–389, 1993.
- [20] H. W. Thomas and C. C. Lefas, "Use of aircraft-derived data to assist in ATC tracking," *IEE Proceedings Part. F*, vol. 129, pp. 281–288, August 1982.
- [21] C. C. Lefas, "Algorithms for improved, heading assisted, maneuver tracking," *IEEE Transactions on Aerospace and Electronics Systems*, vol. 21, pp. 351–359, May 1985.
- [22] C. C. Lefas, "The use of downlinked measurements to track civil aircraft," in *AGARD AG-301*, May 1990.
- [23] C. M. Rekkas, C. C. Lefas, and N. J. Krikelis, "Three-dimensional tracking using on-board measurements," *IEEE Transactions on Aerospace and Electronics Systems*, vol. 27, pp. 617–623, July 1991.

- [24] C. C. Lefas, "Improved tracking with Mode-S data-linked velocity measurements," *IEEE Transactions on Aerospace and Electronics Systems*, vol. 27, pp. 709–714, July 1991.
- [25] C. M. Rekkas, C. C. Lefas, and N. J. Krikelis, "Improved 3-D tracking using the Mode-S down link," *IEEE Transactions on Aerospace and Electronics Systems*, vol. 30, pp. 267–274, January 1994.
- [26] T. Palsson, "GPS based ADS trials in iceland," in *ION GPS - 92*, pp. 417–423, 1992.
- [27] H. J. Rome, "Potential impact of GPS and automatic dependent surveillance on air lane separations in the north atlantic organized track system," in *ION GPS - 90*, pp. 225–236, 1990.
- [28] M. A. Coote, G. W. Schraw, and R. W. Schwab, "Oceanic requirements and benefits modeling for automatic dependent surveillance (ADS)," *Air Traffic Control Quarterly*, vol. 1, no. 1, pp. 31–57, 1993.
- [29] J. S. Morrel, "The mathematics of collision avoidance in the air," *Navigation: Journal of the Institute of Navigation*, vol. 11, January 1958.
- [30] J. M. Holt and G. R. Marner, "Separation theory in air traffic control system design," *Proceedings of the IEEE*, vol. 58, pp. 369–376, March 1970.
- [31] R. L. Ford, "The protected volume of airspace generated by an airborne collision systems," *Journal of Navigation*, vol. 39, pp. 182–187, May 1986.
- [32] R. L. Ford, "The conflict resolution process for TCAS II and some simulation results," *Journal of Navigation*, vol. 40, pp. 283–303, September 1987.
- [33] R. L. Ford and D. L. Powell, "A new threat detection criterion for airborne collision avoidance systems," *Journal of Navigation*, vol. 43, pp. 391–403, September 1990.
- [34] J. A. Deckert, "Integrating TCAS into the airspace management system," in *IEEE PLANS*, 1992.
- [35] H. R. Pilley and L. V. Pilley, "Collision prediction and avoidance using enhanced GPS," in *ION GPS - 92*, 1992.
- [36] D. E. Winer, "The free flight continuum," in *ATM - 95*, 1995.
- [37] R. Braff, J. D. Powell, and J. Dorfler, "Applications of the GPS to air traffic control," in *Principles and Applications of GPS*, vol. 2, ch. 12, AIAA, 1995.

- [38] M. E. Cox, R. C. Rawlings, and P. Kraan, "GPS: Can it contribute to European ATC?," *J. of Navigation*, vol. 45, May 1992.
- [39] P. L. Massoglia and R. D. Till, "Automatic dependent surveillance (ADS) pacific engineering trials (PET)," in *IEEE PLANS*, pp. 167–172, 1992.
- [40] J. L. Baker, V. A. Orlando, W. B. Link, and W. G. Collins, "Mode S system design and architecture," *Proceedings of the IEEE*, vol. 77, pp. 1684–1694, November 1989.
- [41] V. A. Orlando, "The Mode S beacon radar system," *The Lincoln Laboratory Journal*, vol. 2, no. 3, pp. 345–361, 1989.
- [42] W. H. Harman, "TCAS: A system for preventing midair collisions," *The Lincoln Laboratory Journal*, vol. 2, no. 3, 1989.
- [43] J. Walsh and J. Wojciech, "TCAS in the 1990s," *Navigation: Journal of the Institute of Navigation*, vol. 38, no. 4, pp. 383–397, 1991.
- [44] E. H. Phillips, "FAA seeks major cut in primary radars," *Aviation Week & Space Technology*, p. 29, October 1995.
- [45] B. R. Climie, "Automatic dependent surveillance focus of civil avionics integration," in *IEEE PLANS*, pp. 162–166, 1992.
- [46] ICAO Automatic Dependent Surveillance Panel (ADSP). ADSP/3-WP/77 Appendix B, Section 1.3, May 1994.
- [47] M. J. Asbury and R. Johannessen, "The role of GPS in automatic dependent surveillance (ADS)," in *ION GPS-95*, 1995.
- [48] G. Bailey, "Automatic dependent surveillance," in *ATM - 95*, 1995.
- [49] J. J. Fee and T. R. Simpson, "Implementation of GPS-based oceanic air traffic control system," in *ION GPS - 95*, 1995.
- [50] P. R. Drouilhet, "Scanning the issue," *Air Traffic Control Quarterly*, vol. 1, no. 4, pp. 299–301, 1993.
- [51] J. Howland, "Digital air/ground communications for air traffic control," in *AIAA/IEEE 13th Digital Avionics Systems Conference*, pp. 510–514, November 1994.

- [52] L. Kleinrock and F. A. Tobagi, "Packet switching in radio channels: Part I - carrier sense multiple access modes and their throughput-delay characteristics," *IEEE Transactions on Communications*, vol. 23, pp. 1400–1416, December 1975.
- [53] N. Abramson, "The throughput of packet broadcasting channels," *IEEE Transactions on Communications*, vol. 25, pp. 117–128, January 1977.
- [54] L. G. Roberts, "ALOHA packet system with and without slots and capture," *Computer Communication Review*, vol. 5, pp. 28–42, April 1975.
- [55] K. Zhang and K. Pahlavan, "Relation between transmission and throughput of slotted ALOHA local packet radio networks," *IEEE Transactions on Communications*, vol. 40, pp. 577–583, March 1992.
- [56] I. Chlamtac and S. S. Pinter, "Distributed nodes organization algorithm for channel access in a multihop dynamic radio network," *IEEE Transactions on Computers*, vol. 36, pp. 728–737, June 1987.
- [57] D. S. Stevens and M. H. Ammar, "Evaluation of slot allocation strategies for TDMA radio networks," in *IEEE MILCOM*, pp. 835–839, 1990.
- [58] D. S. Stevens and M. H. Ammar, "Evaluation of distributed TDMA rescheduling procedure for mobile packet radio networks," in *IEEE MILCOM*, pp. 1167–1171, 1991.
- [59] D. J. Baker and A. Ephremides, "The architectural organization of a mobile radio network via a distributed algorithm," *IEEE Transactions on Communications*, vol. 29, pp. 1694–1701, November 1981.
- [60] A. Ephremides and T. Truong, "Distributed algorithm for efficient and interference free broadcasting in radio networks," in *IEEE INFOCOM*, pp. 1119–1124, 1988.
- [61] R. Bar-Yehuda, O. Goldreich, and A. Itai, "On the time-complexity of broadcast in multi-hop radio networks: An exponential gap between determinism and randomization," *Journal of Computer and System Sciences*, vol. 45, pp. 104–126, 1992.
- [62] I. Chlamtac and Y. Mansour, "Local cycle generation in multihop radio networks," in *IEEE MILCOM*, pp. 801–805, 1987.
- [63] A. Bhatnagar and T. G. Robertazzi, "Layer net: A new self-organizing network protocol," in *IEEE MILCOM*, pp. 845–849, 1990.

- [64] M. Hofri, "A feedback-less distributed broadcast algorithm for multihop radio networks with time-varying structure," in *Computer Performance and Reliability* (G. Iaseolla, P. J. Courtois, and O. J. Boxma, eds.), pp. 353–368, Elsevier (North-Holland), 1988.
- [65] Y. Bar-Shalom and T. E. Fortman, *Tracking and Data Association*. Academic Press, 1988.
- [66] P. Vacher, I. Barret, and M. Gauvrit, "Design of a tracking algorithm for an advanced ATC system," in *Multitarget-Multisensor Tracking: Application and Advances* (Y. Bar-Shalom, ed.), vol. 2, Artech House, 1992.
- [67] X. R. Li and Y. Bar-Shalom, "Design of an interacting multiple model algorithm for air traffic control tracking," *IEEE Transactions on Control Systems Technology*, vol. 1, pp. 186–194, September 1993.
- [68] W. D. Blair, G. A. Watson, and S. A. Hoffman, "Second order interacting multiple model algorithm for tracking maneuvering targets," in *Signal and Data Processing of Small Targets*, vol. 1954, pp. 518–529, SPIE, 1993.
- [69] H. T. Chou, "An anti-SA filter for non-differential GPS users," in *ION GPS - 90*, pp. 535–542, 1990.
- [70] A. Leick, *GPS Satellite Surveying*. Wiley, 1990.
- [71] R. Conley, "GPS performance: What is normal?," in *ION GPS - 92*, pp. 885–893, 1992.
- [72] P. Y. Hwang, "Recommendations for enhancement of RTCM-104 differential standard and its derivatives," in *ION GPS - 93*, pp. 1501–1508, 1993.
- [73] W. Tang and G. Howell, "Integrated GPS/INS kalman filter implementations issues," in *ION GPS - 93*, pp. 217–224, 1993.
- [74] M. D. Goodwin and J. J. Kusnierek, "Using GPS for airborne formation control," in *ION GPS - 93*, pp. 971–884, 1993.
- [75] A. Gelb, *Applied Optimal Estimation*. The M.I.T. Press, 1974.
- [76] D. J. Mook and I.-M. Shyu, "Nonlinear aircraft tracking filter utilizing control variable estimation," *J. Guidance*, vol. 15, pp. 228–237, January 1992.
- [77] J. D. Kendrick, P. S. Maybeck, and J. G. Reid, "Estimation of aircraft target motion using orientation measurements," *IEEE Transactions on Aerospace and Electronics Systems*, vol. 17, pp. 254–259, March 1981.

- [78] P. S. Maybeck, *Stochastic Models, Estimation and Control*, vol. 1. Academic Press, 1979.
- [79] A. E. Bryson, Jr. and L. J. Henrikson, "Estimation using sampled data containing sequentially correlated noise," *Journal of Spacecraft*, vol. 5, pp. 662–665, June 1968.
- [80] C. K. Chui and G. Chen, *Kalman Filtering*. Springer Verlag, 2 ed., 1990.
- [81] B. D. O. Anderson and J. B., *Optimal Filtering*. Prentice-Hall, 1979.
- [82] S. R. Rogers, "Alpha-beta filter with correlated measurement noise," *IEEE Transactions on Aerospace and Electronics Systems*, vol. 23, pp. 592–594, July 1987.
- [83] G. Chen and C. K. Chui, "Design of near-optimal linear digital tracking filters with colored input," *Journal of Computational and Applied Mathematics*, vol. 15, pp. 353–370, 1986.
- [84] J. A. Guu and C. H. Wei, "Tracking a maneuvering target with correlated measurement noises by maneuver detection method," *Electronics Letters*, vol. 27, pp. 265–267, January 1991.
- [85] J. A. Guu and C. H. Wei, "Maneuvering target tracking using IMM method at high measurement frequency," *IEEE Transactions on Aerospace and Electronics Systems*, vol. 27, pp. 514–519, May 1991.
- [86] L. J. Henrikson, *Sequentially Correlated Measurement Noise with Applications to Inertial Navigation*. PhD thesis, Harvard University, May 1967.
- [87] R. J. Kassel and E. G. Baxa, Jr., "The effect of missing data on the steady-state performance of an α, β tracking filter," in *Proceedings of the 20th Southeastern Symposium on System Theory*, pp. 526–529, March 1988.
- [88] G. Chen, "A simple treatment for suboptimal kalman filtering in case of measurement data missing," *IEEE Transactions on Aerospace and Electronics Systems*, vol. 26, pp. 413–415, March 1990.
- [89] F. R. Castella, "An adaptive two-dimensional kalman tracking filter," *IEEE Transactions on Aerospace and Electronics Systems*, vol. 16, pp. 822–829, November 1980.
- [90] Y. Bar-Shalom and K. Birmiwal, "Variable dimension filter for maneuvering target tracking," *IEEE Transactions on Aerospace and Electronics Systems*, vol. 18, pp. 621–629, September 1982.

- [91] Y. T. Chan, A. G. C. Hu, and J. B. Plant, "A kalman filter based tracking scheme with input estimation," *IEEE Transactions on Aerospace and Electronics Systems*, vol. 15, pp. 237–244, March 1979.
- [92] R. J. McAulay and E. Denlinger, "A decision-directed adaptive tracker," *IEEE Transactions on Aerospace and Electronics Systems*, vol. 9, pp. 229–236, March 1973.
- [93] Y. Bar-Shalom, K. C. Chang, and H. A. P. Blom, "Tracking a maneuvering target using input estimation versus the interacting multiple model algorithm," *IEEE Transactions on Aerospace and Electronics Systems*, vol. 25, pp. 296–300, March 1989.
- [94] A. L. Haines and W. J. Swedish, "Requirements for independent and dependent parallel instrument approaches at reduced runway spacing," tech. rep., FAA-EM-81-8, May 1981.
- [95] "Final monitor aid." [http:// www. tc. faa. gov/ prm/ fma.html](http://www.tc.faa.gov/prm/fma.html), August 1994.
- [96] Anon., "Parallel runway monitor demonstration report," tech. rep., DOT/FAA/RD-91/5, February 1991.
- [97] R. R. LaFrey, "Parallel runway monitor," *The Lincoln Laboratory Journal*, vol. 2, no. 3, pp. 411–436, 1989.
- [98] S. Nagaoka, O. Amai, and Y. Watanabe, "Evaluating the feasibility of a radar separation minimum for a long-range SSR," *The Journal of Navigation*, vol. 42, pp. 403–416, September 1989.
- [99] S. A. Kassam, *Signal Detection in Non-Gaussian Noise*. Springer-Verlag, 1987.
- [100] B. W. Parkinson, "GPS error analysis," in *Global Positioning System: Theory and Applications* (B. W. Parkinson and J. J. Spilker Jr., eds.), vol. 1, ch. 11, AIAA, 1996.
- [101] P. K. Enge and A. J. Van Dierendock, "Wide area augmentation system," in *Global Positioning System: Theory and Applications* (B. W. Parkinson and J. J. Spilker Jr., eds.), vol. 2, ch. 4, AIAA, 1996.
- [102] H. L. Crane and S. V. Massimini, "Simultaneous independent parallel approaches in canada using modernized sensors and displays," Tech. Rep. MP-95W55, The MITRE Corporation, June 1995.
- [103] V. Wulschleger. FAA Technical Center. Private communication, October 1995.

- [104] T. Williamson and N. A. Spencer, "Development and operation of the traffic alert and collision avoidance system (TCAS)," *Proceedings of the IEEE*, vol. 77, pp. 1735–1744, November 1989.
- [105] RTCA/DO-185, *Minimum Operational Performance Standards For Traffic Alert and Collision Avoidance System (TCAS) Airborne Equipment*, 2 ed., 1990.
- [106] V. Czaplyski, "Electronic see and avoid," *AOPA Pilot*, July 1994.
- [107] B. Sridhar and G. Chatterji, "Computer-aided system for detecting runway incursions," in *Sensing, Imaging and Vision for Control and Guidance of Aerospace Vehicles*, vol. 2220, pp. 328–337, SPIE, 1994.
- [108] J. Baldwin, A. Smith, and R. Cassell, "General aviation collision avoidance - challenges of full implementation," in *AIAA/IEEE 13th Digital Avionics Systems Conference (DASC)*, pp. 504–509, November 1994.
- [109] J. W. Andrews, "Modeling of air-to-air visual acquisition," *The Lincoln Laboratory Journal*, vol. 2, no. 3, pp. 475–481, 1989.
- [110] A. K. Barrows, P. Enge, B. W. Parkinson, and J. D. Powell, "Flight tests of a 3-D perspective-view glass-cockpit display for general aviation using GPS," in *ION GPS-95*, September 1995.
- [111] L. G. Culhane and B. M. Horowitz, "Conflict alert and intermittent positive control," in *A Survey of Modern Air Traffic Control*, vol. 1, AGARD AG-209, July 1975.
- [112] K. E. Willis, J. B. Currier, and P. Flanagan, "Intermittent positive control," *Proceedings of the IEEE*, vol. 58, pp. 361–369, March 1970.
- [113] R. G. Dear and Y. S. Sherif, "A prediction model for a ground-based collision avoidance system," *International Journal on Policy and Information*, vol. 13, pp. 69–89, June 1989.
- [114] R. G. Dear and Y. S. Sherif, "Z-Basic algorithm for collision avoidance system," *IEEE Transactions on Systems, Man and Cybernetics*, vol. 21, pp. 915–921, July 1991.
- [115] S. Ratcliffe, "Manoeuvre in response to collision warning from airborne devices," *Journal of Navigation*, vol. 25, pp. 461–466, October 1972.
- [116] S. Ratcliffe, "Collision avoidance and the future of air traffic control," *Journal of Navigation*, vol. 26, October 1973.
- [117] J. E. Lebron, "System safety study of minimum TCAS II," tech. rep., DOT/FAA/PM-83/36, December 1983.

- [118] Y. C. Ho, A. E. Bryson, Jr., and S. Baron, "Differential games and optimal pursuit-evasion strategies," *IEEE Transactions on Automatic Control*, vol. 10, no. 4, pp. 385–389, 1965.
- [119] RTCA SC186 WG2/SG3, "Extended squitter formats." Rev. 1.0, June 1996.
- [120] S. S. Lam, "Packet broadcast networks - a performance analysis of the R-ALOHA protocol," *IEEE Transactions on Computers*, vol. 29, pp. 596–603, July 1980.
- [121] H. Takagi and L. Kleinrock, "Optimal transmission ranges for randomly distributed packet radio terminals," *IEEE Transactions on Communications*, vol. 32, pp. 246–257, March 1984.
- [122] L. Fratta and D. Sant, "Some models of packet radio networks with capture," in *5th Intl. Conf. Computer Communications, Atlanta, GA*, pp. 155–161, October 1980.
- [123] C. Lau and C. Leung, "Capture models for mobile packet radio networks," in *IEEE Intl. Conf. on Communications, ICC*, pp. 1226–1230, 1990.
- [124] G. H. Elkaim, "Brief summary of radar return analysis." Stanford University KGLS group, 1994.
- [125] A. E. Bryson, Jr. and Y. C. Ho, *Applied Optimal Control*. Hemisphere Publishing Corp., 1975.
- [126] R. Gazit, "Digital tracking filters with high order correlated measurement noise," *IEEE Transactions on Aerospace and Electronics Systems*, January 1997.
- [127] J. L. Goodwin and R. L. Ford, "Random air traffic generation for computer models," *Journal of Navigation*, vol. 38, pp. 218–233, May 1985.
- [128] R. A. Singer, "Estimating optimal tracking filter performance for manned maneuvering targets," *IEEE Transactions on Aerospace and Electronics Systems*, vol. 6, pp. 473–483, July 1970.
- [129] B. W. Parkinson and K. T. Fitzgibbon, "Aircraft automatic landing systems using GPS," *Journal of Navigation*, vol. 42, pp. 47–59, January 1989.